Dissertation

Identification and characterization of *Kif1bβ* and *hsSASS-6* as novel disease genes for two hereditary neurological disorders

submitted by

Verena RUPP, BSc. MSc.

for the Academic Degree of

Doctor of Philosophy (PhD)

at the

Medical University of Graz

Institute of Human Genetics

under the Supervision of

Assoz. Prof. Priv.-Doz. Mag. Dr. Christian WINDPASSINGER

2018

Statutory Declaration

I hereby declare that this dissertation is my own original work and that I have fully acknowledged by name all of those individuals and organizations that have contributed to the research for this dissertation. Due acknowledgement has been made in the text to all other material used. Throughout this dissertation and in all related publications I followed the "*Standards of Good Scientific Practice and Ombuds Committee at the Medical University of Graz*".

Please note that parts of this thesis have been published in 'Human Molecular Genetics' (2014).

KHAN, M.A.*, RUPP, V.M.*, ORPINELL, M.*, HUSSAIN, M.S., ALTMULLER, J., STEINMETZ, M.O., ENZINGER, C., THIELE, H., HOHNE, W., NURNBERG, G., BAIG, S.M., ANSAR, M., NURNBERG, P., VINCENT, J.B., SPEICHER, M.R., GONCZY, P. and WINDPASSINGER, C., 2014. A missense mutation in the PISA domain of HsSAS-6 causes autosomal recessive primary microcephaly in a large consanguineous Pakistani family. *Human molecular genetics,* **23**(22). pp. 5940-5949.

* Contributed equally

This work was only possible with the contribution of following people:

Institute of Human Genetics, Medical University of Graz:

Christian Windpassinger, Peter Kroisel, Michael Speicher: recruitment of patients, supervision and project leaders

Department of Neurology, Medical University of Graz:

Christian Enzinger: analysis of MRI data from microcephaly patients

Institute of Molecular Biology and Biochemistry, Medical University of Graz:

Ernst Malle, Chintan Navinchandra Koyani: Western Blot and Pull-down assays for Kif1B

Roland Malli: Kif1B microscopy

UPGON, EPFL Lausanne:

Pierre Gönczy and Meritxell Orpinell Mercadé: supervision and cellular localization studies for hsSAS-6

Gomal Centre of Biochemistry and Biotechnology, Gomal University D.I.Khan:

Muzammil Khan: Recruitment of microcephaly patients

Department of Biochemistry, Quaid-i-Azam University:

Muhammad Ansar: Recruitment of microcephaly patients

Laboratory of Bimolecular Research, Paul Scherrer Institute Villigen:

Michel Steinmetz: generation of protein models for SAS-6

Cologne Center of Genomics:

Peter Nürnberg, Janine Altmüller, Holger Thiele, Gudrun Nürnberg: NGS analysis of microcephaly family

Human molecular Genetics Laboratory, NIBGE Faisalabad:

Shahid M. Baig: NGS analysis of microcephaly family

MiND Lab, The Campbell Family Brain Research Institute, CAMH, Toronto:

John Vincent: Discussion of results

Graz, 15.03.2018

Acknowledgment

At this point, I want to say thank you to all the people who have supported me throughout my time as a PhD student at the Medical University of Graz. I want to express my special gratitude to my principle investigators and mentors, Christian Windpassinger and Michael Speicher, who gave me the opportunity to work at this institute, supported my ideas and helped me finding my own niche in science. Although experiments or projects sometimes turned out to be not as successful as expected, you never gave me the feeling that I screwed it up. I could have not wished for better mentors.

Special thanks goes also towards Ellen Heitzer, who always had an open ear for my scientific questions and problems. Despite lots of other work you came up with several ideas on how to improve my workflow. You are such an inspiring researcher!

I am very thankful for the support of Sasa Frank from the Institute of Molecular Biology and Biochemistry who was part of my PhD committee.

Not to forget my wonderful colleagues at the Institute of Human Genetics who are a warmhearted and supportive crowed of people. Apart from work I found real friends and this is more than one could wish for. Especially, I want to mention Christine, who jumped in for me whenever I was sick or on holiday. Also many thanks to Peter who helped me with questions concerning bioinformatics, to Tom for discussing the trickiest problems with me, and to Erwin, who was very supportive in terms of administrative and study-related questions.

During my PhD I had the chance to visit extraordinarily good research institutes, namely the EPFL in Lausanne and the Stanford University in California. This would not have been possible without the invitation and supervision of Pierre Gönczy and Vittorio Sebastiano - thank you for the wonderful experiences in your labs. Special thanks goes to Meritxell Orpinell Mercadé. You have been taking good care of me at the EPFL – I am so grateful for your time and patience.

Finally, I want to mention my friends and my wonderful family who were so incredibly supportive throughout the years. Whenever I was down, you put me up again and reminded me of why I initially wanted to pursue a career in science. You were always there for me, believed in me, and were happy for me whenever I achieved something new. I want to especially mention Katharina. You initiated my invitation to Stanford

where I was trained the generation of iPSCs. You vouched for me and I highly appreciate this.
I am truly grateful to have you all in my life.

Verena Rupp received funding from the ÖNB Jubiläumsfond, Project Nr. 15093, the FFG Project, Number 8507000, and the Medical University of Graz through the PhD Program ‘Molecular Medicine’ (MolMed).

Table of Contents

Abbreviations

°C	Celsius
A	Adenosine
AA	Amino acid
ABI	Applied Biosystems
ACC	Agenesis of the corpus callosum
ACLSM	Array confocal laser scanning microscope
aIP	Apical intermediate progenitor
AD	Autosomal dominant
ALFY	WD Repeat and FYVE Domain Containing 3 (=WDFY3)
ANKLE2	Ankyrin Repeat And LEM Domain Containing 2
AR	Autosomal recessive
ASPM	Abnormal spindle microtubule assembly
ATP	Adenosine triphosphate
bIP	Basal intermediate progenitor
bp	Base pair
BWA	Burrows-Wheeler aligner
C	Cysteine (amino acid)
C	Cytosine (nucleotide)
Ca^{2+}	Calcium
CaM	Calmodulin
CASC5	Cancer susceptibility candidate 5
CC	Corpus callosum
CDK5RAP2	CDK5 regulatory subunit associated protein 2
cDNA	Complementary DNA
CDK6	Cyclin Dependent Kinase 6
cen	Centrin
CEP	Centrosomal protein
CENPE or J	Centromere Protein E or J
Chr	Chromosome
CIT	Citron Rho-Interacting Serine/Threonine Kinase
cm	Centimeter

cM	Centimorgan
CMT	Charcot-Marie Tooth
CNS	Central nervous system
coMIP	Codon optimized miniplasmid
ConDel	CONsensus DELeteriousness score of missense SNVs
CPAP	Centrosomal P4.1-Associated Protein (=CENPJ)
crSAS-6	Clamydomonas reinhardtii spindle assembly protein 6
CrispR-Cas9	Clustered Regularly Interspaced Short Palindromic Repeats-CrispR associated endonuclease 9
Ct	Carboxy-termianl or C-terminal
CT	Computed tomography
dbSNP	Database of single nucleotide polymorphisms
DMEM	Dulbecco's Modified Eagle medium
DNA	Deoxyribonucleic acid
Dox	Doxycycline
DrSAS-6	Danio rerio spindle assembly protein 6
E plus number	Embryonic day
EDTA	Ethylenediaminetetraacetic acid
EGFP	Enhanced green fluorescence protein
ESP6500	NHLBI Exome Sequencing Project 6500
EtOH	Ethanol
ExPASy	Expert Protein Analysis System
F	Phenylalanine
FBS	Fetal bovine serum
Fg	Femtogram
FHA	Forkhead-associated domain
g	Gram
G	Guanosine
GABA	γ-aminobutyric- acid
GATK	Genome analysis tool kit
Gb	Giga bite
GE	Ganglionic eminence
GFP	Green fluorescence protein
Gsx	GS Homeobox

GW	Gestational week
H_2O	Water
HFB	Human fetal brain
Hg17/19	Human genome version 17 or 19
HGMD	Human genome mutation database
HRP	Horse reddish peroxidase
hsSAS-6/ hsSASS-6	Homo sapiens spindle assembly protein 6
I	Iseoleucine
IBD	Identical by decent
ID	Intellectual development
IDACC	Intellectual disability with agenesis of the corpus callosum
IKM	Interkinetic migration
Ile	Isoleucine
IP	Intermediate progenitor cells
iPSC	Induced pluripotent stem cells
IQ	Intelligence quotient
250K	250 000
KBP	Kinesin binding protein
KCL	Kalium chloride
Kif/KIF	Kinesin family member
kg	Kilogram
L	Leucine
LBC	Lymphoblastoid cells
Leu	Leucine
LOD	Logarithm of odds
LPC	Lysophosphatidylcholine
MAF	Minor allele frequency
MAfftWS	Multiple Alignment using fast furrier transform web service
Mb	Mega bite
MB	Mega base
Mbp	Myelin binding protein
MCPH	Microcephaly primary hereditary

MFSD2A	Major Facilitator Superfamily Domain Containing 2A
min	Minutes
mRNA	Messenger RNA
MRI	Magnet resonance imaging (=MRT)
MRT	Magnetic resonance tomography
MS	Multiple sclerosis
MST	Mitotic somal translocations
Mut	Mutant, mutated
MZ	Marginal zone
N	Asparagine
NaCl	Sodium chloride
NE	Neuroepithelial cell
NHLBI	National Heart, Lung, and Blood Institute
NSC	Neuronal stem cell
NT	Amino-terminal or N-terminal
Olig2	Oligodendrocyte Transcription Factor 2
OMIM	Online Mendelian Inheritance in Men
oRG	Outer radial glial cell
oSVZ	Outer subventricular zone
p75NTR	p75 neurotrophin receptor
PBS	Phosphate-Buffered Saline
PCR	Polymerase chain reaction
Pen/Strep	Penicillin / streptomycin
PH domain	Pleckstrin homology domain
PHC1	Polyhomeotic Homolog 1
Phe	Phenylalanine
PISA	Present in SAS-6
PLK4	Polo-like kinase 4
PNS	Peripheral nervous system
PolyPhen	Polymorphism Phenotyping v2
PP	Preplate
p-ter	End of short chromosome arm
qPCR	Quantitative polymerase chain reaction
Q	Glutamine

q-ter	End of long chromosome arm
R	Arginine
RFP	Red fluorescence protein
RG	Radial glial cell
RNA	Ribonucleic acid
rRNA	Risbosomal RNA
RQ	Relative quantification
rs + number	Reference single nucleotide polymorphism identification number
RTA	Realtime analysis
RT-PCR	Reverse transcription PCR
SCG10	Superior cervical ganglion-10 protein
SCKL	Seckl Syndrome
SD	Standard deviation
Ser	Serine
siRNA	Small interfering ribonucleic acid
SDS-PAGE	Sodium dodecyl sulfate polyacrylamide gel electrophoresis
SE (buffer)	Sodium EDTA
sec	Seconds
SCKL	Seckel syndrome
SNP	Short neural precursors
SNP	Single nuclear polymorphism
SP	Subplate
SSC (buffer)	Saline-sodium citrate
STIL	SCL/TAL1 interrupting locus
STR	Small tandem repeat
SV2	Synaptic vesicle glycoprotein 2
SVZ	Subventricular zone
T	Threonine (amino acid)
T	Thyrosine (nucleotide)
t_0-t_4	Timepoint 1-4
TBST	Tris-buffered saline containing Tween-20
TE (buffer)	Tris-EDTA

Thr	Threonine
UCSC browser	University of California Sana Cruz genome browser
UTR	Untranslated region
Val	Valine
VZ	Ventricular zone
vRG	Ventricular radial glial cell
WDFY3	WD Repeat And FYVE Domain Containing 3 (=ALFY)
WDR	WD-repeat
WES	Whole exome sequencing
WT	Wildtype
ZNF335	Zink finger protein 335

Zusammenfassung

Die Entwicklung des menschlichen Gehirns wird durch die Abfolge hochregulierter Prozesse gewährleistet. Bereits geringe Abweichungen können schwere neurologische Entwicklungsschäden zur Folge haben. Im Zuge dieser Arbeit wurden zwei konsanguine Familien mit autosomal rezessiven neurologischen Erkrankungen untersucht. Während Patienten aus der einen Familie mit einem bekannten Krankheitsbild diagnostiziert wurden (autosomal rezessive primäre Mikrocephalie [MCPH]), zeigten die Betroffenen aus der zweiten Familie eine bis dato unbekannte syndromale Form einer mentalen Entwicklungsstörung mit Balkenagenesie. Aufgrund des konsanguinen Familienhintergrunds ist die Wahrscheinlichkeit einer Homozygotie des betroffenen Allels bei autosomal rezessiven Erkrankungen stark erhöht. Mit Hilfe eines SNP-Arrays war es uns möglich zwei neue homozygote Loci auf Chromosom 1 für die besagten Erkrankungen zu identifizieren. Durch nachfolgende Sanger Sequenzierung und Next Generation Sequencing konnten die potentiell kausalen Mutationen entdeckt werden. Im bis dato unbekannten MCPH14 Lokus auf Chromosom 1p21.3-p13.1 wurde bei allen Betroffenen der Familie die homozygote Fehlsinn-Mutation (c.185T>C) in der hoch-konservierten PISA-Domäne des hsSAS-6 Proteins nachgewiesen. SAS-6 ist ein essentieller Faktor für die Generierung der Prozentriole. Über Knock-down und Co-Lokalisierungsstudien in U2OS Zellen, war es uns möglich eine durch die Mutation induzierte Häufung an monopolaren Spindeln, als auch einen Anstieg der Zellen mit weniger als 4 Zentriolen nachzuweisen. Die Anzahl der letztendlich im Gehirn vorhandenen Neuronen wird durch die Etablierung eines ausreichend großen Pools an neuronalen Stammzellen bestimmt. Unsere Ergebnisse zeigen jedoch, dass die Zellteilung durch die Mutation zum Teil gestört ist, was einen möglichen Pathomechanismus bei der Entstehung einer primären Mikrozephalie darstellt. Durch molekulargenetische Untersuchungen des homozygoten Bereichs auf Chromosom 1p36.31-p36.21 konnten wir in der zweiten Familie eine Splice-site Mutation (c.5270+2T>G) im C-Terminus der β-Isoform des *Kif1b* Gens als potentiell kausale Mutation identifizieren. Durch den Verlust dieser Splice Donor Stelle kommt es zum „skipping“ des vorletzten Exons und einem nachfolgenden Frameshift in der restlichen Sequenz von Kif1Bβ. Kif1B

gehört zur Familie der Kinesin-3 Proteine und ist für den Transport von Vorläufern von synaptischen Vesikeln verantwortlich. Im Zuge dieser Arbeit gelang es uns zu beweisen, dass durch den partiellen Verlust der PH-Domäne, welche für die Vesikelinteraktion notwendig ist, die Lokalisation von Kif1Bβ in der Zelle verändert und eine Interaktion mit $p75^{NTR}$ Vesikeln nicht mehr möglich ist. Es konnte somit ein eindeutiger Funktionsverlust des mutierten Kif1Bβ Proteins nachgewiesen werden. Mit unseren funktionellen Studien konnte die Bedeutung von Kif1B während der Entwicklung des zentralen Nervensystems nachgewiesen werden.

Abstract

Normal corticogenesis is guaranteed by a sequence of tightly regulated processes and interruption of any of these can eventually lead to the development of severe neurological disorders. In this thesis, two consanguineous families with autosomal recessive primary microcephaly (MCPH) and a novel, autosomal recessive syndromal form of intellectual disability with agenesis of the corpus callosum are described. Such rare autosomal recessive diseases occur more frequently in consanguineous families, since the likelihood of inheriting two of the diseased alleles is strongly increased. By homozygosity mapping, we identified potential candidate loci on chromosome 1p21.3-p13.1 in the MCPH family, and on chromosome 1p36.31-p36.21 in the family with the syndromal form of mental disability. By Next Generation Sequencing and Sanger Sequencing, we identified mutations in two novel genes for each disease. For the novel MCPH14 locus, a single missense mutation (c.185T>C), located in a highly conserved domain of the *hsSASS-6* gene, was found. This gene encodes for a protein required for procentriole formation. By performing a variety of knock-down and co-localization studies, we were able to prove the reduced function of the mutated protein, depicted by the higher incidence of monopolar spindles in U2OS cells, as well as the increased amount of cells with less than 4 centrioles. Since cell divisions in neuronal stem cells are essential for establishing a sufficient pool of progenitors, we suggest that this malfunction of hsSAS-6 has led to the described disease phenotype. In the second family with the novel syndrome, we discovered a splice site mutation (c.5270+2T>G) in the β-isoform of *Kif1b* resulting in skipping of the second to last exon and a thus induced frameshift in the remaining gene sequence. Kif1B is a kinesin-3 member highly important for the transport of synaptic vesicle precursors. Here we show that the partial loss of the vesicle-interacting PH-domain induced by the alternative splicing, alters the cellular localization of Kif1Bβ and completely abrogates the co-localization with $p75^{NTR}$-containing vesicles. As many previous studies have proven the need for Kif1Bβ in neuronal outgrowth, our discoveries confirm the importance of Kif1Bβ during embryonic brain development.

1. Introduction

Although the human brain is not the largest across mammalian species, it is said to be the most complex with the highest level of intelligence (Borrell, Calegari 2014). With a total number of around 170 billion cells (half neurons / half glial cells) and weighing approximately 1,5kg it is larger than would be expected for the average human body mass (Andrade-Moraes, Oliveira-Pinto et al. 2013). Hence, a highly sophisticated gyrification system is required to densely pack all the neurons in a 1320-1500cm^3 sized skull (Luders, Steinmetz et al. 2002, Mota, Herculano-Houzel 2015). This small volume is essential, as giving birth to babies with larger brain circumferences would have otherwise been impossible in times before C-section (Stiles, Jernigan 2010). Generally considered as the control center of our body, the brain harbors together with the spinal cord the central nervous system (CNS), one of the two main parts of the nervous system. It receives and processes all information coming in from the body itself as well as external. The second part, the so called 'peripheral nervous system' (PNS), consists of all nerves in the remaining body, connecting the peripheral regions with the CNS (Garzorz 2009). Thus, in order to guarantee constant and flawless neuronal signal transduction it is of essential, that the neuronal system remains functional throughout our life. Due to its highly complex architecture and several tightly regulated developmental steps, it is also prone to severe disorders (Silbereis, Pochareddy et al. 2016). The 'National Institute of Neurological Disorders and Stroke' provides a list of 447 known neurological disorders and syndromes, potential treatment options, prognosis and current clinical trials (National Institute of Neurological Disorders and Stroke 2017).

In the course of a larger ongoing disease gene-identification project we characterized numerous families with complex neurological disorders. For the majority of families, known disease genes were found to be causative during the screening process. However, in two consanguineous families from Pakistan and Austria (latter one with Turkish background) with autosomal recessive brain disorders, namely 'autosomal recessive primary microcephaly' (MCPH) and a novel, previously undescribed syndromal form of intellectual disability that will be hereafter referred to as 'autosomal recessive syndromal intellectual disability with agenesis of the corpus callosum' (IDACC), we were able to identify two novel candidate genes.

However, in order to fully understand these disorders, it is important to gain an overview of how the brain develops.

1.1 Development of the neocortex

Neuronal development in the embryo is initiated by the emergence of neural stem cells (NSC) during gastrulation in the 3rd gestational week (Stiles, Jernigan 2010, Gotz, Huttner 2005). They are located in the ectoderm of the developing embryo and are often referred to as 'neuroepithelial cells' (NE) (Stiles, Jernigan 2010). The final number of neurons, oligodendrocytes and astrocytes in the brain is already determined at this stage. This requires the production of a large enough pool of progenitor cells by generating identical NSC clones through symmetric cell divisions (Homem, Repic et al. 2015, Gotz, Huttner 2005). Around E20 (embryonic day), the neuroepithelial cells can be found aligned to both sides of the neuronal plate which starts to fold inwards due to expansion of the progenitor cells, eventually forming the neuronal tube (Stiles, Jernigan 2010, Sun, Hevner 2014). Upon completion, NEs have moved to the hollow center of the neuronal tube aligning as a single cellular layer along the anlage of the future ventricular system. This so called 'ventricular zone' (VZ) is the apical layer of the future cerebral cortex (Stiles, Jernigan 2010, Homem, Repic et al. 2015). Neuroepithelial cells are attached to both, the basal lamina and the apical surface of the VZ, having a highly apical-basal polarity (Gotz, Huttner 2005, Laguesse, Peyre et al. 2015). Due to the active nuclear movement (interkinetic migration, IKM) in the cytoplasm of NEs throughout the cell cycle, the layer exhibits a so called 'pseudostratified' character, allowing a high number of neuronal stem cells to accumulate in the VZ (Dehay, Kennedy 2007, Florio, Huttner 2014, Gotz, Huttner 2005, Takahashi, Nowakowski et al. 1993).

When the neuronal tube expands along the rostro-caudal axis, it starts to form the three primary brain vesicles, developing later into the fore-, mid-, and hindbrain (pros-, mes- and rhombencephalon, respectively), while the posterior region gives rise to the anlage of the spinal cord. The forebrain segment will further divide into the tel- and diencephalon, while met- and myelencephalon are derived from a subdivision of the rhombencephalon (Silbereis, Pochareddy et al. 2016, Stiles, Jernigan 2010). The cleavage of the prosencephalon around gestational week (GW) 5-6 also gives rise to the paired optic vesicles, the olfactory bulbs and the 2

hemispheres of the brain (Volpe 2000). When the neuronal tube closes around E30, the fluid pressure in the ventricles increases and the brain starts to expand rapidly (Budday, Steinmann et al. 2015). Eventually, during the continuous corticogenesis, a 6-layered cortex will be established (Mountcastle 1997).

1.2 Neuronal stem cells in the fetal brain

Once at the neuronal tube, neurogenesis starts (around E42) and division of NEs switches gradually from symmetric to asymmetric (Stiles, Jernigan 2010). To ensure asymmetric divisions, the radially orientated cleavage plane from NEs has to tilt, resulting in a slightly oblique or horizontal position (Laguesse, Peyre et al. 2015, Gotz, Huttner 2005). This so called 'neurogenic' division will eventually give rise to one identical progenitor cell and one radial glial cell (RG) or other kinds of progenitor cells, such as intermediate progenitor cells (IP) (Gao, Postiglione et al. 2014, Homem, Repic et al. 2015). RGs are a more specialized type of progenitor cells with features similar to NEs but lack tight junctions and start to express astroglial markers, such as GFAP or PAX6 (therefore they are often instead referred to as 'radial glial progenitor' cells) (Malatesta, Hartfuss et al. 2000, Gotz, Huttner 2005, Lui, Hansen et al. 2011). Their divisions are now both, neurogenic (asymmetric) and proliferative (symmetric) (Gotz, Huttner 2005, Gao, Postiglione et al. 2014). In contrast to NEs, interkinetic migration in RGs is now restricted to the part of the cell located in the ventricular and the above located subventricular zone, but not to the more basal areas (Gotz, Huttner 2005). While those RGs that reside within the VZ (vRG) remain attached to both, the lower apical and upper pial surface, throughout the cell cycle and continue proliferating at the ventricular zone (Noctor, Flint et al. 2001), outer radial glial cells (oRG) migrate into a more superficial layer, the outer subventricular zone (oSVZ), where the apical connections are lost (Lui, Hansen et al. 2011). This latter RG type is generated during asymmetric, self-renewing mitotic divisions of vRGs due to the shift from vertical to horizontal cleavage plane orientation. While the daughter cells inherit the basal processes and exit the VZ to become oRGs (also called 'basal radial glial cells' (Ronan, Fletcher 2015, Florio, Huttner 2014)), the daughter vRGs retain the ventricular processes and start to re-grow new pial processes (LaMonica, Lui et al. 2013, Hansen, Lui et al. 2010). It is to note that oRGs are highly abundant in the developing human but not in the rodent

neocortex. This raises the assumption that they could perhaps be responsible for certain neuronal diseases only found in humans but not in rodents (Ostrem, Lui et al. 2014).

In order to invade higher cortical areas upon mitotic divisions, oRGs use so called 'mitotic somal translocations' (MST) (Noctor, Flint et al. 2001). In contrast to the nuclear movements during interkinetic migration, a cell undergoing MST starts to retract its cell body by ascending it upwards shortly before cytokinesis (Ostrem, Lui et al. 2014, Hansen, Lui et al. 2010, Noctor, Flint et al. 2001). This trajectory is seen more frequently in humans than in mice who have a significantly smaller oSVZ. Therefore it has been suggested that MST contributes to the expansion of the oSVZ by pushing the border aligning the subplate more outwards (Ostrem, Lui et al. 2014).

A recent study in mice showed that RGs can only transiently self-renew, giving rise to a defined number of neurons during neurogenesis (Gao, Postiglione et al. 2014). In humans, however, one single oRG has the capability to produce around 800 glial, deep and upper layer neuronal progeny during the peak phase of cortical development (Pollen, Nowakowski et al. 2015), which is up to 100 times more than observed for murine RGs (Gao, Postiglione et al. 2014). Apart from their neurogenic features, RGs also serve as a scaffold for their neuronal offspring helping them to translocate into more superficial areas (Noctor, Flint et al. 2001, Lui, Hansen et al. 2011). Interestingly, in earlier stages of neurogenesis RGs tend to directly differentiate into neurons than in later stages where the number of IP daughter cells increases (Jabaudon 2017). While neurons move to more cortical areas in an inside-out manner (later born neurons are found in more superficial layers than earlier neurons) (Hevner, Daza et al. 2003), IPs start to establish the SVZ (Lui, Hansen et al. 2011). By week 27 the VZ has disappeared and is replaced by a single-cell layer of ependymal cells making the SVZ the major cortical site of progenitor and neuron production (Zecevic, Hu et al. 2011, Zecevic, Chen et al. 2005, Raybaud, Ahmad et al. 2013). It is to note that although IPs are mono to multipolar and divide mostly basally (Pontious, Kowalczyk et al. 2008), they are not attached to either surface (Shitamukai, Matsuzaki 2012). They proliferate symmetrically a few more times (1-3) before they terminally divide into a pair of neurons (Pontious, Kowalczyk et al. 2008, Noctor, Martinez-Cerdeno et al. 2004). IPs are present throughout cortical development, and eventually, differentiate into neurons from all layers, but their progeny are more prevalent in more superficial layers (Kowalczyk, Pontious et al.

2009, Vasistha, Garcia-Moreno et al. 2015). Moreover, it has been shown that every type of projections neuron can be derived from IP progenitors (Mihalas, Elsen et al. 2016) .

In addition to the above mentioned cells, another type of progenitor derived from radial glial cells has been found in the murine brain, so called short neural precursors (SNP) (Gal, Morozov et al. 2006). Together with vRGs they are located in the ventricular zone, giving, like RGs, rise to either stellate or pyramidal neurons that immediately leave the VZ after birth (Stancik, Navarro-Quiroga et al. 2010, Tyler, Haydar 2013). Compared to RGs SNPs undergo only one terminal division (Tyler, Haydar 2013). Therefore, the amount of their neuronal output is much lower. SNP-derived neurons contribute to the establishment of lower cortical layers (studies in mice mapped its localization to layer IV) while neurons derived from RGs rather translocate to upper-layer II/III (Stancik, Navarro-Quiroga et al. 2010). Since both secondary progenitors are derived from radial glial cells, SNPs were renamed 'apical intermediate progenitors' (aIP) and IPs in the SVZ were called 'basal intermediate progenitors' (bIP). However, Tyler et al highlighted that aIPs are an independent subtype of progenitor cells (Tyler, Haydar 2013).

Although neurogenesis completes around GW21, postnatal differentiation and migration of progenitor cells will continue to a certain degree (Stiles, Jernigan 2010).

1.3 Neuronal establishment of the cortex

During neurogenesis two main types of neurons are generated: inhibitory interneurons and excitatory glutamatergic projection neurons (Kwan, Sestan et al. 2012, Florio, Huttner 2014). Excitatory neurons are further divided into pyramidal projection and spiny stellate interneurons, both using glutamate as their neurotransmitter (Kwan, Sestan et al. 2012, Markram, Toledo-Rodriguez et al. 2004). The inhibitory interneuronal neurotransmitter γ-aminobutyric-acid (GABA) is a derivate of the excitatory neurotransmitter, synthesized by decarboxylation of glutamate (National Institute of Neurological Disorders and Stroke 2017).

Pyramidal neurons owe their name to their triangle shaped soma and make up to 80% of all neurons in the neocortex (Kwan, Sestan et al. 2012, National Institute of Neurological Disorders and Stroke 2017). While projection neurons have their origin in the neocortex, interneurons are mainly produced in a thelencephalic area called

ganglionic eminence (GE), but can also be detected in SVZ of the cortex or in the subpial granular layer starting from mid-term (Zecevic, Hu et al. 2011). Their radial glial progenitors can be distinguished by the expression of *Pax6* and *Emx1* (neocortical progenitors) and *Gsx1*, *Gsx2* and *Olig2* (telencephalic progenitors) (Tan, Shi 2013). In contrast to interneurons that interact with more local sites, projection neurons have long axons enabling them to intervene far distant areas (Hevner, Daza et al. 2003). Upon birth, projection neurons start to move upwards to establish the neocortex, the thin, gray layer on the surface of the brain (Stiles, Jernigan 2010). Interestingly, newborn neurons do not directly translocate to their final destination. They rather rest for another 24 hours in the SVZ in a multipolar state before the majority of neuronal progeny becomes again bipolar, reverses their direction and extends their fibers back towards the ventricle. Only after touching and moving closer to the apical membrane, they eventually ascend to the cortical plate. About one third of all post-mitotic neurons however skip retrograde migration but do remain in the SVZ for 24h before their final translocation (Noctor, Martinez-Cerdeno et al. 2004). In contrast to the radial migration of excitatory glutamatergic neurons, inhibitory GABAergic neurons invade the cortex tangentially from the GE (Dwyer, Chen et al. 2016, Budday, Steinmann et al. 2015). Once there, they also switch to a radial migration mode and translocate to their final cortical layer (Zechel, Nakagawa et al. 2016).

The very first neurons to be found in the early phase of neurogenesis are Cajal-Retzius cells. Cajal Retzius cells produce reelin, an important factor controlling the right positioning, branching and growth of newborn neurons in the developing cortical plate (Stiles, Jernigan 2010, Olson 2014). It is to note that reelin as a marker for Caja Retzius cells is only applicable until birth, as after birth reelin is additionally produced by cortical interneurons (Hevner, Daza et al. 2003).

Together with the subplate neurons, Cajal Retzius cells establish the preplate (PP) right above the VZ (Toma, Hanashima 2015). The preplate harbors early born cells that either only have a transient function and die or become cortical or subcortical inhibitory neurons (Budday, Steinmann et al. 2015). While underneath the intermediate and subventricular zones arise (first detectable in GW9), which start to produce pyramidal projection neurons, an event called ‘preplate splitting’ initiates the formation of a well-organized cortical plate that divides the PP into the marginal zone (MZ) and the subplate (SP) around GW8 (Zecevic, Chen et al. 2005, Olson

2014, O'Dell, Cameron et al. 2015). Induced by the dendritic outgrowth of later layer VI neurons, the event itself is of significant importance for proper brain development (Olson 2014). Eventually, the marginal zone will later transform into layer I. The subplate, however, is only a transient layer important for axon guidance and connecting intra- and extracortical areas (Hoerder-Suabedissen, Molnar 2015, Perkins, Hughes et al. 2008, Kwan, Sestan et al. 2012). By week 28 it has reached its maximum size before it starts to degrade around GW35 and will be undetectable by the age of 6 months (Hoerder-Suabedissen, Molnar 2015, Raybaud, Ahmad et al. 2013). The cortical plate will expand until gestational week 18 when finally well-defined layers I-VI have been formed (Budday, Steinmann et al. 2015). The layers are divided in two subgroups: Layer V and VI are known as the subgranular or deep layers (Kwan, Sestan et al. 2012) whereas layers II-IV represent the upper or superficial layers (Gao, Postiglione et al. 2014). In contrast to the deep layer, neurons that can also target subcortical regions such as the thalamus (corticothalamic neurons: mainly layer VI and to a certain extent also layer V neurons), the brain stem and the spinal cord (subcerebral projection neurons are layer V neurons), connections of neurons of the superficial layers are restricted to cortical areas (Gerfen, Economo et al. 2016, Molyneaux, Arlotta et al. 2007).

During establishment of the cortex another important cell type is produced, namely glial cells, including astrocytes, oligodendrocytes and microglial cells (Budday, Steinmann et al. 2015). Differentiation of astrocytes is induced around E108 when radial glia cells switch from neurogenesis to gliogenesis (Stiles, Jernigan 2010, Raybaud, Ahmad et al. 2013). In the postnatal human brain, astrocytes are the most abundant cell type and play a primary role in neuronal synapse formation as well as in controlling their function (Clarke, Barres 2013). Oligodendrocyte progenitor development starts much earlier, around GW 10-15 but they do not become mature oligodendrocytes until GW30 (Raybaud, Ahmad et al. 2013, Budday, Steinmann et al. 2015). They ensure rapid impulse conduction by forming insulating myelin sheets around axons of neurons (Peferoen, Kipp et al. 2014). It is to note that the generation of oligodendrocytes will continue after birth until the age of 9 (Yeung, Zdunek et al. 2014). In contrast to astro- and oligodendrocytes which are derived from radial glial cells, microglial cell originate from yolk sac macrophages that invade the brain and spinal cord anlagen concomitantly with or shortly before the development of the

blood-brain-barrier and serve as the CNS' innate immune system (Waisman, Ginhoux et al. 2015).

Almost simultaneously with the start of gliogenesis and the increasing tangential expansion of the cortex another important developmental step is induced (Yoshida, Ishizu et al. 2017). Due to the constant division, differentiation, migration and axon branching of cells and the concurrent limited space in the scull, around GW 20-21 the cortex starts to fold itself resulting in its typical wrinkled architecture composed of gyri and sulci (Sun, Hevner 2014, Bayly, Taber et al. 2014, Raybaud, Ahmad et al. 2013). They are built in 3 waves, establishing primary (evident around GW31), secondary (mainly present around GW 27) and tertiary sulci, which evolve together with some secondary sulci until after term (Raybaud, Ahmad et al. 2013). While in humans the primary folds are more or less the same, the latter two do vary (Yoshida, Ishizu et al. 2017, Holland, Miller et al. 2015).

Eventually, the intermediate zone will transform into the white matter, harboring mostly long axons wrapped with myelin, responsible for its characteristic white appearance (Tallinen, Chung et al. 2014, Raybaud, Ahmad et al. 2013, Stiles, Jernigan 2010). The neocortex, on the other hand, contains the cell bodies of neurons and therefore appears gray (Stiles, Jernigan 2010) (for easier understanding, see Figure 1).

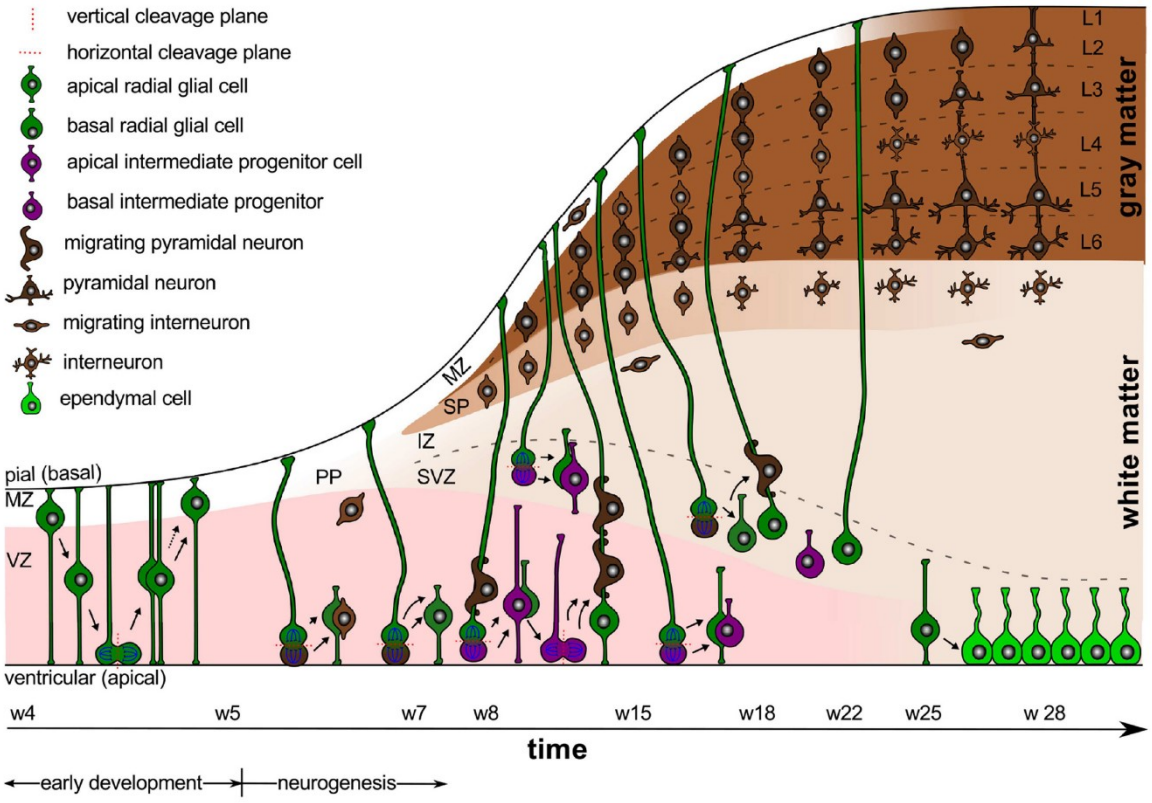

Figure 1: Early human cortical brain development. Initially, progenitors divide symmetrically at the apical surface, thereby increasing their population. Around gestational week 6 neurogenesis starts and asymmetric divisions increase. Over the next couple of weeks the subventricular zone (SVZ), the intermediate zone (IZ), the subplate (SP) and the well-organized 6 layers of the cortical plate are formed. MZ= marginal zone; VZ= ventricular zone; PP= preplate. Figure taken from (Budday, Steinmann et al. 2015) according to the terms of usage of 'Frontiers in cellular neuroscience'.

1.4 Autosomal recessive primary microcephaly

Autosomal recessive primary microcephaly (MCPH) is a rare heterogeneous developmental disease affecting approximately 1 in 1-2 million people. This number decreases to 1:10.000 in the consanguineous population (Woods, Bond et al. 2005). In general, primary microcephaly is diagnosed if the head circumference is 3-4 standard deviations (SD) below the mean centile of a given sex at birth (Roberts, Hampshire et al. 2002, Barbelanne, Tsang 2014). While patients generally exhibit mild to moderate intellectual disability, other features such as short stature or seizures can be present, but are not defined as diagnostic criteria (Barbelanne, Tsang 2014). Anatomically, the degree of gyrification is significantly reduced,

associated with a thinner than normal cortex but no other brain malformations. To date, 18 MCPH loci and the corresponding genes have been identified (see Table 1)

Table 1: Primary microcephaly genes

Locus	Gene	Chrom. location (hg38)	Inheritance mode	Gene function	Phenotype	Gene first published
MCPH1	*MCPH1*	8p23.1	AR	Responsible for chromosome condensation and decondensation. Regulates *cdk1* activation and thus the entry into mitosis. Late neurogenesis and symmetric cell divisions are negatively affected upon knock-down (Gruber, Zhou et al. 2011)	Mild- to moderate intellectual disability, microcephaly	(Jackson, Eastwood et al. 2002)
MCPH2	*WDR62*	19q13.12	AR	Expressed in ventricular and subventricular zone. Assembles kinetochore microtubules to control mitotic spindle orientation (Miyamoto, Akutsu et al. 2017)	Microcephaly, intellectual disability, thickened cortex, no boarder between white and gray matter, pachygyria, polymicrogyria, lissencephaly, schizencephaly, subcortical heterotopia, brainstem atrophy, abnormal corpus callosum, cerebellar hypoplasia, seizures	(Yu, Mochida et al. 2010, Bilguvar, Ozturk et al. 2010)
MCPH3	*CDK5RAP2*	9q33.2	AR	Controls orientation of mitotic spindles in neuronal progenitors and *Cdk5rap2* knockout cells show premature cell cycle exit (Pagnamenta, Murray	Microcephaly with sensorineural deafness (Pagnamenta, Murray et al.	(Bond, Roberts et al. 2005)

				et al. 2012, Lizarraga, Margossian et al. 2010, Barrera, Kao et al. 2010)	2012). Knockout animals show thinner superficial cortical layers (Lizarraga, Margossian et al. 2010)	
MCPH4	*CASC5*	15q15.1	AR	Expressed in the ventricular zone. Controls segregation of sister chromatids by directing the kinetochore to the microtubule. Controls spindle assembly checkpoint signaling (Caldas, DeLuca 2014, Genin, Desir et al. 2012)	Microcephaly with simplified gyri	(Genin, Desir et al. 2012)
MCPH5	*ASPM*	1q31.3	AR	Controls spindle pole position in neuroepithelial cell to ensure correct mitotic cleavage plane orientation (Fish, Kosodo et al. 2006, Bond, Roberts et al. 2002)	Microcephaly with simplified gyral patterns, short growth (Abdel-Hamid, Ismail et al. 2016)	(Bond, Roberts et al. 2002)
MCPH6	*CENPJ*	13q12.12 -q12.13	AR	Strong expression in neuroepithelial cells. Required for centriole formation (Kohlmaier, Loncarek et al. 2009)	Microcephaly with intellectual disability, seizures, joint stiffness (Darvish, Esmaeeli-Nieh et al. 2010)	(Bond, Roberts et al. 2005)
MCPH7	*STIL*	1p33	AR	Found at spindle poles during metaphase. Required for centriole assembly and duplication (Vulprecht, David et al. 2012)	Microcephaly with intellectual disability, short stature, ataxia, seizure (Darvish, Esmaeeli-Nieh et al. 2010)	(Kumar, Girimaji et al. 2009)
MCPH8	*CEP135*	4q12	AR	Important for procentriole formation and regulates mitotic spindle assembly (Y. C. Lin, Chang et al. 2013)	Microcephaly with intellectual disability, speech problems	(Hussain, Baig et al. 2013)
MCPH9	*CEP152*	15q21.1	AR	Expressed in ventricular zone, important for centriole duplication. Assists in recruiting of	Microcephaly with simplified gyri, mild cognitive	(Guernsey, Jiang et al. 2010)

				pericentriolar material (Firat-Karalar, Rauniyar et al. 2014)	impairment, mirror movements, aggressive, impulsive, tics, obsessive and compulsive traits, jerky movements, tics	
MCPH10	*ZNF335*	2q13.12	AR	Interacts with H3K4 chromatin methyltransferase complex to regulate methylation and thus the expression of genes important for brain development. Essential for neuronal progenitor proliferation and neuronal differentiation. Loss of *ZNF335* results in depletion of mitotic cells due to premature neuronal fate determination.	Most severe form of microcephaly with extremely simplified gyral pattern, skull larger than cerebral cortex, high amount of subarachnoid fluid, thinned cerebral cortex with neuronal disorganization, only low percentage of normal 6-layered cortical areas, barely no pyramidal neurons, abnormal cerebellum and Purkinje cell layer. Death within a few months after birth	(Yang, Baltus et al. 2012)
MCPH11	*PHC1*	12p13.31	AR	Part of PRC1 complex, which ubiquitinates histone H2A. Important for DNA damage repair.	Microcephaly with normal brain architecture and slightly lower IQ	(Awad, Al-Dosari et al. 2013)
MCPH12	*CDK6*	7q21.2	AR	Expressed in apical progenitor cells. Localizes around nucleus and the centrosome. Knockdown results in reduction in cell proliferation, disorganized spindles and microtubules, abnormal nuclei and an	Microcephaly with simplified gyral pattern, sloping forehead, mild intellectual disability	(Hussain, Baig et al. 2013)

				increase in the number of centrosomes.		
MCPH13	*CENPE*	4q24	AR	Dimeric kinesin that captures microtubules to kinetochore.	Microcephaly, micrognathia, sloping forehead, simplified gyri, thinned cortex, cerebellar hypoplasia severe intellectual disability, little to no language, short stature, small hand and feet, seizures, increased tone, cardiac problems, developmental delay of motor skills	(Mirzaa, Vitre et al. 2014)
MCPH14	*SASS6*	1p21.2	AR	Essential for procentriole formation	Microcephaly with severe intellectual disability, poorly defined basal ganglia, internal capsule was not delineated, hypoplasia of vermis cerebelli, abnormal frontal convexity , attention problems, aggressive, little speech, reading disability, seizures	(Khan, Rupp et al. 2014) reported in detail in this thesis
MCPH15	*MFSD2A*	1p34.2	AR	Essential for omega-3 fatty acid docosahexaenoic acid (DHA) uptake in blood- brain epithelium. Transports DHA in form of lysophosphatidylcholine (LPC) through the blood-brain barrier.	Microcephaly with intellectual disability and developmental delay, normal gyral pattern, dilated ventricles, cerebellar	(Alakbarzade , Hameed et al. 2015, Guemez-Gamboa, Nguyen et al. 2015)

					hypoplasia, thinned corpus callosum, hypoplastic brainstem, loss of white matter in posterior regions,spastic gait, some have talopes eqinovarus, limited to no speech, pulmonary insufficiency and dysphagia, spastic quadriparesis, lethal in case of inactivating mutation	
MCPH16	*ANKLE2*	12q24.33	AR	Important for neuroblast production. Mutations do not affect mitotic spindle orientation, centriole formation or centriole number but has a negative impact on cell proliferation. Important for nuclear envelope reassembly after cell division (Kaufmann, Kukolj et al. 2016).	Extremely sloping forehead, enlarged extra axial space, extremely reduced gyrification, agenesis of the corpus callosum, ptosis, slightly thicker cortex, small jaw, hyper- and hypopigmented macules, spastic quadriplegia, anemia, glaucoma, seizures	(Yamamoto, Jaiswal et al. 2014)
MCPH17	*CIT*	12q24.23	AR	Localized at central spindle and cleavage furrow. Interacts with KIF14 to promote chromosome segregation during cytokinesis	Microcephaly with mild-to-moderate intellectual disability, simplified gyral pattern, extra-	(Basit, Al-Harbi et al. 2016)

				(Gruneberg, Neef et al. 2006).	axial space enlarged	
MCPH18	*ALFY/ WDFY3*	4q21.23	AD	Autophagy mediating scaffold protein that controls neuronal progenitor differentiation.	Microcephaly with mild-to-moderate intellectual disability	(Kadir, Harel et al. 2016)
MCPH19	*Kif14*	1q32.1	AR	Interacts with CIT to promote cytokinesis (Gruneberg, Neef et al. 2006).	Reduced cortex with simplified gyral pattern, enlarged lateral ventricles, sloping forehead and moderate to severe intellectual disability, impaired speech, spastic tetraparesis, total agenesis of corpus callosum, thicker cortex, small kidneys	(Moawia, Shaheen et al. 2017)

AR=autosomal recessive; AD=autosomal dominant

Sir et al. (Sir, Barr et al. 2011) found that another centrosomal gene, *CEP63*, is mutated in primary microcephaly patients. Due to the accompanied growth retardation seen in patients, the *CEP63* locus was listed in OMIM as being causative for Seckel Syndrome-6 (OMIM 614728) even though the authors remained unclear about the categorization. This, however, questions the above listed MCPH loci and whether all truly account for primary microcephaly, since dwarfism and growth retardation were also reported for some MCPH genes. The initial classification of MCPH defining it as a birth defect characterized by a smaller head and simplified gyri but no other brain abnormalities (Woods, Bond et al. 2005) does not match with all known MCPH types. In the end only seven MCPH types fulfill these requirements, while the rest display additional syndromal phenotypes and/or brain abnormalities. Some genes are even listed for both Seckel syndrome and autosomal recessive primary microcephaly, such as *CENPJ* (MCPH6 and SCKL4), *CEP152* (MCPH9 and SCKL5) and *PHC1* (MCPH11 – has no SCKL locus entry, but the phenotype has not been classified). However, the clinical spectrum for MCPH has widened and now

includes seizures, slight growth retardations (up to -3SD), mild spasticity as well as hypoplasia of the cerebellum and hindbrain (Verloes, Drunat et al. 1993).
An interesting aspect of microcephaly genes is that most of them play an essential role during cell division and cell cycle progression. As already discussed in detail in chapter 1.2, a large enough neuronal progenitor pool has to be generated via symmetric cell divisions before neurogenesis takes place. A premature switch from vertical to horizontal division plane orientation during mitosis can prevent the establishment of the adequately sized neuronal stem cell pool and leads to premature neuronal differentiations (Homem, Repic et al. 2015). The recent epidemic Zika virus outbreak on the American continent depicts an elegant example which highlights the importance of an undisturbed symmetric progenitor division. This Arbovirus is transferred to humans via *Aedes* mosquitoes and causes symptoms such as fever, headache, painful joint movements, a skin rash, inflammation of the eyes and diarrhea within a few days (Javed, Manzoor et al. 2018). While it is not life-threatening for the general population, fetuses of infected pregnant women have an increased danger of developing microcephaly (Al-Qahtani, Nazir et al. 2016). Li et al. (C. Li, Xu et al. 2016) found that the virus targets only neuroepithelial cells, which divide at high rates in the developing brain of fetuses, thus suppressing further cell divisions and thereby leading to microcephaly in the embryo. This neurovirulent feature is untypical for the original wildtype strain and was only recently associated with a specific mutation (S139N) in the contemporary Cam/2010 virus (F. Zhang, Wang et al. 2017) exhibiting an enhanced replication rate in human neuronal progenitor cells, which is eventually responsible for an increase in neuronal apoptosis (Yuan, Huang et al. 2017). Furthermore, studies on brain organoids have provided proof of interference with centrosomal protein recruitment and shown that spindles in apical progenitor cells are tilted, thus inducing premature asymmetric divisions (Gabriel, Ramani et al. 2017).

1.5 Agenesis of the corpus callosum

While the left hemisphere of the brain is the center for language, which controls our speech and auditory perception, the right half of the brain is responsible for processing what we see and supports spatial awareness (Wolman 2012).

Connection of these two by sending axons via the corpus callosum to the opposite hemisphere enables us to develop higher cognitive skills (Edwards, Sherr et al. 2014). The corpus callosum (CC) is a large tract of commissural fibers comprised of around 200 million axons of excitatory and, to a lesser extent, inhibitory neurons that are vital for the integration of sensory and motor information, support the learning of languages, and have an impact on emotions and the development of social skills (Paul 2011, Bloom, Hynd 2005). It is the largest known structure of white matter only evident in placental mammals (van der Knaap, van der Ham 2011). However, the CC is not the only axonal connection between the two cerebral hemispheres. Beside this primary interhemispheric tract, anterior, posterior, habenular and hippocampal commissures also exist (Palmer, Mowat 2014, Bloom, Hynd 2005).

The earliest precursor of this connective bridge, the commissural plate, arises shortly after the prosencephalic cleavage in GW5-6 (Dobyns 1996, Achiron, Achiron 2001). Navigated by guidance- and repulsive molecules expressing glial cells in the midline, the first callosal pioneering axons from the cingulate cortex start to cross the midline around gestational week 13-14 (Edwards, Sherr et al. 2014, Ren, Anderson et al. 2006, Unni, Piper et al. 2012). It has been shown that the remaining axons of the CC then simply follow the pioneer axons through this glial zipper after they have finally made it to the other hemisphere (Klose, Bentley 1989, Kuwada 1986, Tovar-Moll, Moll et al. 2007). Although recent studies suggest a bidirectional development of the CC, enhanced growth of the anterior part is evident in the first weeks (Paul 2011). The corpus callosum as a structure can first be visualized around GW15, but its final structure is not manifested before GW17 (embryonic day 115) (H. Huang, Xue et al. 2009, Achiron, Achiron 2001). It mainly constitutes of axons of superficial layers II and III neurons, but harbors projection fibers from layer V and VI neurons as well (O'Leary, Koester 1993, Lavado, Ware et al. 2014). By term, the total amount of callosal axons is established, but due to pruning and myelination, the CC undergoes most of its maturation within the first 4 years of life. However, it will evolve until early adulthood before it starts to slightly decrease in size by the age of 40 (Luders, Thompson et al. 2010, Fitsiori, Nguyen et al. 2011). The mature CC consists of four different regions, starting in the front with the rostrum, followed by the genu, the body (anterior, posterior body and isthmus) and finally the splenium at the posterior end (Filippi, Cauley 2014). Studies on adult split-

brain patients that have undergone callosotomy to treat epileptic seizures have shed most light onto the function of the corpus callosum (Wolman 2012). Additionally, lesions in different callosal areas have helped to unravel regional callosal functions: among other abnormalities, injuries in the anterior sections of the CC impair movements and speech, while patients exhibiting posterior lesions have reading disabilities, but interestingly maintain writing skills (Filippi, Cauley 2014). Nevertheless, it has been suggested that subcortical commissures take over some integrative tasks after transection of the CC, which has to be kept in mind when studying the connective role of CC in these patients (Bloom, Hynd 2005).

In a few cases, the formation of the CC is disturbed during embryogenesis. There are four forms of aberrant callosal morphologies, including hypoplasia (thinner than usual CC), dysplasia (structurally malformed CC), hypoplasia with dysplasia and complete agenesis of the corpus callosum (ACC indicates a total absence of the CC) (Hanna, Marsh et al. 2011). The frequency of the latter can be as rare as 0.5-1 affected in 10.000 and increases to 2-2.3% in people with additional intellectual disabilities (Jeret, Serur et al. 1985, Fratelli, Papageorghiou et al. 2007). A list of syndromal and non-syndromal inherited diseases that are associated with ACC can be found in the 'Online Mendelian Inheritance in Man' Database (McKusick-Nathans Institute of Genetic Medicine, Johns Hopkins University (Baltimore, MD) 2012). Entering the term 'corpus callosum agenesis' will reveal 849 OMIM entries of syndromes associated with callosal abnormalities (, OMIM Clinical Synopsis Search - corpus callosum agenesis). In general, there are two types of ACC distinguished by the presence or absence of so-called 'Probst bundles'. These are longitudinal fibers, which have not crossed the midline and accumulate diffusely along the medial wall on their hemisphere of origin. In ACC patients lacking these Probst bundles, either the formation of commissural neurons or the extension of projecting axons is disturbed (Dobyns 1996, Schell-Apacik, Wagner et al. 2008). A recent study revealed that patients with Probst bundles actually exhibited significantly better social and adaptive functions (Al-Hashim, Blaser et al. 2016). Complete absence does not indicate a concurrent bad or worse neurodevelopmental outcome than in partial agenesis. Sotiriadis and Makrydimas (Sotiriadis, Makrydimas 2012) showed that children with prenatally diagnosed isolated ACC (partial and complete ACC without additional brain abnormalities) developed normally in 75% of cases with a favorable development in 80% in infants with complete ACC. Interestingly, in

their study partial ACC was associated with a slightly higher rate of severe outcome than observed for complete ACC. However, due to the small number of participating partial ACC patients with severe outcome, this finding was not statistically significant. In addition, the researchers noted that prognosis worsens with the parallel occurrence of other brain malformations.

Preterm delivery, viral infections, maternal phenylketonuria, alcohol abuse during pregnancy or genetic predispositions may contribute to developmental callosal abnormalities (Jo, Cho et al. 2012, Riley, Mattson et al. 1995, Schell-Apacik, Wagner et al. 2008, Paul, Brown et al. 2007). These factors can affect neuronal progenitor proliferation, neuronal faith, neuronal translocation, midline patterning, the formation of the two hemispheres as well as the extension, projection and navigation of axons to their target cells in the contralateral hemisphere (Edwards, Sherr et al. 2014). Interestingly, only 32-37% of ACC patients have an identifiable underlying genetic cause with 48% of them carrying mutations in single genes and 30% showing chromosomal aberrations. While the remaining 63-68% of ACC patients present with known clinical syndromes, these have as yet not been link to causative genes (Al-Hashim, Blaser et al. 2016, Schell-Apacik, Wagner et al. 2008). This indicates that the genetic testing for syndromal ACC remains challenging even in times of Next Generation Sequencing.

1.6 Consanguinity and the inheritance of rare diseases

As mentioned above, disturbance of any of these tightly regulated developmental steps during cortical development can lead to severe disorders. In the course of this dissertation I came across two of such rare developmental disorders, which have a major impact on the patients' architecture of the brain, their mental performance, social skills and behaviors.

In Europe, a disease is by definition considered as 'rare' if the probability of inheritance is 1:2000 (information taken from https://www.eurordis.org), while the US has set the threshold to less than 200.000 affected (information taken from National Institute of Health https://rarediseases.info.nih.gov). The majority of all known rare conditions (around 80%) is due to inherited genetic defects (Institute of Medicine (US) Committee on Accelerating Rare Diseases Research and Orphan Product Development 2010). Especially when it comes to consanguineous

marriages, the chance of giving birth to children suffering from extremely rare autosomal recessive traits increases significantly (A. Bittles 2001, Zlotogora 1997). In North African, Arab and some Western and Southern Asian countries, the rate of such marriages is above 20% and increases to over 50% in Pakistan and Sudan (A. H. Bittles, Black 2015). Despite the common knowledge that their genomes share a larger number of homologous regions, 1/3rd of all consanguineous couples are not aware of the fact that they thus face higher reproductive risks (Teeuw, Loukili et al. 2014). While it is rather difficult to find the causative gene in affected children of unrelated parents, children of consanguineous parents share blocks of homozygous (in this case called 'autozygous') regions, which are identical by decent (IBD). Thus, homozygosity mapping is the method of choice when it comes to identifying autosomal recessive disease loci in consanguineous families (Hildebrandt, Heeringa et al. 2009). The easy - and nowadays affordable - massive parallel sequencing of the target loci allows the detailed screening of all genes located in the filtered regions (Alkuraya 2010).

In this thesis two consanguineous families with inherited neurodevelopmental diseases were screened for the genetic cause of their autosomal recessive disorder. Applying a positional cloning strategy we were able to identify two novel disease-causing genes suspected to play a major role during brain development.

2. Material and Methods

Some passages have been quoted verbatim from the following source: '*A missense mutation in the PISA domain of HsSAS-6 causes autosomal recessive primary microcephaly in a large consanguineous Pakistani family'* published in Human Molecular Genetics (Khan, Rupp et al. 2014).

2.1 Sample collection

After obtaining informed consent, blood was collected into EDTA vacutainer tubes (BD Bioscience) from the two affected IDACC patients, the healthy brother of VI:1 and their parents. For the microcephaly family, blood was drawn from 3 affected patients, 7 healthy family members and 116 healthy Pakistani individuals. DNA was isolated according to our in-house desalting protocol. Briefly, whole blood was overlaid with 4-5 volumes of blood lysis buffer (16,58g NH_4Cl, 2g $KHCO_3$, 0,074g EDTA [all from Sigma] dissolved in 2l dH_2O) and incubated on ice for 30min followed by a second lysis step for another 10min in lysis buffer before the resulting pellet was subjected to protein digestion (5ml 1xSE buffer supplemented with 250µl of 20% SDS and 25µl of a 10mg/ml Proteinase K [Qiagen] stock) overnight at 37°C. The following day DNA was precipitated with 6M NaCl, washed with 100% EtOH and dissolved in 1xTE buffer.

For cDNA analysis, blood from both IDACC patients and MCPH patients V-3, IV-7 and two healthy controls was collected into PAXgene RNA blood tubes (PreAnalytiX) and RNA was isolated using PAXgene RNA Kit.

The study on the IDACC family was approved by the ethics committee of the Medical University of Graz (approval number 24-421 ex 11/12) and conducted according to the Declaration of Helsinki. The study on the MCPH family was approved by institutional ethical review boards of Gomal University, Dera Ismail Khan, and Quaid-i-Azam University, Islamabad, Pakistan.

2.2 Karyotyping

Metaphases of lymphoblastoid cells (see 2.10.1) were prepared according to our in-house protocol. Briefly, lymphoblastoid cells were resuspended in 10ml of fresh

media. 2ml were supplemented with 100µl of KaryoMAX Colcemid Solution (10µg/ml stock solution from Gibco, ThermoFisher) and incubated for 1h at 37°C and 5%CO_2. After 1h the remaining 8ml of cell suspension were added and incubated for another 30min at 37°C. Subsequently cells were pelleted at 2000rpm for 8min. The pellet was resuspended in 300µl supernatant and 5ml of pre-warmed 0,075M KCl (37°C) were added dropwise. Cells were left at 37°C for 20min and harvested at 1200rpm for 8min. The pellet was carefully resuspended in 300µl supernatant and ice-cold fixative (3:1 ratio of methanol:glacial acetic acid) was added dropwise. After adding a total of 5ml, cells were centrifuged (1200rpm, 8min) and washed for three more times with fixative solution. Eventually, cells were resuspended in fixative and dropped from about 20cm on pre-cooled glass-slides which were stored in H_2O. Slides were dried and aged for 2 days at room temperature before they were transferred into SSC-buffer (35,06g NaCl, 17,648g tri-sodium citrate dehydrate in 2L H_2O) and 60°C for 7h. Subsequently, they were transferred into 4% Giemsa solution for 8 min and rinsed with water afterwards. Slides were scanned with a scanner from Metasystems and analyzed with Metafer 4 program.

2.3 Genotyping and LOD score calculation

All affected individuals were genotyped on an Affymetrix GeneChip Human Mapping 250K NspI Array at the 'Center for Medical Research' at the Medical University of Graz. Data were analyzed with dChip software (M. Lin, Wei et al. 2004) available from http://www.hsph.harvard.edu/cli/complab/dchip/. For haplotype analysis of the IDACC family, a total of 3 highly polymorphic STR markers covering the autozygous region of interest were selected for fine mapping and segregation analysis, including D1S214 (6.962 Mb), D1S450 (9.585 Mb) and D1S2667 (11.486 Mb) from the ABI Prism Linkage Mapping Set v2.5 (Applied Biosystems).

To genotype the MCPH family six highly polymorphic STR markers were selected, including D1S206 (101,6MB) and D1S2726 (111,18MB) from the ABI Prism Linkage Mapping Set v2.5, as well as D1S2719 (96,81Mb), D1S2739 (98,93Mb), D1S2671 (101,67Mb), and D1S495 (102,56MB) from the UCSC browser mapping track (build 37/ hg19) (Khan, Rupp et al. 2014, Kent, Sugnet et al. 2002). PCRs were performed

with ABI Prism True Allele PCR Premix (Applied Biosystems) according to the program listed in Table 2.

Table 2: Temperature profile for microsatellite marker PCR

1	95°C	12min
2	94°C	15sec
3	55°C	15sec
4	72°C	30sec
Go to step 2 for 10x		
5	89°C	15sec
6	55°C	15sec
7	72°C	30sec
Go to step 5 for 20x		
8	72°C	10min
9	6°C	∞

Amplicons were denaturated using HiDi Formamide supplemented with Gene Ruler 500-Liz Size Standard (both from Applied Biosystems). Genome scan data were generated on the ABI3130xl and analyzed with Peak Scanner Software v1.0 (Applied Biosystems).

For the MCPH family a genome wide linkage analysis with 20,044 SNP markers from the Affymetrix array was conducted and LOD scores were calculated with ALLEGRO (Gudbjartsson, Jonasson et al. 2000). Data handling, evaluation and statistical analysis were performed as described previously (Hussain, Baig et al. 2013). For linkage analysis using STR marker results an autosomal recessive trait with full penetrance and a disease allele frequency of 0,001 were assumed. The two point LOD score was calculated using Superlink, for the multipoint LOD score calculation Merlin (Abecasis, Cherny et al. 2002) was used. Sex-averaged recombination rates between markers were obtained from Rutgers map (build 37, patch 4) (Matise, Chen et al. 2007).

2.4 Whole-Exome sequencing

Whole exome sequencing of the two IDACC patients was performed at Macrogen Inc. DNA was enriched using EZ Human Exome Library v2.0 kit from NimbleGen (Roche) and 76bp paired end reads were generated on Illumina Sequencing machines resulting in a mean sequencing depth of 142,4. We filtered the received excel data files for the target loci, splice site mutations, deletions, insertions, non-synonymous-, and stop gain mutations. Subsequently data were filtered for high-quality (coverage = PASS) rare (MAF<0.005) homozygous variants (dbSNP build 135).

Exom sequencing of the affected MCPH family members was performed at the Cologne Center for Genomics in Cologne, Germany. Briefly, 1 µg of DNA was fragmented using sonification technology (Covaris). The fragments were end-repaired and adaptor-ligated including incorporation of sample index barcodes. After size selection, the library was subjected to the enrichment process. For that SeqCap EZ Human Exome Library v2.0 kit from NimbleGen (Roche NimbleGen) was chosen. The enriched library was subsequently sequenced on an Illumina HiSeq 2000 sequencing instrument using a paired end 2 × 100 bp protocol.

This resulted in 8.4 Gb of mapped sequences, a mean coverage of 89-fold, a 30x coverage of 87%, and a 10x coverage of 97% of target sequences. For data analysis, the Varbank pipeline v.2.3 and filter interface was used (unpublished, https://varbank.ccg.uni-koeln.de/). Primary data were filtered according to signal purity by the Illumina Realtime Analysis (RTA) software v1.8. Subsequently, the reads were mapped to the human genome reference build hg19 using the BWA (H. Li, Durbin 2009) alignment algorithm. GATK v1.6 (McKenna, Hanna et al. 2010) was used to mark duplicated reads, to do a local realignment around short insertion and deletions, to recalibrate the base quality scores and to call SNPs and short indels.

Scripts developed in-house at the Cologne Center for Genomics were applied to detect protein changes, affected donor and acceptor splice sites, and overlaps with known variants. Acceptor and donor splice site mutations were analysed with a Maximum Entropy model (Yeo, Burge 2004) and filtered for effect changes. In particular, we filtered for high-quality (coverage >15; quality >25) rare (MAF<0.005) homozygous variants (dbSNP build 135, the 1000 Genomes database build 20110521, and the public Exome Variant Server, NHLBI Exome Sequencing

Project, Seattle, build ESP6500). They also filtered against an in-house database containing variants from 511 exomes from epilepsy patients to exclude pipeline related artefacts (MAF<0.004) (Khan, Rupp et al. 2014).

2.5 Mutation screening

Primers covering the coding exons and splice sites of *HsSAS-6, NGF, PSCR1* and *WDR47* were designed with Primer3 (http://www-genome.wi.mit.edu/genome_software/other/primer3.html) (Rozen, Skaletsky 2000) and ordered from Microsynth AG (this applies to all subsequent primer sequences mentioned in this thesis). A list of all oligonucleotides can be found in Table 3.

Table 3: PCR primers for screening genes in MCPH14 locus (table reproduced from (Khan, Rupp et al. 2014) with permission of Human Molecular Genetics).

Primer	**Oligonucleotide Sequence**	**Product length (bp)**
HsSAS-6		
SASS6_E1 f	AGGCTAATCCCGAGGGC	200
SASS6_E1 r	AGAACCGCCATCTTTCCC	
SASS6_E2 f	GAGAACACCTGTGGAAAGTCTTG	304
SASS6_E2 r	CCAACAGTTGCAAAATAGCC	
SASS6_E3 f	TATGATACACTGATGTTGTTGGATTTC	310
SASS6_E3 r	ACAAATAGCCCAATATTCCCAA	
SASS6_E4 f	AGCCTGGGTGATGGAGTG	309
SASS6_E4 r	ACGGAAAAGATTTTGCCATC	
SASS6_E5 f	TGGGAGTCCTCAATGTGCTC	454
SASS6_E5 r	TCCCGACTATACCTTGACTAAATAAG	
SASS6_E6 f	CTTTGAGTAGCATGGCTATAGATG	195
SASS6_E6 r	CAAGGAAGCAATTCAGTGCC	
SASS6_E7 f	ATTGGGTGGTAAAGAGCCAG	717
SASS6_E7 r	GACCCCATTAGTATAGAACAAAACC	

SASS6_E8 f	TTTTCAGAATGGGGATCTAAAG	449
SASS6_E8 r	AGCATCCAGAGGAACACCAC	
SASS6_E9-10 f	TAAATAACCAGATGAGGCAGC	526
SASS6_E9-10 r	TTTCATTTGCCTATAAAAGAGCTTC	
SASS6_E11 f	GGTGGTTTTAGAAGAAAATGGTG	502
SASS6_E11 r	CAAACTGAAACAGGTTATTACCATC	
SASS6_E12 f	TGATTCAGATACCTTGATTGCTC	496
SASS6_E12 r	TTAGCTGAGTGTGGTGGTGC	
SASS6_E13 f	TGAACCTATATTGCTCTCCTGTG	381
SASS6_E13 r	GGTATCAGCACCTTAAATCATGG	
SASS6_E14 f	GGCATGATAAACAAGACTGGC	345
SASS6_E14 r	AAAAGATGTGAAATGTTTGTATGC	
SASS6_E15 f	CCCTCTGCCCAAAACTGTC	286
SASS6_E15 r	TCTCAGGTAAACAGGTGGGC	
SASS6_E16-17f	AAACCAGTGAAGAATGTGTTCTG	530
SASS6_E16-17 r	TGAGGATCTGGTTTGTGTTGAC	
NGF		
NGF_E3_1f	CCCAGAAACTGCCTTTTGAC	485
NGF_E3_1r	ACACCGAGAATTCGCCC	
NGF_E3_2f	ACTTCGAGGTCGGTGGTG	483
NGF_E3_2r	ACAGGTTGAGGTAGGGAGGG	
PSCR1		
PSRC1_E2-3f	GGGCAGAATGGATACCTGAG	321
PSRC1_E2-3r	AGGGATTCGAGACAAAGAGG	
PSRC1_E4f	GTTGTGGGGCTTTTATGCAG	582
PSRC1_E4r	TCATGGCACACACCATGTC	

PSCR1_E5f	ATTTCTTAATTCCTTAAGCCACAG	614
PSCR1_E5r	ACAGCTCTGGGAGGGTGAG	
PSCR1_E6-7f	ACTAATCCCACACTCGCTCC	527
PSCR1_E6-7r	CAGAATCTGCTGGAGTCAGG	
WDR47		
WDR47_E2f	ATGTGTAGTTGCCAGGCAGT	354
WDR47_E2r	CATAGCCTTTTCATGATTATAAAGTTC	
WDR47_E3f	TGCTGTTTTGTCATCTGTTCTG	271
WDR47_E3r	TTCAAGGCCAGTGGAGAAAG	
WDR47_E4f	GGCTTCAATGTGATAAGAAGCCTA	300
WDR47_E4r	TGCTAATCCTTCGTTTTAGTGAC	
WDR47_E5af	TCGTTTTCATATTTCATAGCATGT	494
WDR47_E5ar	TGGAAGATTCTGAAGCCATGA	
WDR47_E5bf	GAAAGCGAAGTGCTTCTTGG	527
WDR47_E5br	ACAGGCATAAGCCACTGCAC	
WDR47_E6f	GTCGGGGCTACAGAGAGAGA	357
WDR47_E6r	TTTCCTACTCCCAAATATCAGAAAA	
WDR47_E7f	TGTTTCCGTGGAATAAAGCA	498
WDR47_E7r	TTCAAATGCGTAAAAAGCCTTA	
WDR47_E8f	TGTGCATATTTTTACCTTTTCACAC	435
WDR47_E8r	AAGGCTCCAAAGACAAGTTCA	
WDR47_E9f	GAAAAATTAGTGTTTGAAAGGGTAAA	240
WDR47_E9r	TTCTTTGAATTGAAAATTTCTTAGCA	
WDR47_E10f	GGCAGTAAACCTAACATGATCCA	359
WDR47_E10r	GGCAATTCTGAAAAAGGAACC	
WDR47_E11f	TGAAAACTATTAATAAGCTGTTGTCTG	383

WDR47_E11r	AAGACAATACAGAAATACAACATGGAG	
WDR47_E12f	AAACCATTATTCTTGACCAGTTTTG	380
WDR47_E12r	TGGACAGTAAGAGCAAGACCC	
WDR47_E13f	TATAGGCATGAGCCACCTTG	392
WDR47_E13r	CAAATGCAAGTATTGTGAAAGAAC	
WDR47_E14f	ATTTTGTTTAGGCCTTGGGC	610
WDR47_E14r	AAACCTAACAATAAGACTATTCACTGC	
WDR47_E15f	CAATCTATACATATACTTATTTTGCATTGTA	290
WDR47_E15r	TGGACACTATGTTCTTCAGATTTGT	

CAPZA1_cDNA_forw 5'GGAAGTTCACCATCACACCA and CAPZA1_cDNA_rev 5'GGCCTTGAATGTGGTATCTGA primers were used to investigate the effect of the splice site mutation in exon 8 of CAPZA1 in the IDACC patients on mRNA level. To verify the splice site mutation detected in Kif1bβ PCR primers Kif1b_mut_f (5'-ATTGCTGTCTCTGTAGTAACTTTCTTG) and Kif1b_mut_r (5'-AAGACCAAGCCACTGCACTT) were designed. All PCRs were performed using HotStarTaq Master Mix Kit (Qiagen) with the following cycling conditions: 94°C for 15 min, followed by 35 cycles of 95°C for 25 s, 57°C for 30 s and 72°C for 1 min with no final elongation step (subsequently referred to as 'HS57' program). The sequencing reaction was set up with the Big Dye v3.1 cycling sequencing kit (Applied Biosystems) according to the manufacturers' protocol. Prior to sequence analysis, dye remnants were removed with Centri-SepTM columns (Applied Biosystems) and samples were bidirectionally sequenced on the ABI3130xl (Applied Biosystems). Resulting data were analyzed with ChromasLite software (Technelysium Pty Ltd.) and the UCSC browser (Kent, Sugnet et al. 2002, Fujita, Rhead et al. 2011).

The impact of the mutation on splicing was investigated on mRNA level. For cDNA generation, blood derived total RNA was transcribed with Omniscript RT Kit (Qiagen). The region of interest was amplified by PCR (with KIF1b_Isocheck_f (5'-TGAAGAAATTAGACCAAGCTCAGTG) and KIF1b_cDNA_r (5'-TGTATTTCGACTGGCTCGG) using HotStarTaq Master Mix Kit (Qiagen) with the

following cycling conditions: 94°C for 15 min, followed by 35 cycles of 95°C for 25 s, 55°C for 30 s and 72°C for 1 min with no final elongation step. Sequencing was performed as described above.

To check the presence or absence of exon 25 in the mRNA we used primers kif1b_E25_check_f (5'- tggatttgatgcgagagatgt) and Kif1b_E25_check_r (5'- acttcacctttctcactgacga) to amplify the region of interest with HotStarTaq Master Mix (Qiagen) applying the same cycle conditions as mentioned above.

2.6 RT-PCR and qPCR

To measure absolute quantities of *Kif1A*, *Kif1bα* and *Kif1bβ* expressed in human fetal brain total RNA (Clontech), U2OS cells and lymphoblastoid cells of patients and a healthy control, 1µg RNA was transcribed with QuantiTecht reverse transcription kit (Qiagen). To generate templates for the corresponding standard curves, first, a conventional PCR using HotStar Taq Mastermix and HS57 program was performed to amplify *Kif1bβ*, *Kif1bα* and *Kif1A* target sequences using following primer pairs: Kif1b_alpha_cDNA_f (5'- TCTTCTTTTGGAGCAGCAGAG) and Kif1b_alpha_cDNA_r (5'- TTTCCAGCTCTCTTCACACG), Kif1b_beta_cDNA_f (5'- CTCACCCACACTTTCAACAGAG) and Kif1b_beta_cDNA_r (5'- TGCTGAAACTGGACTCAGAGG) as well as KIF1A_RTf (5'- CGGACATAGGCCACAGATG) and KIF1A_RTr (5'- CGTGTGACTGGTGTGTACGA). Subsequently, the PCR products were run on a 1% agarose gel for 30min at 130V, and corresponding lanes were cut out and extracted using GenElute Gel Extraction Kit (Sigma). DNA amounts were measured with Qubit 2.0 Fluorometer and pre-diluted to 1pg. To create standard curves 1:5 (for *KIF1A*: 1000, 200, 40, 8, 1.6, 0.32, 0.064, 0.0128fg) and 1:3 (for *Kif1bα* and *Kif1bβ:* 1000, 333.3, 111.1, 37.04, 12.34, 4.12, 1.37, 0.457fg) serial dilution series of the corresponding template DNAs were prepared. Sample cDNAs were applied either diluted or undiluted (according to Qubit (Invitrogen, ThermoFisher) concentrations) to make sure that concentrations were within the standard curve. To measure relative quantities of *Kif1b* isoform expression in brain and muscle, RNA from muscle tissue was isolated as described recently (Y. Xue, Schoser et al. 2016). cDNAs were transcribed as mentioned above and levels were measured relative to

the expression of 18s rRNA (primer 18s_f 5'GAGACTCTGGCATGCTAACTAG and 18S_r 5'GGACATCTAAGGGCATCACAG).

All reactions were set up in triplicates with 10µl Fast SYBR Green master mix (Applied Biosystems), 8µl sterile water, 1µl cDNA and 1µl of a 10µM primer mix on the StepOne Plus Real-time PCR System (Applied Biosystems) according to the manufacturer's instructions. PCR was performed using following cycling conditions: a holding stage of 95°C for 20min, followed by a cycling stage of 40 cycles at 95°C for 3 sec and 60°C for 30sec. Finally, the melt curve was generated at 95°C for 15sec, 60°C for 1min and a final increase of 0.3°/sec from 60 to 95°C where the temperature was held for another 15sec. Data were analyzed with the StepOnePlus Software v.2.3 and quantities, fold changes and diagrams were then calculated and generated in Excel according to the guidelines from applied biosystems.

2.7 HsSAS-6 homology analysis in Jalview

HsSAS-6 Ile62 homology among nine different species (from NCBI *Homo sapiens* (AAI01027), *Danio rerio* (AAI65167), *Pan troglodytes* (JAA36473), *Aligator mississippienis* (XP_006277337), *Apis melifera* (XP_395972), *Mus musculus* (NP_082625), *Caenorhabditis elegans* (CAA16384), *Drosophila melanogaster* (AAF56983), *Chlamydomonas reinhardtii* (BAF94334)) was investigated with the desktop version of Jalview2.8 (Waterhouse, Procter et al. 2009). For Kif1bβ, PH domain amino acid sequences of following species were aligned in Jalview 2.10.3 (accession numbers according to *UniProt): Homo sapiens (O60333), Rattus norvegicus* (O88656), *Mus* musculus (Q60575), *Danio Rerio* (C0LSN9_DANRE), *Drosophila melanogaster* (A1ZAJ2), *Alligator sinensis* (A0A1U8DAW3_ALLSI), *Erinaceus europaeus* (A0A1S3WSN7_ERIEU), *Gallus gallus* (E1C889_CHICK) and and *Xenopus tropicalis* (F7DRH5_XENTR). Sequences were aligned with MafftWS alignment using the default settings (Katoh, Kuma et al. 2005). Regions that were highly conserved in terms of their hydrophobicity are highlighted in red and blue.

2.8 Kif1bβ splice site prediction

We analyzed the mutagenic potential of the splice site variant with the 'Berkley Drosophila Genome Project: Splice Site Prediction by Neural Network' online tool (available at http://www.fruitfly.org/seq_tools/splice.html) (Reese, Eeckman et al. 1997). We applied 0.40 as the donor and acceptor score cutoff value.

2.9 Cloning

2.9.1 Kif1bβ

WT *Kif1bβ* cDNA was amplified from Human Fetal Brain Marathon Ready cDNA (Clontech) with Phusion Hot Start II High-Fidelity Polymerase (Thermo Scientific) using the GC buffer and kif1b_cDNAf_long (5'-TAAAATGTCGGGAGCCTCAGTGAAG) and kif1b_cDNAr_long (5'-TGTATTTCGACTGGCTCGGGC) in a two-step protocol: 98°C for 30 sec, followed by 40 cycles of 98°C for 10sec and 72°C for 3min28sec, and a final elongation step at 72°C for 10min. We derived multiple PCR products which were separated on a 0.8% agarose gel. The correct band was extracted with the GenElute Gel Extraction Kit (Sigma) and eluted in 30µl H_2O. Subsequent A-tailing of 25µl of the eluted product was performed with Taq DNA Polymerase with Standard Taq Buffer, 1.5 mM $MgCl_2$ (all from New England Biolabs) and 200µM dATP (Roche) for 14min at 72°C. 4µl of the A-tailing mix was used for cloning into a eukaryotic expression vector with the pcDNA™3.1 vector⁄ CT-GFP-fusion TOPO® Expression kit (Invitrogen, Life Technologies) in order to create pcDNA3.1-Kif1Bβ-WT-GFP.

For pcDNA3.1-kif1Bβ-MUT-GFP, we first amplified an extended version of Kif1b beta (up to the new Stop codon, resulting from the frame shift) from human fetal brain cDNA using the same cycle conditions as for the WT construct and the following primer pair: kif1b_cDNAf_long and kif1b_Mut_cDNAr (5'-CCAAAGAGAAATGAGAGGTAACGCTTTC). After A-tailing, the product was cloned into pcDNA™3.1 vector⁄ CT GFP-fusion TOPO®. Clones with the same isoform as the WT construct were selected for *in-vitro* mutagenesis. The mutagenesis reaction was set up with Ultra Pfu HF DNA Polymerase (Stratagen) and 5' phosphorylated primers kif1b_mut_rev (5'-CTTCACCATGGCCTGCTGGTCCTCACT) and kif1b_mut_f (5'-

GTCAAAGCTTTCCCGCAGATGCCCGA). An initial step of 2min at 92°C was followed by 10 cycles at 92°C for 10sec, 59°C for 30sec and 68°C for 23min with a subsequent 20 cycles at 92°C for 10sec, 59°C for 30sec and 68°C for 23min+10sec/cycle. The 11kb lane was isolated from a 0,8% agarose gel with GenElute Gel Extraction kit (Sigma), and the linear PCR products were ligated with Quick ligase (New England Biolabs) and transformed into TOP10 chemical competent cells (LifeTechnologies). For the cloning of NT-GFP-Kif1bbeta_CtailWT and NT-GFP-Kif1b_CtailMUT, the *Kif1bβ* tail region was amplified from the corresponding pcDNA3.1-Kif1bβ-WT-GFP or pcDNA3.1-kif1bBβ-mut-GFP plasmid, respectively, with primers Kif1b_PH_NTf (5'-ATGGTCCCAGCTGTGGAAACACCATATT) and and Kif1b_PH_NTr (5'-TTATTTCGACTGGCTCGGGC) or Kif1b_deltaPH_NTr (5'-TTACAAAGAGAAATGAGAGGTAACGCTTTC) using HotStarTaq Mastermix (Qiagen). The following cycling conditions were used: initial 15min at 94°C followed by 35 cylces of 95°C for 25sec, 57°C for 30sec and 72°C for 1min. Resulting PCR products were directly used in the cloning reaction with pcDNA™3.1 vector⁄NT-GFP TOPO® vector (LifeTechnologies). Clones containing correctly orientated sequences were identified by colony PCR using primers T7f (5´-TAATACGACTCACTATAGGG) and Kif_fulllength_r (5'-GATCTTCGGGTGAGGTATGAG) for full-length *Kif1bβ* WT and MUT constructs or GFP_f (5´-CGACACAATCTGCCCTTTCG) and Kif1b_PH_NTr for WT and MUT C-terminal constructs. To cover all exons by sequencing, in addition to T7f and GFP_f primers, the following primers listed in Table 4 were used.

Table 4: Primers for sequencing *Kif1bβ* clones

Primer	Sequence
Kif1b_2f	5'atcattccacagttatgtgaagaact
Kif1b_3f	5'actgtgaaagagtacgagatttgct
Kif1b_4f	5'acagggattctgtacttacttggct
Kif1b_5f	5'taaaacagaggccatcagaatg
Kif1b_6f	5'atcatcatgggtaaaaaccatgt
Kif1b_7f	5'agtttacttcattacgggacttactct
Kif1b_8f	5'tgtgtgaacgagcgcctt
Kif1b_9f	5'tcgtctgttgcaatgactcgt
Kif1b_10f	5'actgaatcatttgtggattacatca
Kif1b_11f	5'tgatgccatcctctcccta
Kif1b_12f	5'agaacttagcaggctggcg
Kif1b_13f	5'tctccaattggacgggat
kif1b_cDNA_r_v2	5'tgtatttcgactggctcgg

The p75-RFP was a gift from Moses Chao (Addgene plasmid #24092, unpublished).

2.9.2 HsSASS-6

Cloning of *HsSASS-6* was performed at the UPGON group at the EPFL in Lausanne. pEBTet-GFP plasmids (Bach, Grigat et al. 2007) were a gift from Dirk Gründemann. The oligos GW-F (5'CGCGGGTACCGCCGGCAGCTAGCGGCGCGCCCGGCCGATAT) and GW-R (5'ATATCGGCCGGGCGCGCCGCTAGCTGCCGGCGGTACCCGCG), were annealed and digested with KpnI and EagI and ligated into KpnI and NotI cut pEBTet-GFP producing the pEBTet-MCS vector. This plasmid was then used to insert fluorescence proteins and Gateway cassette (Invitrogen), generating the destination vector pEBTet-GW-EGFP. The multiple cloning site of pENTR 1A (Invitrogen) was modified by introducing single restriction sites between the attR1 and attR2 sites (3′-AgeI and XbaI-5′), generating the entry vector pENTR-SD-Age-

AGT. Full length *HsSASS-6* (NM_194292.1) was amplified using the primers Age-Ko-HsSAS6-F (5'CGCGACCGGTACCATGAGCCAAGTGCTGTTCCAC) and Xba-noST-S6-R (5'CGCGTCTAG ATAACTGTTTGGTAACTGCCCA), and cloned into pENTR-SD-Age vector by restriction digest with AgeI and XbaI.
Mutations of the I62 residue in HsSAS-6 were generated by site-directed mutagenesis on pENTR-SD-Age-HsSAS-6 using the following primers: S6-I62T-fwd, *ACA*TCTGAGGAAGATTTTCAAAGT and S6-I62T-rev, AACAAGGTTATATAAAAAAAATGG (mutated codon is italicized). Gateway reaction was then performed according to the manufacturer's protocol to generate the expression plasmids pEBTet-HsSAS-6-GFP and pEBTet-HsSAS-6-I62T, which were sequence verified' (Khan, Rupp et al. 2014).
All plasmids were isolated with EndoFreePlasmid Maxi Kit (Qiagen).

2.10 Cell culture and transfection

2.10.1 Kif1bβ

The human choriocarcinoma cell line JAr (ATCC) was cultured as previously described. U-2 OS cells were kindly provided by the 'Cell Culture Core Facility' of the Medical University of Graz. They were maintained in DMEM with 10% FBS and 1% Pen/Strep (all from Life Technologies) at 37°C and 5% CO_2. Cells were transfected with pcDNA3.1-kif1bβ-WT and FuGENE HD Transfection Reagent (Promega) at 50% confluence with a ratio of 3,5:1 (FuGENE:DNA) according to the manufacturer's protocol. For co-transfection with p75-RFP, cells were first transfected with the pcDNA3.1-kif1bβ-WT plasmid applying a 4:1 ratio. The day after, cells were transfected with p75-RFP (addgene #24092) applying a 3:1 ratio of FuGENE:DNA. 24h later, cells were monitored under an array confocal laser scanning microscope (ACLSM) built on a fully automated inverse microscope (Axio Observer.Z1, Zeiss) at the Institute of Biochemistry of the Medical University of Graz.
For electroporation $4x10^6$ cells were transfected with 12µg plasmid DNA using the NEON transfection system (Invitrogen). Cells were co-transfected with 500ng p75-RFP and 13µg pcDNA3.1-GFP-Kif1bβ-delta-PH or pcDNA3.1-GFP- kif1bβ-PH. The following conditions were used: 1230V, 10ms, 4 Pulse. Cells were analyzed 18h later.

To generate lymphoblastoid cell lines, lymphocytes were isolated from heparinized peripheral blood by density gradient centrifugation using Lymphocyte Separation Medium LSM 1077 (PAA) according to the manufacturers protocol. Lymphozytes were further resuspended in 2ml of blood media (RPMI 1640 with hepes, 10%FBS, 1%Pen/Strep; all from Gibco, Life Technologies) and supplemented by the same volume of filtered B-95-8 culture supernatant. After 24h at 37°C half of the media was removed and new media with 3-4 drops of cyclosporine (Sandoz) was added to the cells. Cells were maintained in cyclosporine supplemented media for 3 more weeks. When cells had finally reached a high division rate, media was changed to normal blood media (see above).

2.10.2 HsSASS-6

Transfection and co-localization studies were performed at the UPGON group in Lausanne. U2OS cells were obtained from the EACC and maintained in McCoy's 5A GlutaMAX medium (Invitrogen) supplemented with 10% fetal bovine serum (FBS) for U2OS cells or tetracycline-negative FBS (Brunschwig) for the inducible episomal cell lines (iU2OS). To generate such iU2OS lines, U2OS cells were transfected with pEBTet-HsSAS-6-GFP or pEBTet-HsSAS-6[I62T]-GFP using Lipofectamine2000 (Invitrogen). Transfected cells were selected with 1 µg/ml puromycin one day after transfection and amplified. Early passage cells were used, inducing expression with 1ug/ml doxycycline for 48 hr.
Endogenous HsSAS-6 was depleted using a Stealth RNAi siRNA (Invitrogen) targeting the 3′UTR of HsSAS-6 (5-GAGCUGUUAAAGACUGGAUACUUUA-3). Stealth RNAi siRNA negative control LO GC (Invitrogen) was used as a control.
siRNA transfection was performed using Lipofectamine RNAiMax (Invitrogen) according to the manufacturer's protocol, and cells were analyzed 48-72 hr after siRNA treatment (Khan, Rupp et al. 2014).

2.11 Cell-extract preparation and biochemical assays

2.11.1 HsSAS-6

Cells were collected, washed in PBS, and lysed on ice for 1 hour in lysis buffer (50 mM Tris-HCl [pH 7.5], 150 mM NaCl, 0.5 mM EDTA, 0.5% NP-40, Complete Mini Protease Inhibitor Cocktail [Roche Diagnostics]). Lysates were cleared by centrifugation for 10 min at 12,000 × g at 4°C and the supernatant collected. SDS-PAGE was performed using 10% polyacrylamide gels (BioRad), followed by transfer on nitrocellulose membrane (Amersham). The membrane was probed with mouse HsSAS-6 antibody (Santa Cruz, 1:1000) or mouse Tubulin antibody (Sigma, 1:10000), followed by incubation with their respective HRP-conjugated secondary (Promega) and the signal detected with chemiluminescence. Western Blots were performed at the UPCON group at the EPFL in Lausanne.

2.11.2 Kif1Bβ

For protein isolation, cells were washed twice with ice cold PBS and lysed with 100µl lysis buffer (50 mM HEPES, 150 mM NaCl, 1 mM EDTA, 10 mM $Na_4P_2O_7$, 2 mM Na_3VO_4, 10 mM NaF, 1% (v/v) Triton X-100, 10% (v/v) glycerol and Complete Mini protease inhibitor cocktail tablets; pH 7.4) for 10 min on ice (Semlitsch, Shackelford et al. 2011). Scraped cells were centrifuged at 13,000 rpm and 4°C for 10 min to remove insoluble cell debris. Protein contents of cell lysates were determined using the BCA™ Protein Assay Kit (Thermo Scientific) according to the manufacturer's instructions.

Fifty µg of total protein was added to 10 µl of 4x NuPAGE LDS sample buffer (Invitrogen) containing 2 µl sample reducing agent (Invitrogen) and heated (70°C, 10 min). Proteins were separated by electrophoresis on 6% Bis-Tris gel and transferred to nitrocellulose (Invitrogen, 40 µM). Membranes were blocked with 5% (w/v) non-fat milk in TBST (Tris-buffered saline containing Tween-20) (25°C, 2 h) and incubated with polyclonal rabbit anti-KIF1Bβ (1:2000, Bethyl, A301-055A) overnight at 4°C. After washing, membranes were incubated with HRP-conjugated goat anti-rabbit IgG (Biomol-8101102, 1:100,000 or Pierce, 1:50,000) at 25°C for 2h. Immunoreactive bands were visualized using Super Signal West Pico Chemiluminescent substrate (Thermo Scientific) and developed using Bio-Rad ChemiDoc MP Imaging System.

Co-immunoprecipitation was performed by incubating protein lysates (1 mg) from WT, V:1, VI:2, and VI:4, respectively; with anti-KIF1Bβ antibody (1 µg) according to the manufacturer's suggestions (GE healthcare). Immunoprecipitates were separated by 6% (KIF1Bβ) or 15% (CaM) SDS-PAGE Bis-Tris gels and transferred to nitrocellulose membranes. Immunoreactive bands were visualized using anti-KIF1Bβ or rabbit polyclonal anti-CaM (1:500, Santa Cruz, sc-5537) as the primary antibody followed by HRP-labelled secondary antibody as described above. This work was conducted at the Institute of Biochemistry at the Medical University of Graz.

2.12 Immunofluorescence and microscopy for hsSASS-6 transfected cells

Centriole and monopolar spindle quantification was performed at the UPCON group at the EPFL in Lausanne. U2OS cells grown on glass coverslips were fixed for 7–10 min in –20°C methanol, washed in PBS, and blocked in 1% bovine serum albumin and 0.05% Tween-20 in PBS. Cells were incubated 2 hr at room temperature with primary antibodies, washed three times for 10 min in PBST (0.05% Tween-20 in PBS), incubated 45 min at room temperature with secondary antibodies, stained with ~1 µg/ml Hoechst 33258, washed three times in PBST, and mounted. Primary antibodies were 1:4000 mouse centrin (20H5; gift from Jeffrey L. Salisbury) and 1:500 rabbit GFP (gift from Viesturs Simanis). Secondary antibodies were 1:1000 goat anti-rabbit coupled to Alexa 488 and 1:1000 goat anti-mouse coupled to Alexa 568. For quantification of centrioles, mitotic cells (prophase to metaphase) with similar cytoplasmic GFP expression were used; highly expressing cells that often harbored GFP aggregates were not retained for analysis. Imaging was done on a Zeiss LSM710 confocal microscope. Optical sections were acquired every 0.12µm, and planes containing centrioles were projected together. Images were processed using ImageJ and Adobe Photoshop, preserving the relative image intensities within a series.

2.13 Confocal Imaging for Kif1Bβ and p75 transfected cells

Co-Localization of p75 and KIF1Bβ was investigated by recording GFP and RFP signals using the array confocal laser scanning microscope (ACLSM) built on a fully

automatic inverse microscope (Axio Observer.Z1, Zeiss) equipped with VoxCell Scan® (VisiTech, Visitron Systems) using a 100 × objective (Plan-Fluor 100 × /1.45 oil, Zeiss) at the Institute of Biochemistry of the Medical University of Graz. Live cells were cultured and transfected on glass slides (see 2.10.1) and excited with diode lasers (Visitron Systems); GFP was excited at 473nm (50mW) and RFP was excited at 561nm (50mW). Emitted light was collected with filters ET525/50m for GFP and ET480/40m for RFP (Chroma Technologies Corporation). Pictures were captured using a photometrics CCD camera (CoolSnap HQ2, Photometrics), Images were processed with ImageJ (Schindelin, Arganda-Carreras et al. 2012, Schneider, Rasband et al. 2012) and movies were subsequently generated with MetaMorph 7.7.0.0 software (Visitron) (Bischof, Rehberg et al. 2017, Waldeck-Weiermair, Bischof et al. 2015).

3. Results

3.1 Autosomal recessive syndromal intellectual disability with agenesis of the corpus callosum

Family IDACC is a consanguineous Turkish family living in Corinthia, Lower Austria. Two first cousins of this family were affected with a to date unreported autosomal recessive syndromal intellectual disability accompanied with complete agenesis of the corpus callosum (pedigree see Figure 2).

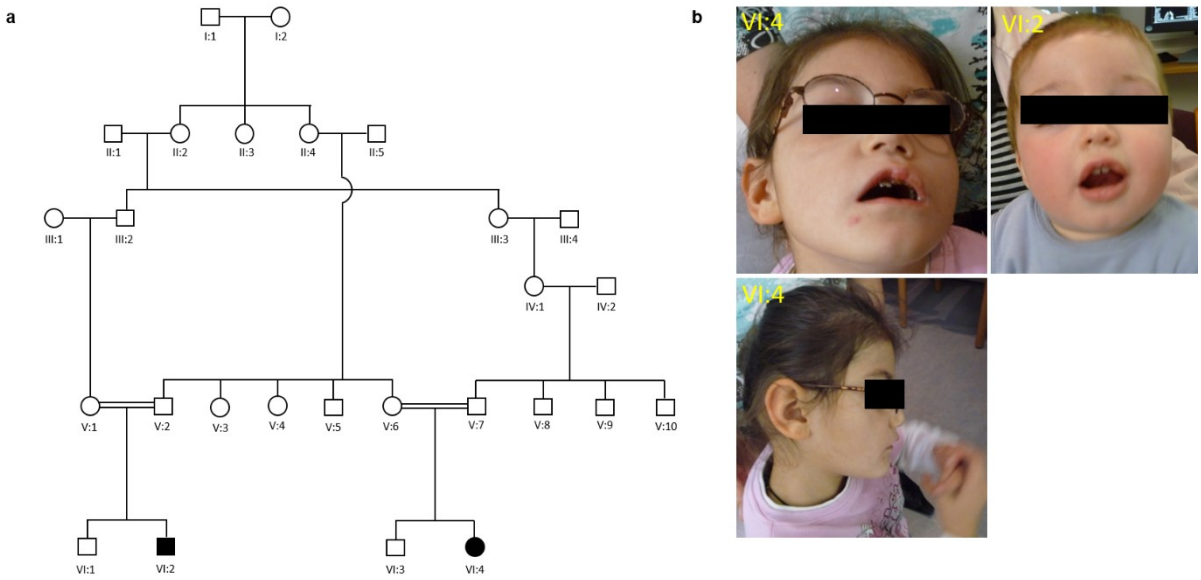

Figure 2: Pedigree of the IDACC family and pictures of patients. **a.** Pedigree. Black symbols indicate the two affected children while the white symbols indicate the non-affected. Circles represent girls, squares represent boys. Double lines connecting parents depict a consanguineous marriage. **b.** Patients VI:2 and VI:4. Both children have ptosis (dropping of the eye lid - hidden by bar); hypotonia is reflected by the open lip posture (low muscle tone). Additionally, VI:4 has a brachycephalic head (flattened back on lower picture).

VI:2 (see Figure 2b) was the first child of V:1 and V:2. Prenatal ultrasound of VI:2 revealed hydronephrosis grade IV and grade II on the right and left side, respectively. After an uneventful pregnancy, the child was delivered at full-term with

a birth weight of 2,610 g (date of birth: October 2007). The lab values were within the normal range, beside a cirrhosis of the right kidney associated with vesicoureteral reflux grade IV-V and a grade III reflux on the left side. At the age of three months, bilateral ptosis and nystagmus were diagnosed. Subsequent brain magnetic resonance tomography (MRT) at the age of four months revealed a complete agenesis of the corpus callosum, a hypoplastic gyrus cinguli, deformation of both frontal horns and slightly enlarged occipital horns (colpocephaly). Furthermore, the third ventricle was slightly enlarged and reached cranial to the interhemispheric fissure between the lateral ventricles and communicated with the interhemispheric fissure anteriorly. Basal ganglia, posterior cranial fossa and myelination were normal (see Figure 3). Developmental delay, hypotonia with delayed motor development and some mild dysmorphic features were diagnosed after the first month of life. Chromosome analysis was inconspicuous showing a normal male karyotype (46,XY). At four months of age he had 5.5 kg, and his head circumference was 40.5 cm. At 10 months of age his growth parameters were at the 3rd percentile. Around his first birthday his weight was 7.8 kg, and the head circumference was 45 cm. In addition to the known bilateral ptosis ophthalmologic examination at the age of two (26 months) revealed strabismus that could be due to oculomotor nerve palsy. At four years of age, a neurologic examination diagnosed an atactic gait with an external rotation of the right leg. There was no evidence for a peripheral nerve disorder, confirmed by a nerve conduction study, which showed no evidence for an axonal or demyelinating disorder. His fine motoric skills are impaired, spoken language and expressive speech development is severely retarded. He has issues maintaining eye contact, exhibits significant attention and concentration problems and is reported to be a restless child.

V:6 had four pregnancies, including one still birth in the 20th week of gestation. A second pregnancy revealed bilateral hydronephrosis and megacystis during an ultrasound examination. Due to these findings the pregnancy was terminated despite showing a normal male karyotype (46, XY) during prenatal testing.

The pregnancy with VI:4 was normal. The girl (Figure 2b) was delivered at full term (date of birth: February 2004), with a birth weight of 3,730 g and lab values that were within the normal range. Chromosome analysis showed a normal female karyotype (46,XX). Within the first year of life severe developmental delay with a congenital left facial nerve paresis was diagnosed. As for patient V:2, brain MRTs revealed

complete agenesis of the corpus callossum. Characteristic lateral convexity of the frontal horns, parallel lateral ventricles and dilated posterior ventricles (occipital horns) were noted. Hence colpocephaly was diagnosed. The third ventricle showed continuity with the interhemispheric fissure. Myelination was normal for the age (Figure 3).

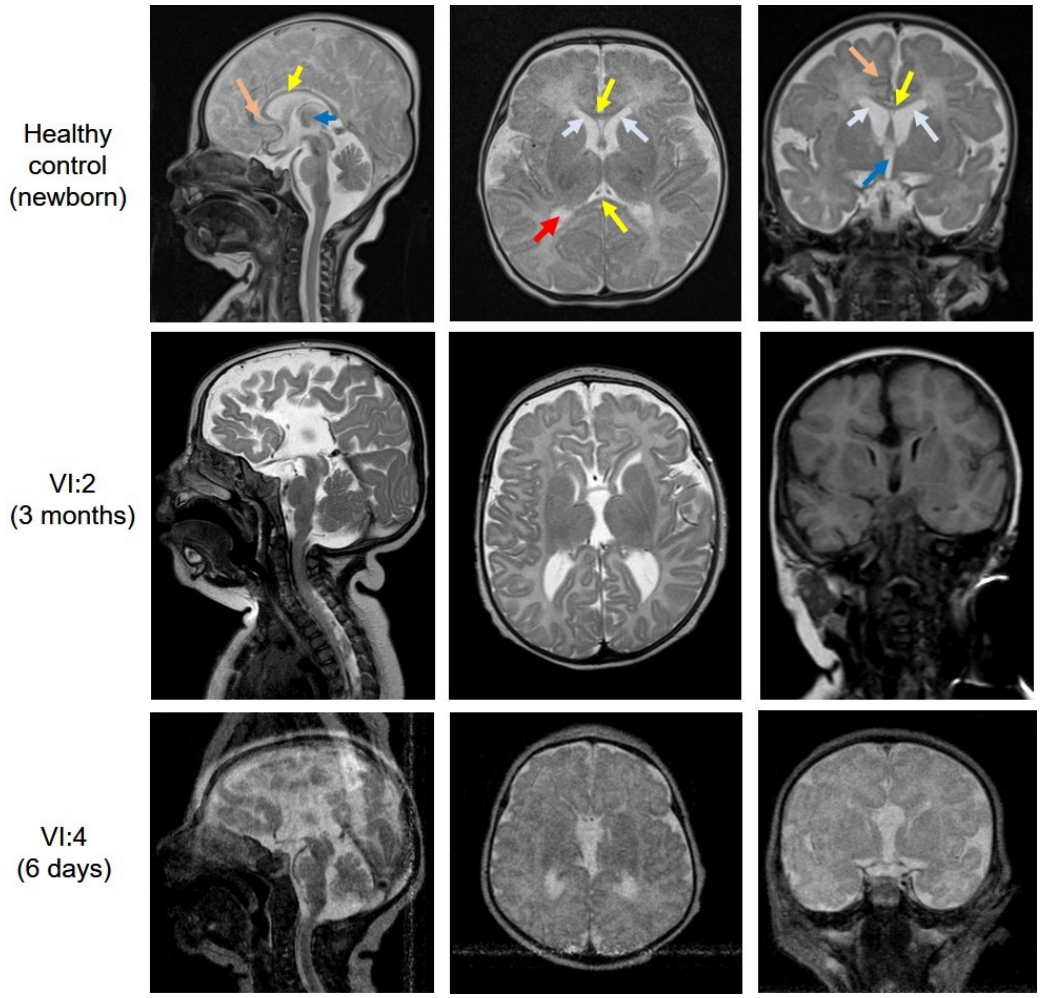

Figure 3: MRI pictures of the 2 patients and a healthy control. Sagittal, axial and coronal cross sections of the brain were selected (left to right). Yellow arrows indicate the corpus callosum, which is absent in the two patients. The gyrus cingula is hypoplastic (light red), the third ventricle is dilated and reaches cranial (dark blue arrow) in both patients. Frontal horns (lateral ventricles; light blue arrow) are deformed in VI:2 while the occipital (posterior) horns (red arrow) are enlarged in both patients.

At two months of age she weighted 5,500 g (>97th percentile), was 60 cm tall (>97th percentile), and had a head circumference of 36.5 cm (25th – 50th percentile). At 8.2 kg (>25th percentile) and 74 cm (>50th percentile), her weight and size were still within the normal range by the age of 10 months. However, her head circumference was clearly below the 3rd percentile (41cm). Though her vision was normal, at one year and two months of age, ophthalmologic examination revealed bilateral ptosis, strabismus, and a congenital oculomotor nerve palsy. At one year and seven months she was still not able to walk and her motor movements were reduced. At 3 years and 7 months her weight and height were still within the normal range for the given age (12.5 kg [3rd - 10th percentile], 98 cm [>50th percentile]), whereas her head circumference was significantly smaller compared with children her age (44cm). She showed a hypoton-atactic gait which was slightly asymmetric. She understood and followed instructions relatively well but had problems paying attention. A neurological examination by the age of 11 ½ found pronounced dysmorphic facial features and aggressive behavior. Due to ocular motor apraxia she exhibited dystonic movements of her head. Her coordinative functions were strongly reduced, intellectual development was severely delayed and cognitive functions were impaired. She was reported to show motoric clumsiness, speech and language delay. There was no evidence for a peripheral neurologic disorder.

The clinical data of both patients are summarized in Table 5.

Table 5: Clinical data of IDACC patients

Pedigree ID	**VI:2**	**VI:4**
Chromosomes	46,XY	46,XX
Kidneys	hydronephrosis	normal
Delivery	Full-term	Full-term
Apgar	Normal	Normal
Birth weight	2,610 g	3,730 g
Eyes	Bilateral ptosis Strabismus	Ophtalmoplegia Bilateral ptosis Strabismus
Brain	Complete agenesis of the corpus callossum 3rd ventricle enlarged reaching to the interhemispheric fissure Deformation of both frontal horns Enlarged occipital horns	Mild microcephaly/ brachycephaly Complete agenesis of the corpus callossum 3rd ventricle enlarged reaching to the interhemispheric fissure Deformation of both frontal horns Enlarged occipital horns
Cranial nerves	Congenital oculomotor nerve palsy	Congenital oculomotor nerve palsy Congenital left facial nerve paresis
Growth parameters	All at the 3rd percentile	Head circumference below 3rd percentile
Dysmorphic facial features	Mild	More pronounced
Motor development	Severely delayed Hypoton	Severely delayed Hypoton
Gait	Atactic	Atactic
ID	Severely delayed	Severely delayed
EEG	Normal	Normal
Speech	5 words	5 words
Sense of hearing	Normal	Hearing aid on left ear

ID=intellectual development; EEG= electroencephalography

We collected blood from both affected children (VI:2 and VI:4), the mother (V:1) and the brother (VI:1) of VI:2, as well as from the parents (V:6 and V:7) of VI:4. In addition to DNA and RNA isolation, lymphoblastoid cell lines were generated from the blood of both affected and from V:1. As mentioned above, karyotyping revealed no chromosomal abnormalities (Figure 4).

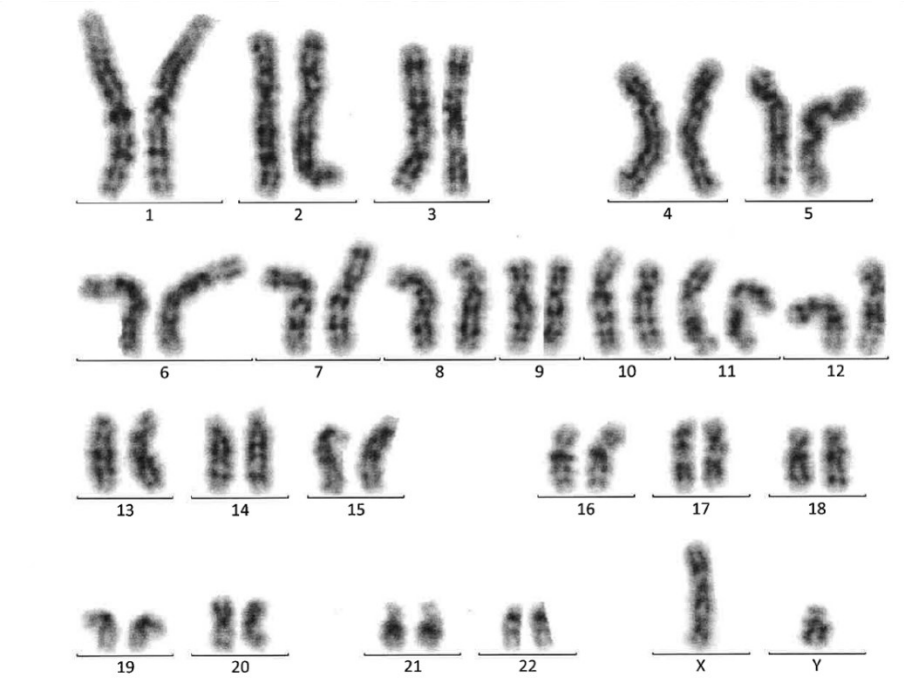

Figure 4: Chromosome analysis of lymphoblastoid cells shows a normal karyotype (chromosomes of VI:2)

The affected children's consanguineous background suggested the disease-causing gene to be located in an autozygous region of the genome. Hence a SNP 250K array was conducted for both affected. Analysis of the data in dChip revealed four homozygous stretches with identical haplotypes on chromosome 1p36.31-p36.32 (6,775 MB), 2q22.1-q23.3 (8,534MB), 3p14.1 (2.86MB) and 9q21.13-q21.2 (positions according to chromosome build hg17) (Figure 5).

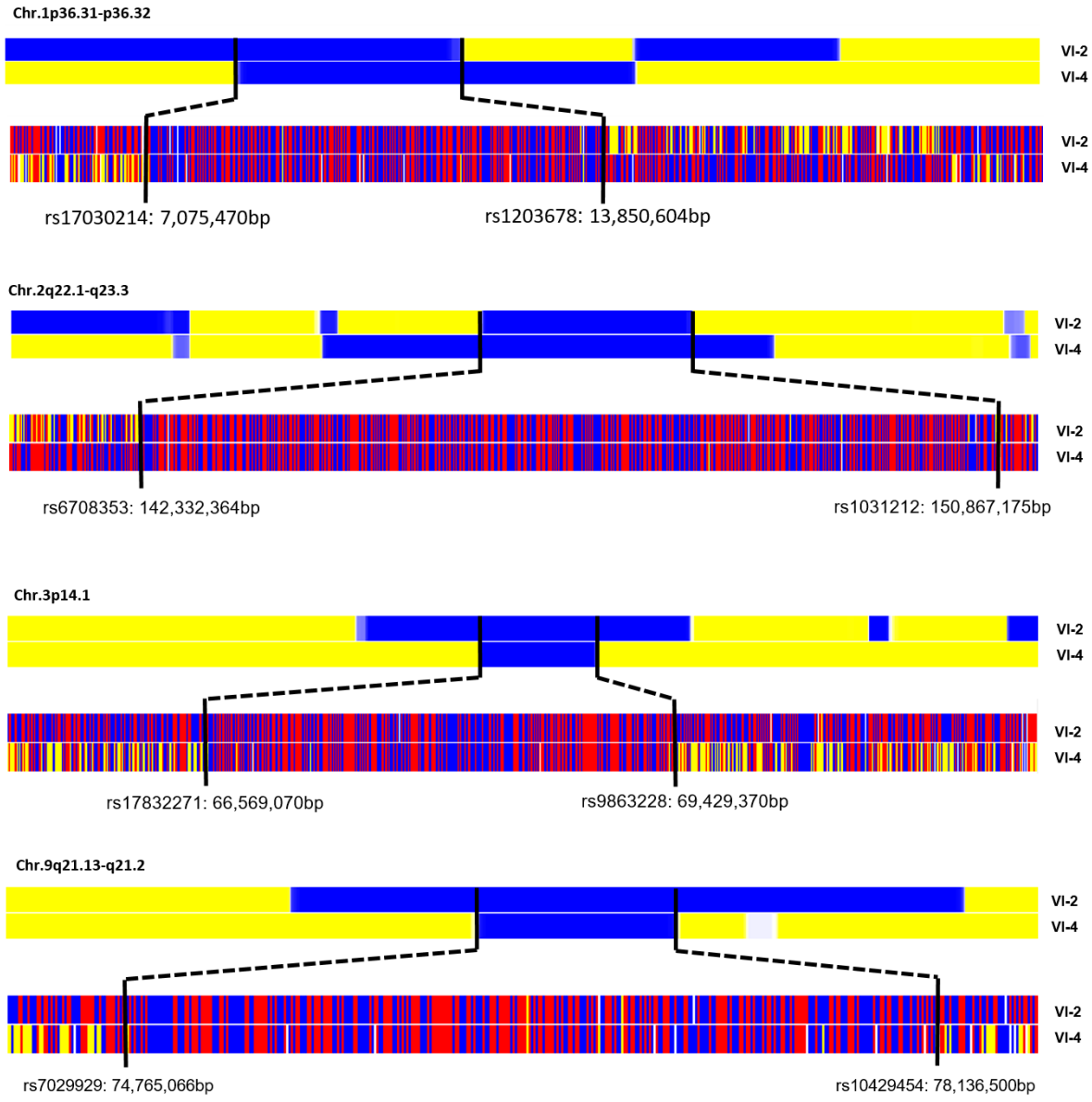

Figure 5: 250K NspI SNP array of patients VI:2 and VI:4. Blue and yellow bars represent homozygous and heterozygous regions, respectively. Identical red and blue SNP haplotypes depict autozygous regions. Red is homozygous for SNP A, blue is homozygous for SNP B, yellow is heterozygous for SNP A and B. SNPs restricting the homozygous stretch are noted as rs numbers with their corresponding location on the chromosomes (according to genome build hg17).

Due to the large number of genes located in these loci, we decided to send the DNA for whole exome sequencing (WES). Since data received from WES were matched with the hg19 build, positions of our loci changed to 1p36.31-p36.21 (7,141,204-14,105,298bp), 2q22.2-q23.3 (142,498,632-151,041,667bp), 3p14.1 (66,486,380-69,346,680bp) and 9q21.13-q21.2 (77,535,512-80,906,946bp). Filtering for rare and

high quality variants revealed only three candidate genes all located in the locus on chromosome 1, including two nonsynonymous mutations with reported rs numbers in *PRAMEF11* (c.A308G; p.E103G; rs2994114) and LOC440563 (c.A434G; p.H145R; rs28713604) and an unknown splice site mutation c.5270+2T>G in the donor splice site of exon 47 in the β isoform of the *KIF1b* gene (NM_015074.3; exon number according to the longest isoform of *Kif1bβ*). The RNA expression data on UCSC clearly showed that *PRAMEF11* and *LOC440563* were both only very weakly expressed in brain tissue whereas *KIF1b* displayed an extremely high expression pattern in diverse brain regions and in skeletal muscle. Moreover, we were not able to find the mutation in the NHLBI Exome Variant Server (http://evs.gs.washington.edu/EVS/). Zhao et al found that Kif1Bβ is a kinesin required for synaptic vesicle precursor transport in neurons (Zhao, Takita et al. 2001). Most interestingly, in the same paper they associated this gene with an autosomal dominant hereditary motoneuropathy, Charcot-Marie-Tooth disease type 2A. Brain sections of the *Kif1b* knock-out mouse generated by this research group showed an impaired development of the commissural fibers, which is in accordance with the MRI data from our patients. With regards to these background data our hypothesis that *Kif1bβ* was our candidate gene was therefore strengthened.

To check whether the mutation indeed affects splicing, we carried out several experiments to confirm its mutagenic potential. First, we used the online splice site prediction program on http://www.fruitfly.org. By entering the last 2382bp's of the genomic wildtype and mutant sequence of *Kif1bβ*, the program calculated the donor and acceptor splice site probabilities. In the wildtype sequence the donor splice site achieved the highest maximum score of 1 while the donor splice site was lost in the mutated sequence (Figure 6). The predicted acceptor splice sites, however, remained unaffected.

WT

Start	End	Score	Exon	Intron
254	268	1.00	gaccaag	gtgagtac
336	350	0.40	ctgtgag	gtctgtac
393	407	0.51	gtctggg	gtgagagg
809	823	0.40	gagtaca	gtgaggac
835	849	0.77	ggtgaag	gtccgtcc
1162	1176	1.00	caatacg	gtaagaag
1680	1694	0.40	ctcccag	gttcaagc
1827	1841	0.73	acctcag	gtgatcca
1871	1885	0.60	tacaagc	gtgagcca

MUT

Start	End	Score	Exon	Intron
254	268	1.00	gaccaag	gtgagtac
336	350	0.40	ctgtgag	gtctgtac
393	407	0.51	gtctggg	gtgagagg
809	823	0.40	gagtaca	gtgaggac
835	849	0.77	ggtgaag	gtccgtcc
1680	1694	0.40	ctcccag	gttcaagc
1827	1841	0.73	acctcag	gtgatcca
1871	1885	0.60	tacaagc	gtgagcca

Figure 6: Splice site prediction using www.fruitfly.org. The maximum score for a splice site prediction in the wildtype (WT) sequence was achieved for the position between 1162 and 1176bp's containing our target splice site (red square). In the mutant (MUT), however, the splice site was predicted to be lost.

To verify the mutation, we performed Sanger Sequencing on the DNA of all affected and unaffected family members. Only the patients were homozygous for the splice site mutation, while the unaffected were all heterozygous carriers (Figure 7).

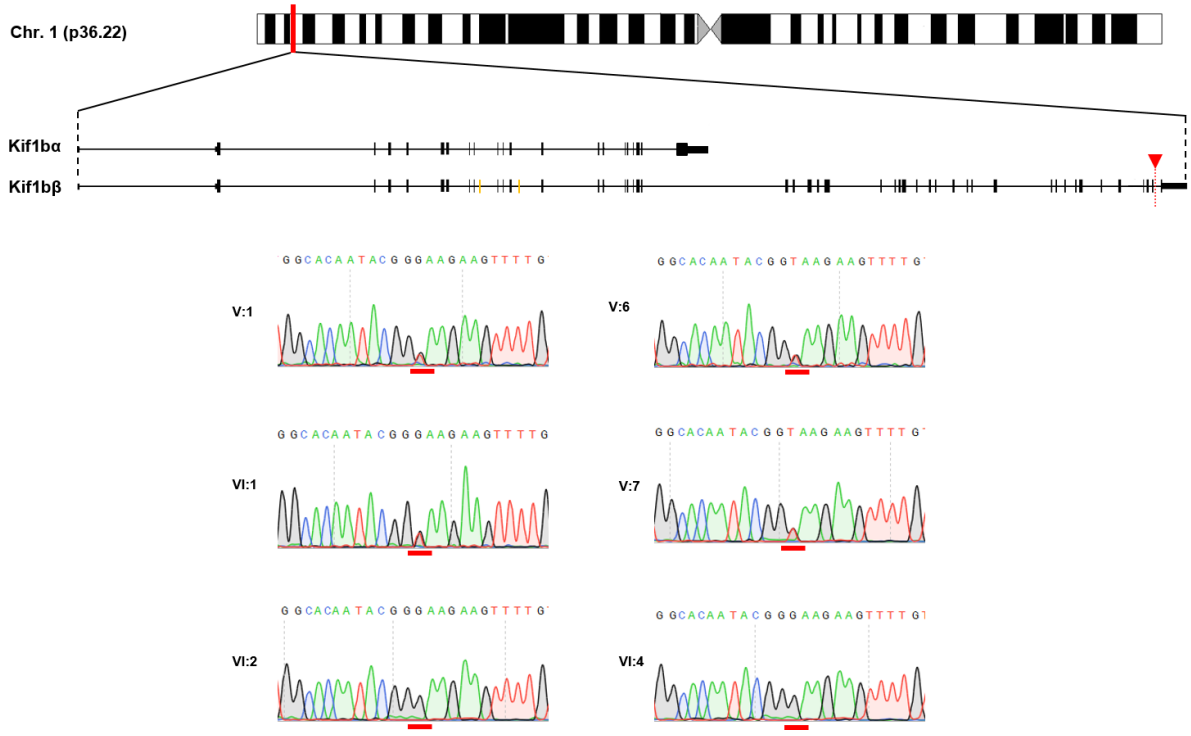

Figure 7: Sanger sequencing confirmed the c.5270+2T>G transition in the long isoform of *Kif1b*, *Kif1bβ*. The red arrow marks the mutation site. Exons in orange are present in the longest known isoform of *Kif1bβ* but are not included in the refseq sequence of NM_015074.3. The affected are homozygous for the mutation; the unaffected are heterozygous.

In parallel, we analyzed the segregation of the disease locus on chromosome 1 within the IDACC family using highly polymorphic markers D1S214 (6.962 Mb), D1S450 (9.585 Mb) and D1S2667 (11.486 Mb) (positions according to genome build hg19). This confirmed the disease-specific autosomal recessive inheritance pattern of the red haplotype, as only the affected were homozygous for the mutation and had two of the red alleles, while the healthy family members were heterozygous for the disease haplotype (Figure 8).

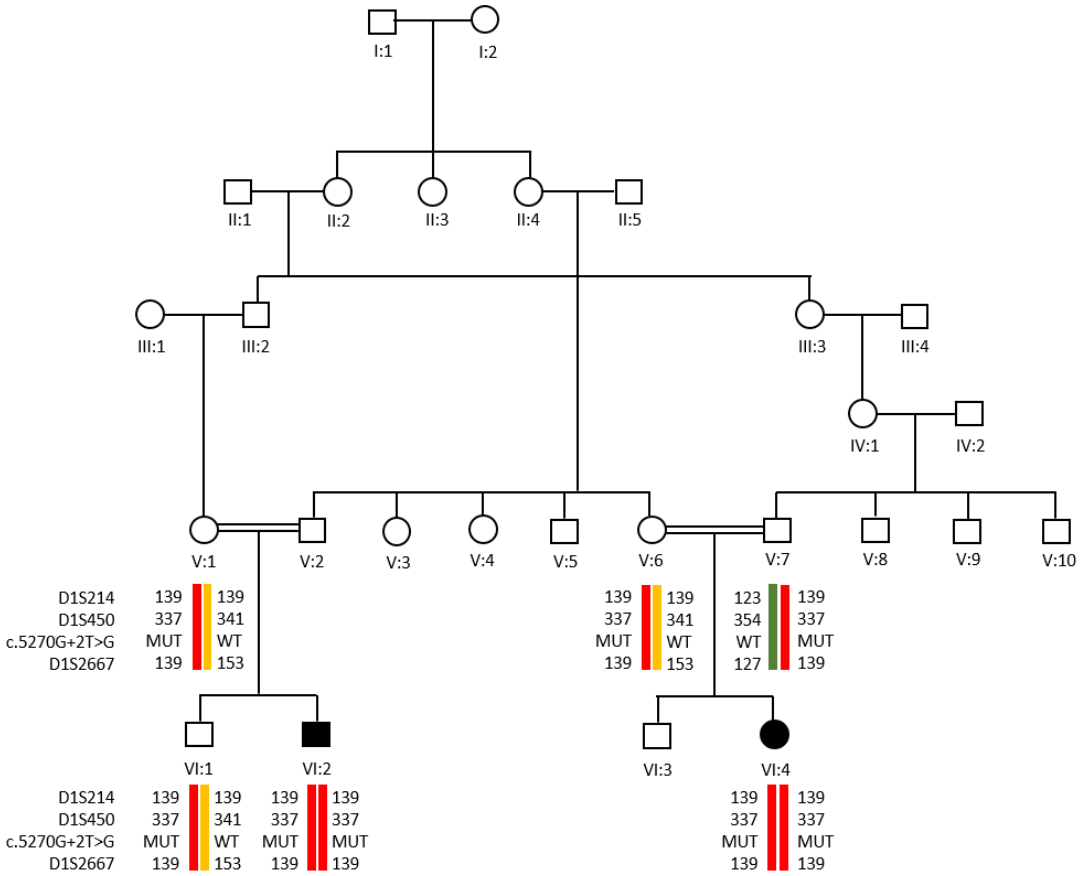

Figure 8: Segregation analysis. Highly polymorphic microsatellite markers confirm that only patients VI:2 and VI:4 are homozygous for the same haplotype (red) including the c.5270G+2T>G transition, while the non-affected family members are all heterozygous carriers.

To investigate how the mutation affects splicing, we analyzed the cDNA of VI:2 and VI:4. Primers located within exon 45 and 48 to span the entire exon 47 were selected. No alternative splice variants are known for this region. Therefore, all PCR products were expected to show the same size if the mutation has no impact on splicing. Already in the gel it was visible that the amplified product of both patient cDNAs was significantly smaller in size than the band derived from the human fetal brain control PCR (Figure 9A). Sanger sequencing confirmed the loss of exon 47 and the fusion of exon 46 with exon 48 (Figure 9B).

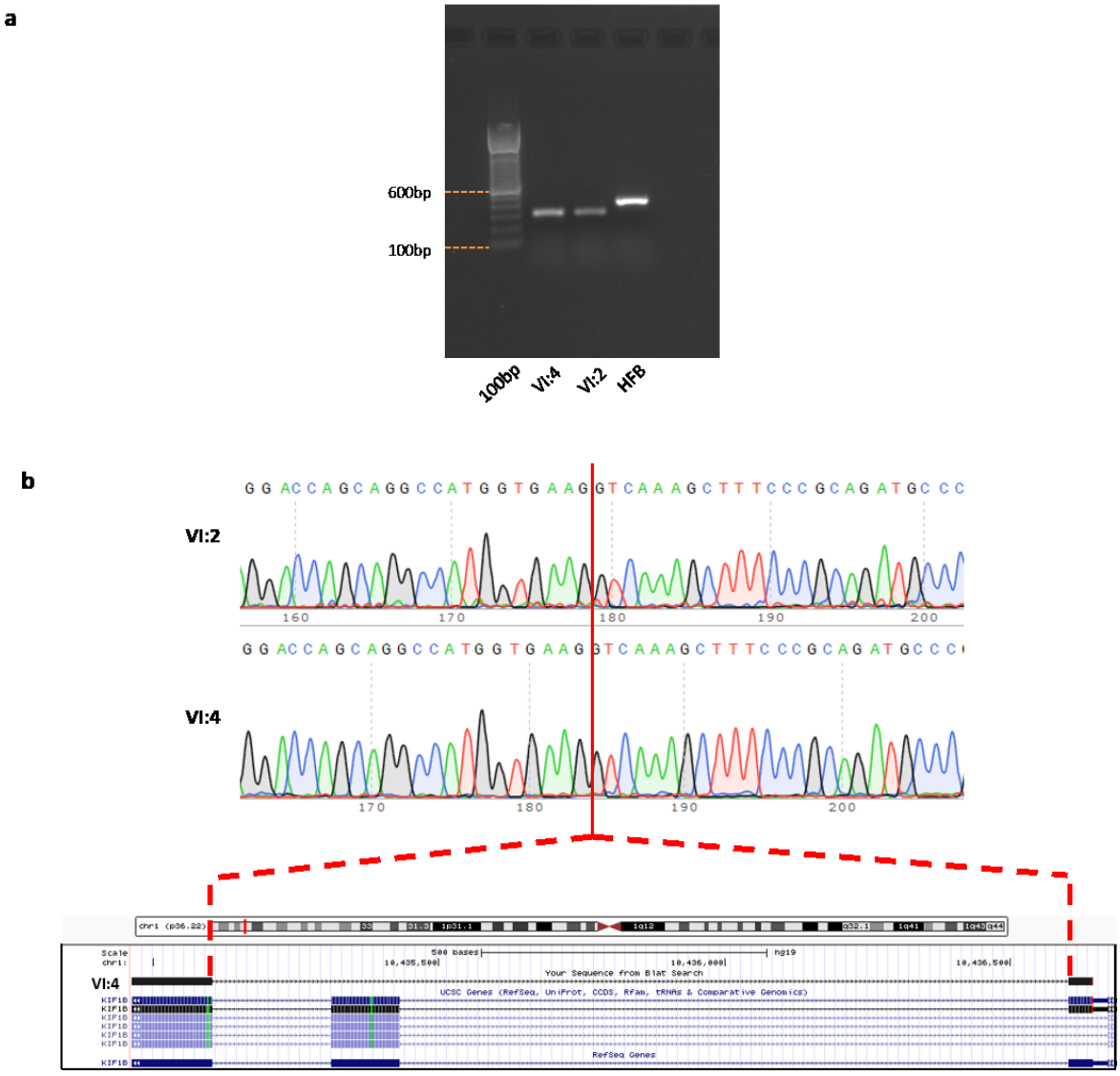

Figure 9: cDNA analysis of VI:2 and VI:4. **a**. PCR from human fetal brain (HFB) cDNA reveals a band at the expected size around 371bp while the PCR product of both patients is approximately 100bp smaller. Exon 47 is 119bp in size, which would be in line with the observed shift in size. No remaining WT splicing can be recognized on the gel. **b**. Sanger sequencing confirmed the fusion of exon 46 and 48 upon splicing. Sequence alignment using BLAT in the UCSC browser displays the missing exon (alignment of cDNA sequences of VI:4 are indicated in black).

Frameshift mutations eventually might lead to mRNA degradation after transcription. We thus questioned, if this alteration has a potential impact on mRNA stability. We therefore measured the total quantities of both *Kif1b* isoforms in lymphoblastoid cells derived from patients and an unrelated control LBC line and calculated its relative quantities to the amount of *Kif1b6* expressed in brain (Figure 10a).

As the shorter α isoform is not affected by the mutation, we expected its expression profile to remain consistent in all samples tested. qPCR data revealed equal mRNA levels in patients and the healthy controls. Moreover, this experiment also confirmed previously published data showing the much higher expression level of *Kif1bβ* in the brain compared with *Kif1bα* (Conforti, Dell'Agnello et al. 2003).

We further wanted to exclude a nonsense-mediated decay on protein level, as protein and mRNA expression levels do not always correlate. To test this, we performed a Western Blot in the laboratory of Ernst Malle comparing the expression in lymphoblastoid cells of both affected, the heterozygous mother of VI: 2, V:I, and two cancer cell lines (Hela and Jar). For this, we chose an antibody from Bethyl derived against the amino acid residues between 1575 and 1625 amino acids (CAC16629.1; GeneID 23095), targeting specifically the β isoform but not the mutated tail area. While KIF1Bβ levels in the lymphoblastoid cells were equal, the cancer cell lines the amount of KIF1Bβ protein varied, as expected (Figure 10b).

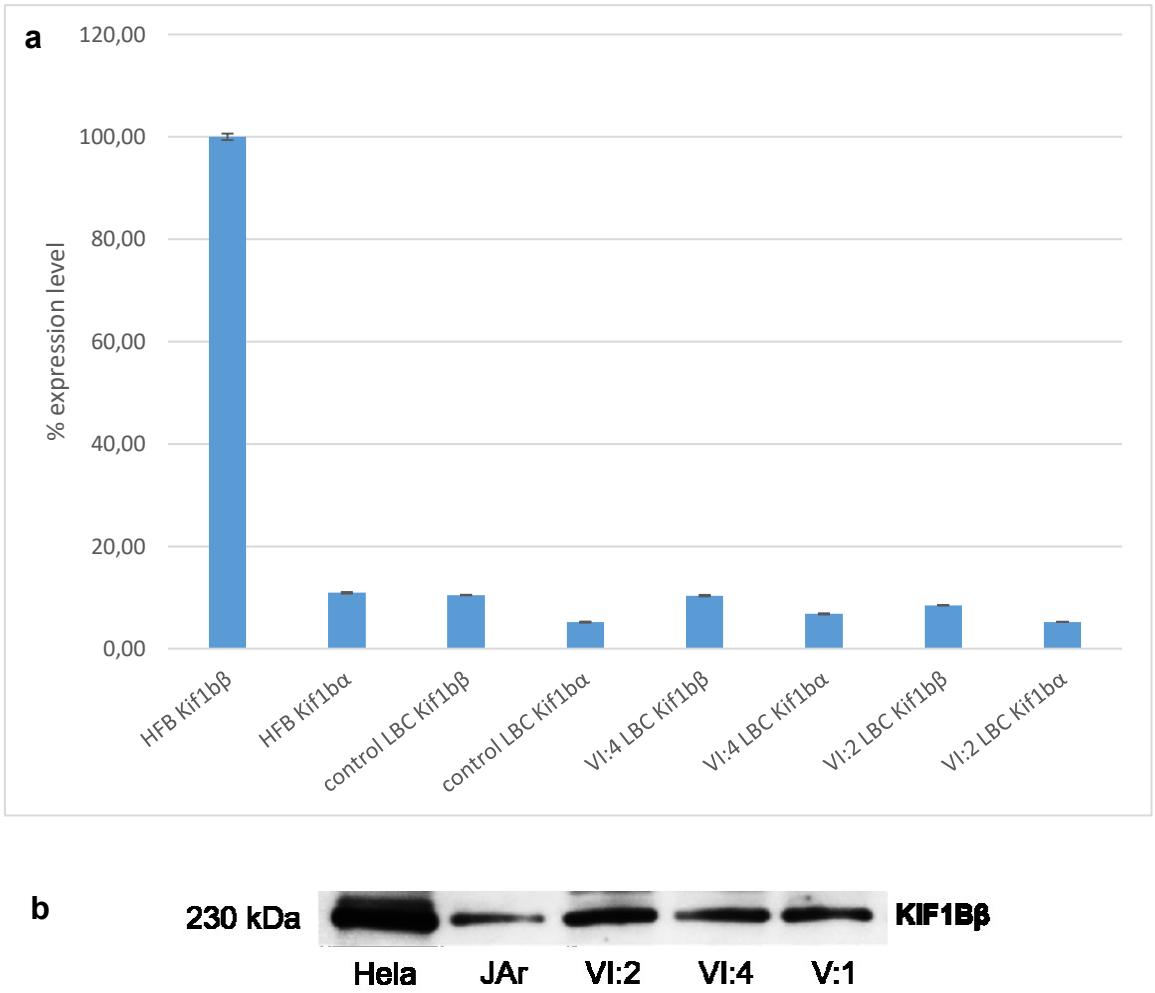

Figure 10: mRNA and protein expression of *Kif1bβ* and Kif1Bβ. **a.** Relative mRNA expression levels of *Kif1bα* and *Kif1bβ* in lymphoblastoid cells (LBC) from patients and a healthy, unrelated control compared to Kif1Bβ expression in human fetal brain. No decrease of *kif1bβ* mRNA levels compared to a wildtype *Kif1bβ* control LBC line were detectable. **b.** Western Blot with extracts from control cancer cell lines (Hela – suggested as a positive control by the company- and Jar) and from lymphoblastoid cells of VI:2, VI:4 and V:1 confirms the stability of the protein despite an altered tail domain.

This novel construct, however, induces a frameshift altering the entire C-terminal domain of *Kif1bβ* shifting the Stop codon into the 3'UTR region. This was confirmed by the online translation tool from the ExPASy Bioinformatics Resource Portal (https://web.expasy.org/translate/) (Gasteiger, Gattiker et al. 2003). Although the novel tail is longer, the entire protein sequence of the mutant is shorter due to the missing exon 47 (Figure 11).

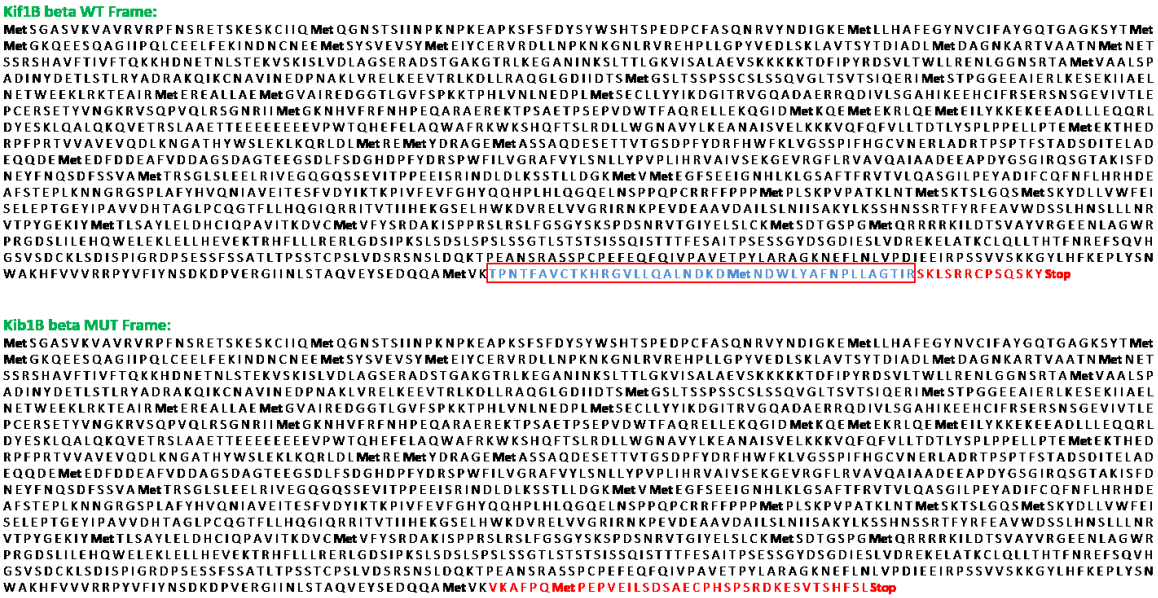

Figure 11: Predicted changes in DNA translation upon skipping exon 47. The blue sequence in the red square indicates the amino acid sequence which is lost in the mutated isoform upon splicing (lower protein sequence block). However, the sequence following the ablated exon is not identical with the C-terminal domain of the mutated protein (indicated in red letter).

To investigate the influence of the altered carboxy terminus on cellular localization, we cloned the full-length versions of wildtype and mutant Kif1bβ C-terminally fused to GFP into the pcDNA3.1 expression vector (pcDNA3.1-Kif1Bβ-WT-GFP and pcDNA3.1-Kif1Bβ-MUT-GFP) and overexpressed these in U2OS cells. For cloning we chose the 46 exon long isoform of *Kif1bβ* (NM_015074 with 1770 amino acids) (construct displayed in Figure 7 without the orange exons), which is associated with synaptic vesicle precursor transport. Since the motor domain that interacts with the microtubules remained intact we did not expect major changes in localization. Indeed, a brief first look did not reveal any interesting aberrations, but upon more detailed analysis we observed accumulated GFP granules in the wildtype Kif1bβ expressing cells. The mutant, however, showed a diffuse distribution of the GFP signal throughout the cytoplasm leaving cell organelles empty (Figure 12).

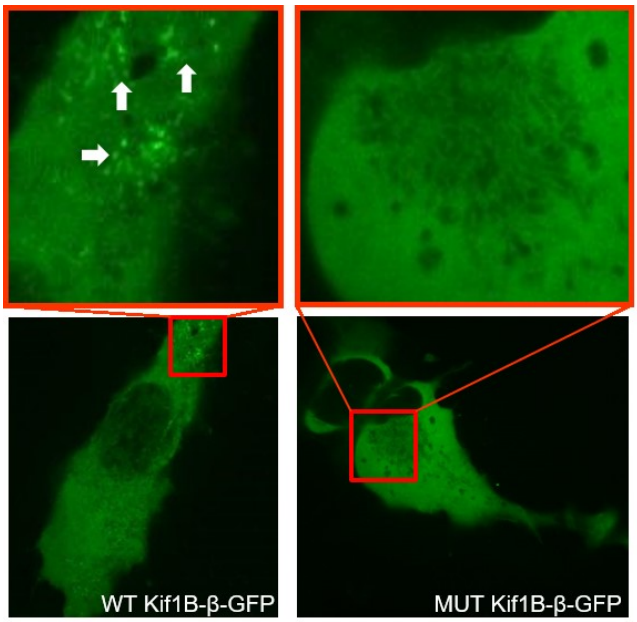

Figure 12: Overexpression of pcDNA3.1-Kif1Bβ-WT-GFP and pcDNA3.1-Kif1Bβ-MUT-GFP in U2OS cells 48 hours after transfection. Dense GFP expressing spots were recognized in the KIF1Bβ WT expressing cells, while they were undetectable in the cells overexpressing the mutated isoform.

Skipping of the second to last exon and the thus induced frameshift depletes a third of the highly conserved Pleckstrin homology (PH) domain of Kif1bβ required for the vesicle transport in neurons (see Figure 13).

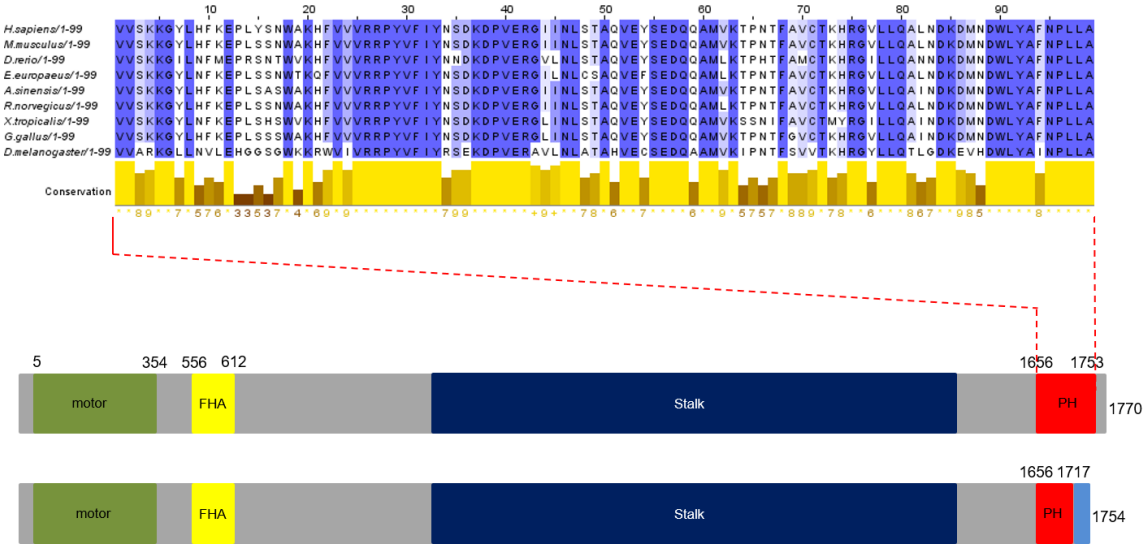

Figure 13: PH domain conservation and schematics of Kif1bβ WT and MUT protein isoforms. MAfftWS alignment in Jalview2.10.3 compares PH domain of various species (see material and methods). This highlights a high conservation grade. Blue grading indicates 100% (darkest blue) to 50% (lightest blue) conservation. The conservation grade bar on the bottom depicts extremely high conserved residues in yellow and those with lower conservation in brown. Schematic of altered protein tail domain of Kif1bβ compared to the 1770 AA long wildtype isoform. Motor= motor domain, FHA= forkhead-associated domain, stalk= stalk domain, PH= Pleckstrin homology domain.

Synaptic vesicle precursor transport is initiatedby the interaction of the PH domain with phosphatidylinositol 4,5-bisphosphate in the membrane of vesicles (Klopfenstein, Tomishige et al. 2002, Klopfenstein, Vale 2004). In particular, together with its PH domain containing kinesin-3 family member Kif1A, Kif1Bβ plays a major role in the post-Golgi transport of the neurotrophin receptor p75 ($p75^{NTR}$) in non-polarized cells (X. Xue, Jaulin et al. 2010). While *Kif1a* is indeed much more highlyexpressed in human fetal brain samples than *Kif1bβ* (see Figure 14) they are expressed at different time points during brain development (Zhao, Takita et al. 2001).

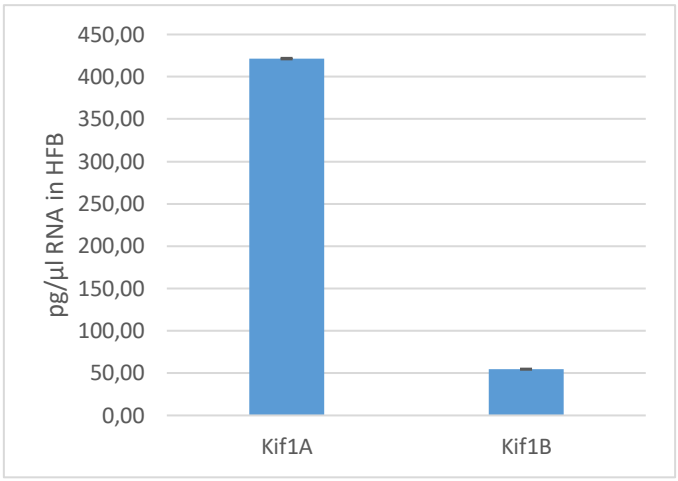

Figure 14: Quantification of *Kif1bβ* and *Kif1A* cDNA in human fetal brain (HFB) RNA.

P75^{NTR} is known to interact with all neurotrophins (NGF, BDNF, NT-3, NT-4) (Escudero, Lazo et al. 2014). It controls apoptosis in developing neurons and is essential for axonal outgrowth (E. J. Huang, Reichardt 2001). Thus we asked whether p75^{NTR} vesicle trafficking was affected. Therefore we simultaneously co-expressed p75-RFP (Addgene plasmid #24092, unpublished) with either wildtype or the mutated *Kif1bθ*. In *pcDNA3.1-Kif1bβ-WT-GFP* expressing cells, Kif1Bβ was clearly accumulating around vesicles containing p75-RFP (Figure 15a). Timelapse experiments allowed us to track vesicle movements within a co-expressed cell over several seconds. This demonstrated very clearly, that p75^{NTR} granules move along with KIF1Bβ. For the *pcDNA3.1-Kif1Bβ-MUT-GFP* transfected cells, however, co-expression could not be observed. In these cells vesicle membranes were solely visualized by p75-RFP expression (Figure 15b).

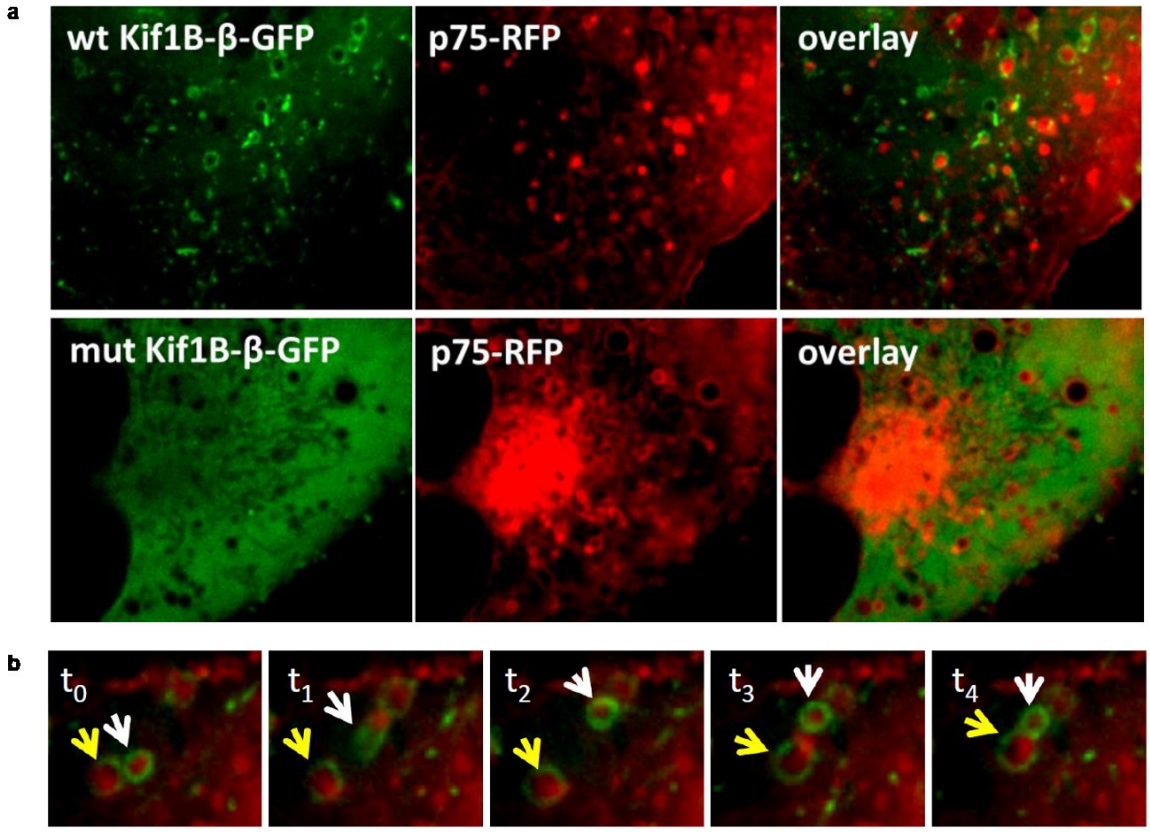

Figure 15: Co-expression of pcDNA3.1-Kif1Bβ-WT-GFP and pcDNA3.1-Kif1Bβ-MUT-GFP with p75-RFP. **a**. KIF1Bβ-WT accumulates around p75NTR containing vesicles. In KIF1B-MUT expressing cells co-localization is impaired. **b**. Recording of vesicle movement in co-expressed WT cells. $P75^{NTR}$ vesicles transported by KIF1Bβ-WT move synchronously through the cell. t_0-t_4 indicate time points. Yellow and white arrows mark two recorded vesicles for easier tracking of movements.

As we wanted to confirm that this phenotype is caused by the impairment of the PH-domain, we cloned the wildtype and mutant tail domain into the pcDNA3.1 vector containing an N-terminal GFP fusion protein (starting with amino acid 1669) (Figure 16a). Figure 16b illustrates the overexpression of the recombinant proteins in U2OS cells. Although the GFP expression was now detected across the entire cell (even in the nucleus), we observed the same differences as when expressing the full-length constructs. Co-localization occured when the wildtype tail domain was simultaneously overexpressed with p75-RFP. In cells transfected with the novel alternatively spliced tail domain, $p75^{NTR}$ vesicles failed to co-localize with the mutated Kif1bβ tail.

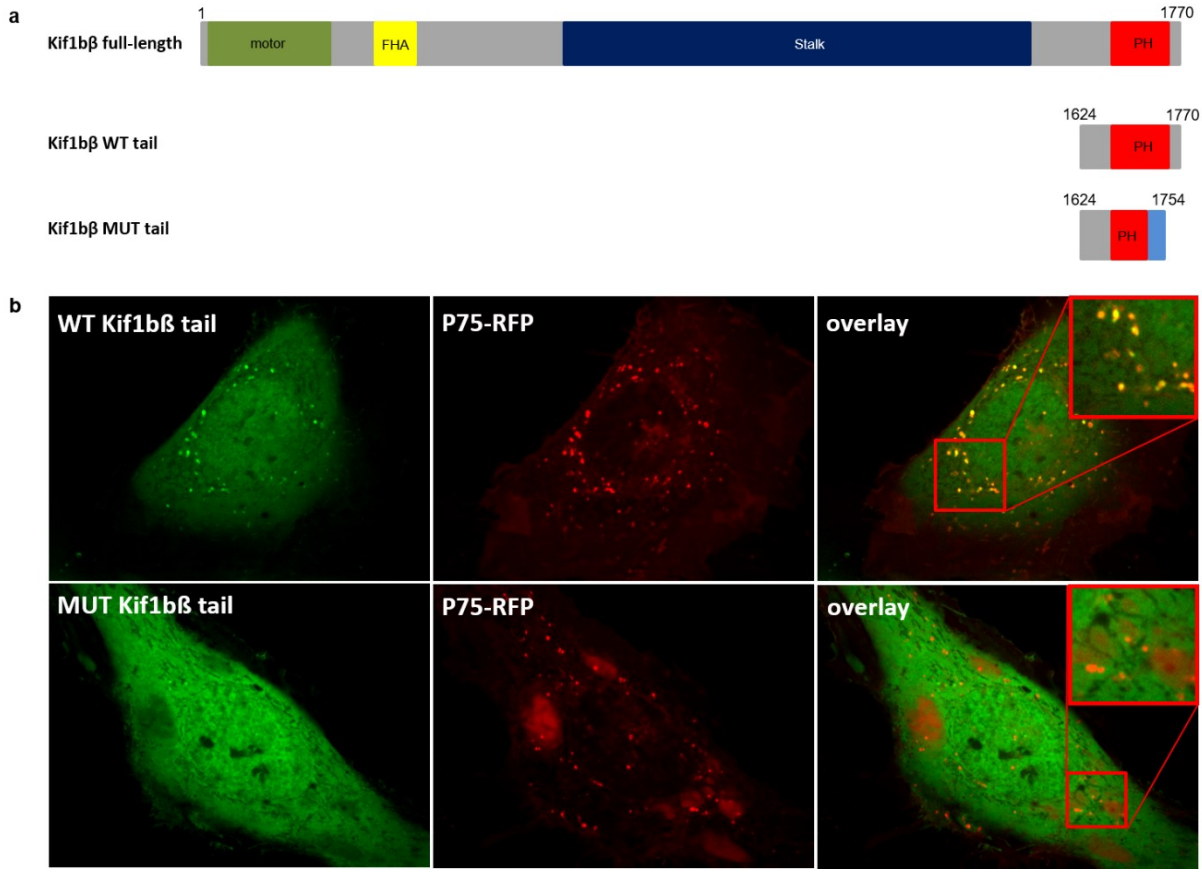

Figure 16: Co-expression of WT and MUT C-terminal domains with p75-RFP. **a**. Schematic presentation of KIF1Bβ WT and MUT tail domains cloned into pcDNA3.1-NT-GFP. Numbers indicate amino acid positions in the full-length reference protein. Motor= motordomain, FHA= forkhead-associated domain**,** Stalk= stalk domain, PH= Pleckstrin homology domain **b**. GFP-expressing granules of the wildtype KIF1Bβ tail domain are overlapping with p75 expression. Expression of the mutated KIF1Bβ tail construct is found throughout the cell with no preferential localization.

As before, we recorded the movements of the expressed KIF1Bβ-tail domains. Pronounced GFP-expressing areas in cells expressing the WT tail domain show full-length construct-like movements while upon expression of the mutated carboxy terminus, the GFP signal remains diffusely distributed within the cell with no recognizable movements. We therefore concluded that $p75^{NTR}$ vesicle transport is severely impaired upon loss of the second to last exon of *Kif1bβ*.

Recently, the C-terminal part (the last 552 amino acids) of KIF1Bβ was reported to interact with calmodulin (CaM), the major receptor for intracellular calcium (Charalambous, Pasciuto et al. 2013). In addition to the fact, that CaM is known to play a crucial role in axon extension and guidance through the midline by controlling

the response of the commissural fibers to the repulsive signals (Kim, Furman et al. 2001), it has been shown to recruit KIF1Bβ to synapses upon presynaptic depolarization induced by Ca^{2+} influx, thereby controlling thereby vesicle exocytosis (Charalambous, Pasciuto et al. 2013). Although only a small portion of the tail is altered in the mutant (last 33 AA's), we wanted to see if this influences the binding of CaM to KIF1Bβ. This Pull-Down assay was performed by Chintan Navinchandra Koyani in the laboratory of Ernst Malle. After immunoprecipitating native KIF1Bβ from lymphoblastoid cells of the patients, the heterozygous mother and an unaffected control, we checked whether we were able to find CaM in the precipitate. Interestingly, while we did not observe altered CaM levels in the co-immunoprecipitated fraction of the heterozygous mother compared with the healthy control, CaM interaction with KIF1Bβ was almost completely abolished in the lymphoblastoid cells of the patients (Figure 17).

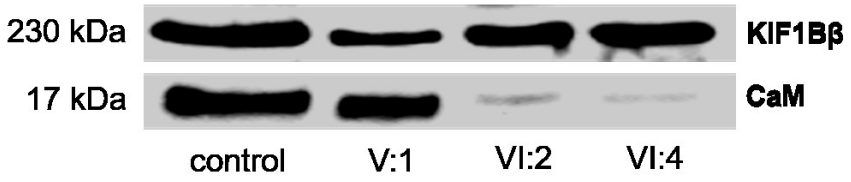

Figure 17: Co-immunoprecipitation of KIF1Bβ (upper line) and calmodulin (CaM; lower line). Respective protein sizes are indicated on the left. Only a faint band is seen for CaM in the fraction of VI:2 and VI:4 indicating a loss of interaction between KIF1Bβ and CaM.

In summary, these data suggest that our splicing defect in *Kif1bβ* is most likely associated with the developmental central nervous defect found in our IDACC family. However, it is interesting that mutations in the same gene can account for different neurological diseases. CMT2A is an autosomal dominant (rare recessive cases have been reported) axonal peripheral sensorimotor neuropathy affecting the lower rather than the upper limbs and is caused mostly by mutation in the mitofusin2 gene (Bombelli, Stojkovic et al. 2014). Disease onset is within the first 10 years or later primarily due to degeneration of peripheral axonal fibers (Sole, Ferrer et al. 2009). Abnormal mitochondria morphologies are typical hallmarks when investigating affected neurons. As for axons are highly dependent on synaptic mitochondria delivery, this has been suggested to be the molecular cause of CMT2A

(Chen, Chan 2006). Kif1Bα but not β is known to be associated with mitochondrial transport (Conforti, Dell'Agnello et al. 2003). As shown, in the brain, the α isoform is expressed at significant lower levels than the β isoform. Thus, we wondered if the expression pattern of *Kif1bα* and *β* in muscle is reversed. By relative quantification of both isoforms in human fetal brain and muscle RNA we saw that compared to the longer *Kif1bβ* the *α* isoform was indeed higher expressed in muscle tissue (Figure 18). The CMT2A mutation is located in the motor region of the gene thus affecting both isoforms. This could therefore offer an explanation for the influence of the Q98L mutation on peripheral neuron degeneration and why we do not see neuropathy-related signs in our patients and the heterozygous, non-affected family members.

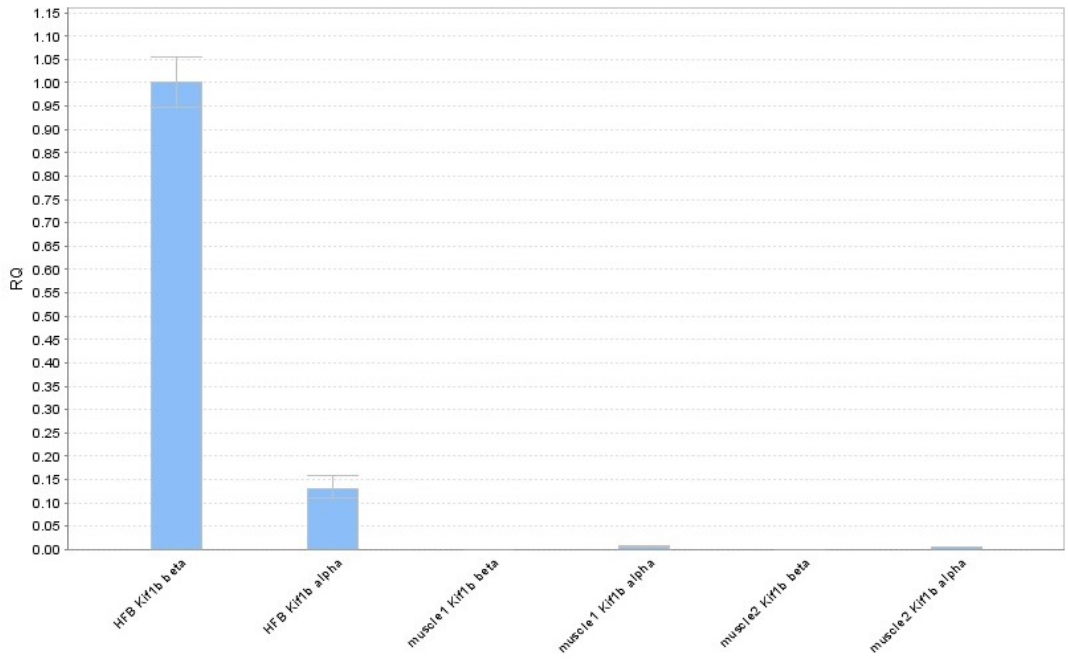

Figure 18: Quantification of *Kif1bβ* and *Kif1bα* levels between human fetal brain and muscle tissue relative to *Kif1bβ* levels in human fetal brain. The *Kif1bβ* isoform is expressed at significantly higher levels in brain than *Kif1bα.* However, in muscle tissue of 2 different donors, the α isoform is more abundant compared to *Kif1bβ.* HFB= human fetal brain; RQ= relative quantification level

More recently homozygous *Kif1bβ* mice deleterious for the second last exon of *Kif1bβ* were generated by David Keays' research group at the Research Institute of Molecular Pathology (IMP) in Vienna. Detailed phenotypic characterizations are still pending, but all homozygous littermates died shortly after delivery and showed

severe brain abnormalities (personal communication), which is in line with previous observations in *Kif1b* complete knockout mice (Zhao, Takita et al. 2001). These results confirm that Kif1Bβ is fundamental during brain development and that the homozygous splice site mutation is causative for the brain developmental disorder detected in our patients.

3.2 HsSASS-6 is mutated in autosomal recessive primary microcephaly

The following findings have been published in Human Molecular Genetics in 2014 (Khan, Rupp et al. 2014). Pictures and tables are identical with those in the publications; some text passages may also overlap.

As mentioned in chapter 1.5, MCPH is a rare disease in the non-consanguineous population. In Pakistan, however, first-cousin marriages are still common, with a frequency of 54% in rural areas (Agha 2016). We here report about a Pakistani family from Dera Ismail Khan, a city in the Khyber Pakhtunkhwa province, with four individuals affected with autosomal recessive primary microcephaly (MCPH), including two girls at the age of three and six (V:3 and V:1) and two adult brothers (VI:7 and VI:8). All MCPH patients were progeny from consanguineous marriages (Figure 19).

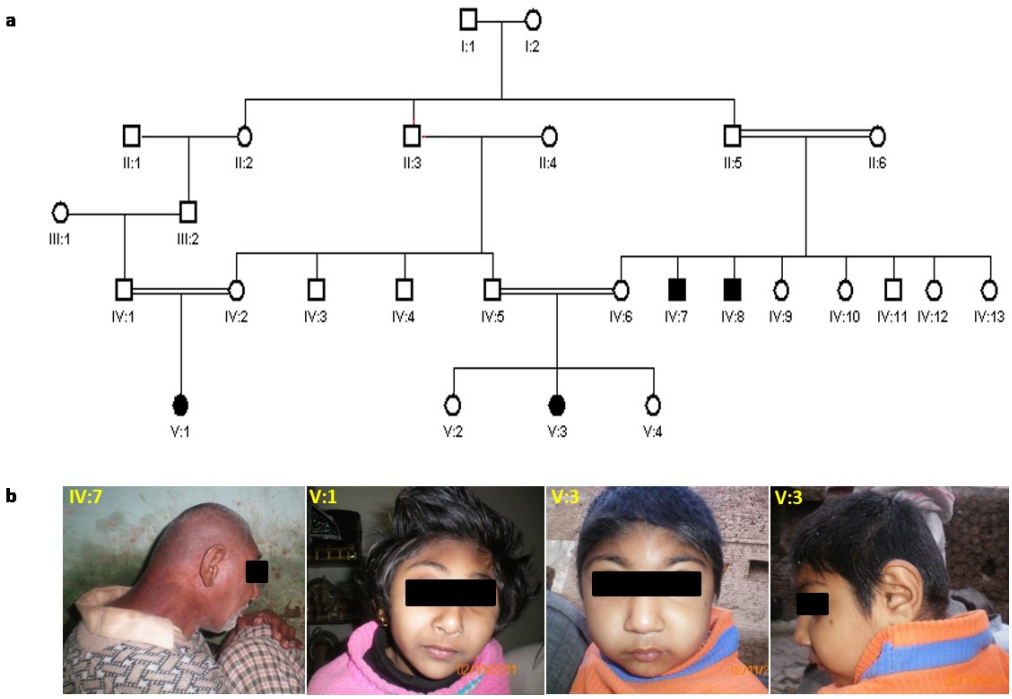

Figure 19: Pedigree and pictures of the MCPH family. **a.** Affected are children of consanguineous parents. **b.** Patients VI:7, V1 and V:3. Due to the small head ears, nose and eyes (not shown here) appear larger than normal (pictures reproduced from (Khan, Rupp et al. 2014) with permission of Human Molecular Genetics).

All affected had a significantly smaller head with an occipitofrontal head circumference clearly below the 3rd percentile. This was combined by intellectual disability (IQ levels ranging between 20 and 40) and seizures in VI:7 and VI:8. Although the two older patients had a smaller height compared to other people their age, this was not a feature reported to differ much from the other family members. Although muscle tone and bone development were normal, V:1 was not able to walk by the age of six. All patients struggled to pay attention and showed aggressive behavior. Communication with the affected was difficult due to limited speech and severe pronunciation problems. Routine tasks, such as going to the toilet or dressing were not manageable without help. Moreover, for V:I strabismus on the right eye was diagnosed. Clinical data are summarized in Table 6.

Table 6: Clinical data of affected MCPH patients (table reproduced from (Khan, Rupp et al. 2014) with permission of Human Molecular Genetics).

Pedigree ID	**VI:7**	**VI:8**	**V:3**	**V:1**
Age (Years)	50	42	3.5	6
Gender	Male	Male	Female	Female
Occipitofrontal circumference	47 cm (SD= -6,63)	41.5 cm (SD= -10,26)	35 cm (SD= -19,6)	38.5 cm (SD= -15)
Height	155 cm	157 cm	82 cm	95 cm
Behavior	Aggressive	Aggressive	Aggressive	Aggressive
General physique	Weak	Normal	Weak	Normal
Epileptic shock	Yes	Yes	No	No
Facial expression	Active	Active	Dull	Active
Attention	No	Low	Low	Low
Muscle tone	Normal	Normal	Normal	Normal
Adaptive Behavior				
Self-Feeding	Yes	Yes	Yes	Yes
Toilet training	No	Weak	No	No
Dressing/undressing training	No	No	No	No
Reading/Writing	No	No	No	No
Self-care	No	No	weak	No
Level of conveying their message	Very weak	Very weak	Very weak	Very weak

SD= standard division

Computed tomography (CT) of patient V:3 confirmed a microcephalic brain with poorly defined ganglia. Additionally, delineation of the internal capsule was missing, infratentorial abnormalities, a hypoplastic vermis cerebellar and deformation of lateral ventricles were noted (Figure 20).

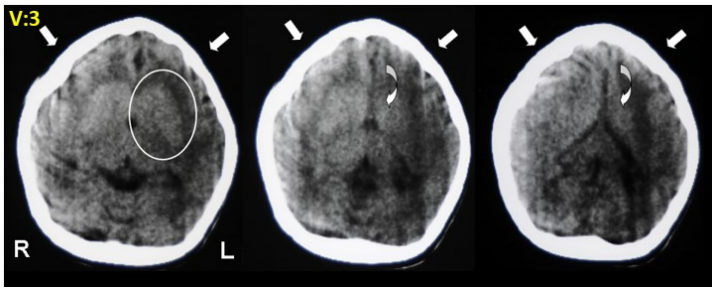

Figure 20: Computed tomography of V:3. Selected axial slices of cranial computed tomography. Notwithstanding compromised image quality, some distinct features can be noted: diminished cranial circumference with symmetrically poorly developed frontal lobes (arrows; also note deformed shape of the skull), poorly confined basal ganglia (oval) with missing delineation of the internal capsule, dysmorphic lateral ventricles (curved arrows; slit-like frontal horns), and infratentorial abnormality with hypoplasia of the vermis cerebelli (images not shown) (figure and text reproduced from (Khan, Rupp et al. 2014) with permission of Human Molecular Genetics).

Due to the aggressive behavior of patient IV:8 DNA could only be collected from patients IV:7, V:1 and V:3 as well as from several other unaffected family members. Assuming that the disease causing gene was located within an autozygous area of the genome, SNP genotyping was performed on individuals IV:7, V:3 and V1 using a 250K array from Affymetrix. Most interestingly, only one homozygous locus with identical haplotype patterns was shared by all three spanning a 18,53Mb region on chromosome 1p21.3-p13.1. This interval was restricted by SNPs rs555557 (98,912,075bp) and rs2251406 (117,445,365bp) and did not harbor any known MCPH genes (Figure 21a). This suggested the discovery of a novel MCPH locus, namely MCPH14. Full scale linkage analysis calculated a maximum multipoint LOD score of 3.9 for this locus (Figure 21b).

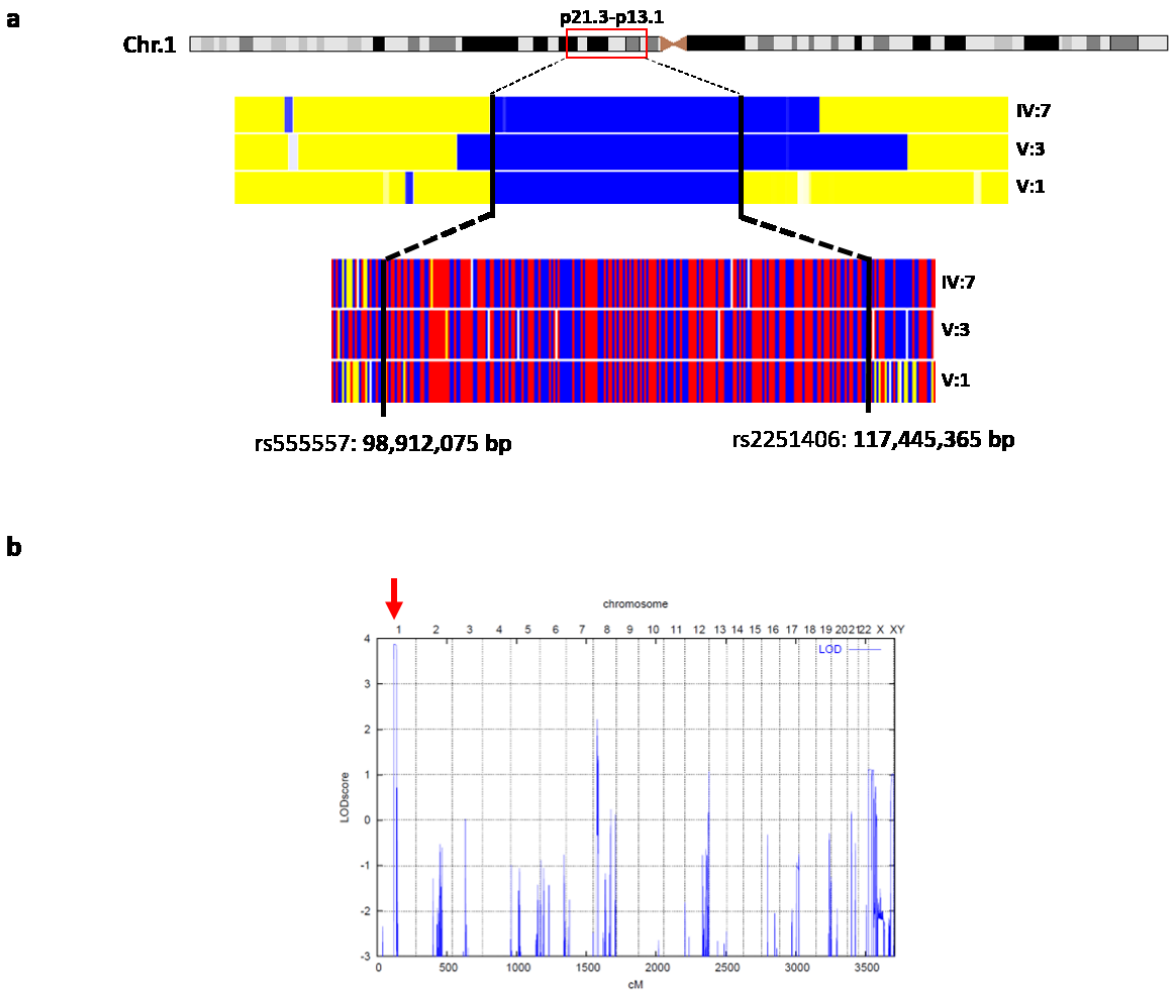

Figure 21: Homozygosity mapping and linkage analysis. **a.** 250K NspI SNP array reveals a homozygous 18,53Mb stretch (blue) with identical haplotype on chromosome 1p21.3-p13.1 restricted by SNP rs555557 and rs2251406 in all three patients. **b.** Parametric linkage analysis of the family. LOD scores (y-axis) are plotted over genetic distance in cM (centi Morgan) across the genome (x-axis), where chromosomes are concatenated from p-ter to q-ter from left to right. A single LOD score peak at 3.9 cM (red arrow) marks the locus on chromosome 1 (figures and text reproduced from (Khan, Rupp et al. 2014) with permission of Human Molecular Genetics).

To confirm intrafamilial segregation we conducted STS marker analysis using 6 highly polymorphic microsatellite markers, including D1S2719 (96,8Mb), D1S2739 (98,9Mb), D1S2671 (101,6Mb), D1S206 (101,6MB), D1S495 (102,56MB) and D1S2726 (111,18MB) (Figure 22). All affected were homozygous for the same haplotype between marker D1S2671 and D1S2726 whereas the healthy family members did either carry one copy of the green haplotype or none (as for V:2).

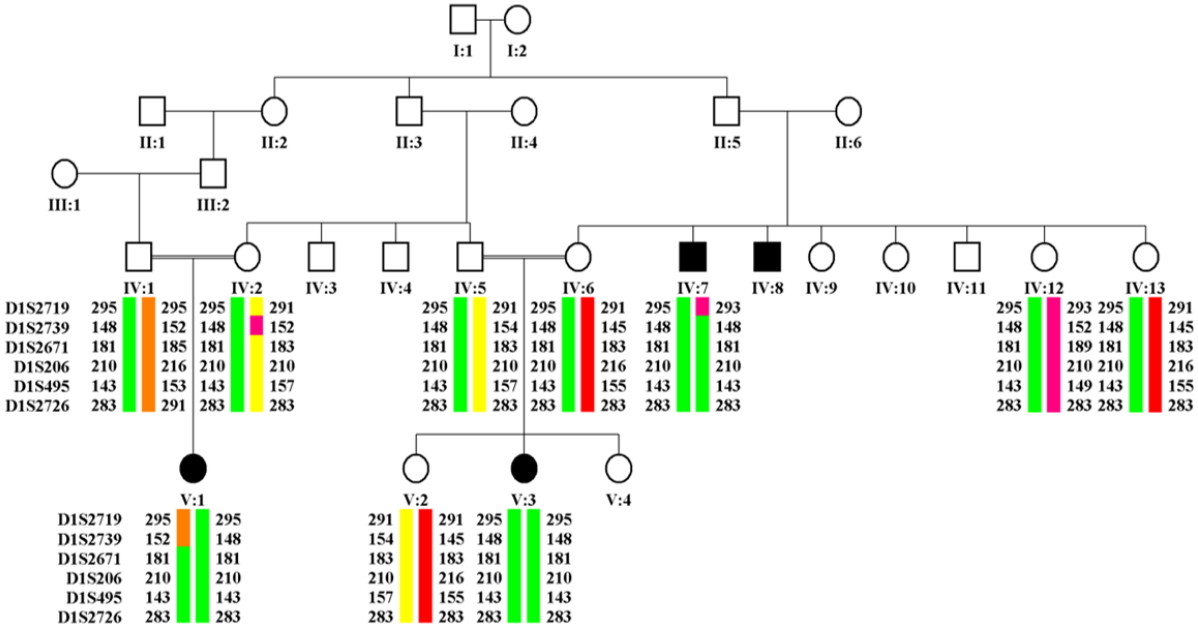

Figure 22: Microsatellite marker analysis. The green allele between STR marker D1S2671 and D1S2726 segregates in the family in an autosomal recessive manner (figure reproduced from (Khan, Rupp et al. 2014) with permission of Human Molecular Genetics).

We also calculated the two-point and multipoint LOD scores for these STR markers, achieving maximum values of 2.8 and 3.53, respectively (Table 7).

Table 7: Two-point and multipoint LOD score analysis. Highest two-point LOD score was achieved for marker D1S495, for multipoint LOD score calculation, a maximum score of 3.53 was calculated for the area between marker D1S2671 and D1S495 (table reproduced from (Khan, Rupp et al. 2014) with permission of Human Molecular Genetics).

Marker information		Two point LOD score at θ							Multipoint LOD score
Marker name	Genetic position in cM	0	0.01	0.05	0.1	0.2	0.3	0.4	
D1S2719	125.36	1.1878	1.1663	1.0671	0.9244	0.6203	0.3429	0.1322	1.9798
D1S2739	127.1	0.5384	0.8588	1.129	1.0802	0.7298	0.3472	0.1028	-0.0809
D1S2671	129.55	2.5335	2.4658	2.1917	1.844	1.1526	0.5427	0.1518	**3.5256**
D1S206	129.55	0.8813	0.8575	0.756	0.6219	0.3614	0.1569	0.0406	-
D1S495	131.32	2.7667	2.6977	2.4179	2.0615	1.3456	0.6948	0.2348	**3.527**
D1S2726	139.6	0.4233	0.4088	0.3525	0.2866	0.1732	0.0886	0.0324	**3.0448**

Next, we screened the target locus for potential disease genes that either play a role during cell division or cell cycle control as for most of the 13 known MCPH genes have a major impact on either of these (see table Table 1: Primary microcephaly genes We selected four genes for subsequent Sanger Sequencing, including *WDR47, PSRC1, NGF* and *SASS6* (hereafter referred to as *HsSASS-6*). Only in *HsSASS-6,* a well-characterized gene encoding for a protein involved in procentriole formation during cell division (Gonczy 2012, Rodrigues-Martins, Bettencourt-Dias et al. 2007, Leidel, Delattre et al. 2005, Strnad, Leidel et al. 2007, van Breugel, Hirono et al. 2011, Gopalakrishnan, Guichard et al. 2010), we eventually detected a homozygous missense mutation, c.185T>C (NM_194292.1; Chr.1:100588787A>G). Lying within a highly conserved region in exon 3, the transition leads to an amino acid replacement of the non-polar and hydrophobic isoleucine with a hydrophilic and polar threonine (p.Ile62Thr). All available family members were further screened for the mutation. Results were in line with the STR marker analysis. While all affected were homozygous for the mutation, the healthy family members were either heterozygous carriers or displayed the wildtype sequence (V:2) (Figure 23).

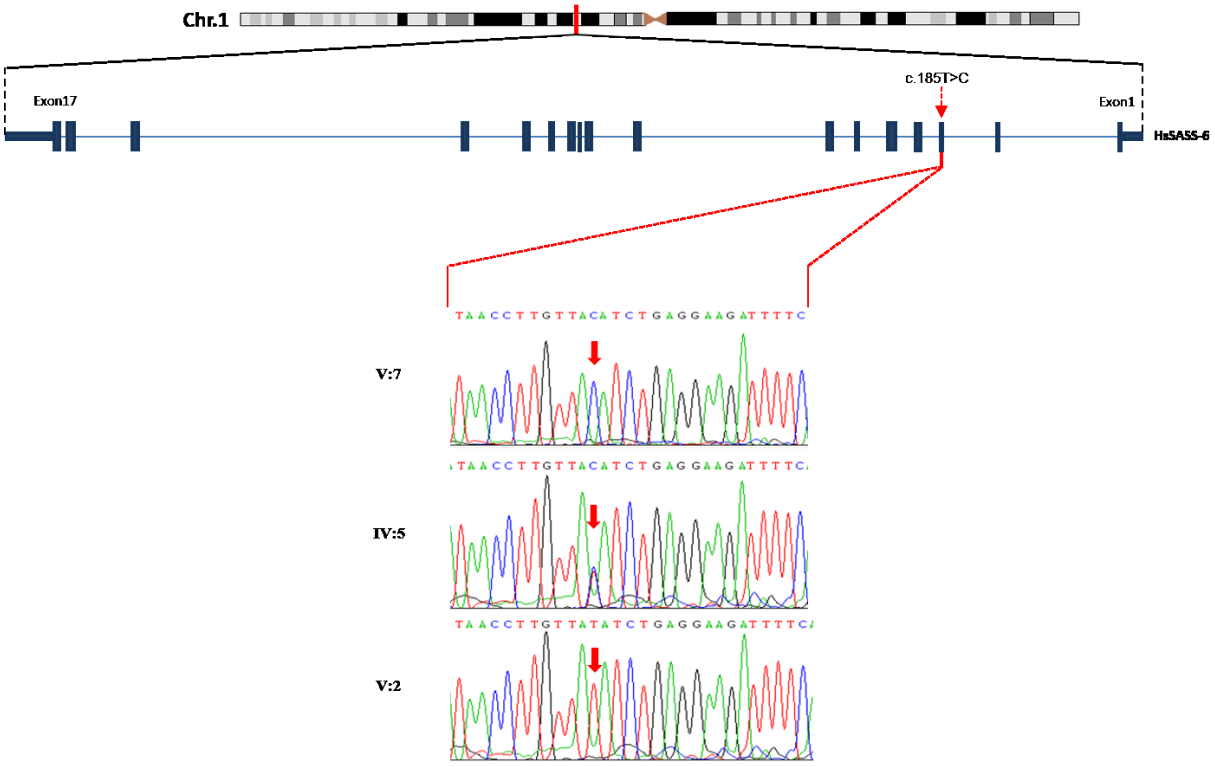

Figure 23: Sanger sequencing confirmed a homozygous c.185T>C mutation in *HsSASS-6* in the patients (represented by sequence of V:7) and either heterozygous (IV:5) or wildtype sequences in non-affected family members (mutation site indicated by red arrow). The gene itself is oriented in reverse (sequencing traces are reproduced from (Khan, Rupp et al. 2014) with permission of Muzammil Khan et al and Human Molecular Genetics).

As a control we sequenced the mutation site in 116 healthy, unrelated Pakistani individuals with no result. Additionally, 19 more unresolved MCPH families from Pakistan were unsuccessfully screened for mutations in *HsSASS-6*.

Although we only had a single locus, we wanted to exclude all other known microcephaly genes for potential compound heterozygous mutations as well as all remaining genes in the MCPH14 locus. Therefore, whole exome sequencing was conducted. Although we were able to definitely exclude all 13 MCPH genes, we found another mutation in a gene situated in the homozygous interval on chromosome 1 and encoding for a protein regulating actin polymerization, namely *CAPZA1* (Maun, Speicher et al. 1996). The c.656C>T (p.Ser219Leu) missense mutation was located in the splice site of exon 8 and as the mutation in *HsSASS-6*, it was not listed in the NHLBI Exome Variant Server (http://evs.gs.washington.edu/EVS/).

Analysis in PolyPhen2 and ConDel predicted the mutation in *Hs-SASS6,* but not the mutation in *CAPZA1* to be potentially pathogenic (PolyPhen2: HsSAS-6 p.Ile62Thr: score = 1.0; CAPZA1: p.Ser219Leu: score = 0.014; and ConDel: HsSAS-6 p.Ile62Thr: score = 0.847; CAPZA1: p.Ser219Leu: score = 0.001). Alternative splicing variants caused by the *CAPZA1* mutation were excluded by RNA analysis. For this we picked primers spanning the region between exon 7 and the last exon 10. However, gel electrophoresis of the PCR products already clearly highlighted that no alternative transcripts were present as we obtained the same band sizes as in the analysis of mRNAs from two healthy and unrelated controls (Figure 24). Sanger sequencing confirmed normally spliced wildtype *CAPZA1* transcripts. Additionally, knock-out experiments in mice did not show any association of this gene with any cell division defects (Neumann, Walter et al. 2010). Thus, we excluded *CAPZA1* as a potential MCPH disease gene.

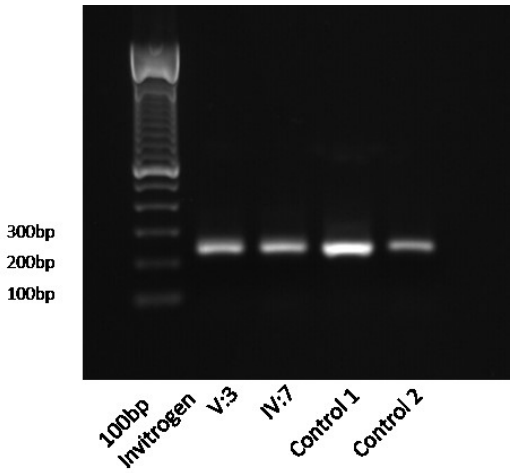

Figure 24: cDNA analysis of *CAPZA1*. cDNA analysis of the two patients V:3 and IV:7 reveal the same 242bp PCR products as the amplicons from the unaffected controls. Relevant 100bp standard sizes are shwon on the left side (figure reproduced from (Khan, Rupp et al. 2014) with permission of Human Molecular Genetics).

HsSAS-6, however, has already been studied in detail and is known to be essential to ensure proper cell division (Strnad, Leidel et al. 2007, Leidel, Delattre et al. 2005, Nakazawa, Hiraki et al. 2007). The gene itself consists of 17 exons coding for a 657 amino acid long protein. Upon procentriole formation, HsSAS-6 dimerizes and

interacts via the head domain with nine more homodimers to form the hub and spokes of a cartwheel like ring structure and initiates the establishment of the daughter centriole (Kitagawa, Vakonakis et al. 2011, Hilbert, Erat et al. 2013, Gonczy 2012). The Ile62 residue is located within the highly conserved PISA domain supporting the formation of the N-terminal head domain of HsSAS-6 (Figure 25).

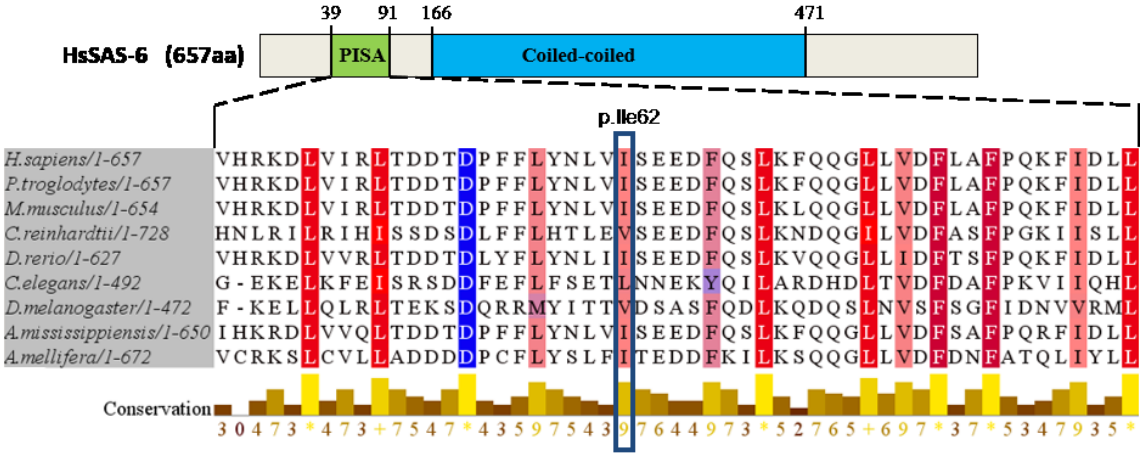

Figure 25: Conservation and location of the Ile62 residue in the DrSAS-6 head domain. a. Conservation of the SAS-6 PISA domain in nine different organisms is highlighted by MAfftWS alignment analysis in Jalview2.8. Residues are colored according to the hydrophobicity table of Kyte and Doolittle (Kyte, Doolittle 1982). Red indicates conserved hydrophobic, blue the conserved hydrophilic residues. Shading intensities represent the conservation grade of the hydrophobicity (dark=very conserved; white= not conserved) (figure and text reproduced from (Khan, Rupp et al. 2014) with permission of Human Molecular Genetics).

So far, crystal structures of the human HsSAS-6 are not available since recombinant human SAS-6 proteins are not soluble (own, unpublished experiments). Thanks to existing high resolution crystal structure of the head of the *Danio rerio* homolog, DrSAS-6, the exact position of the mutated residue was determinable. This highlighted that the Ile62 residue (green spheres) is located within the hydrophobic core of the head together with the highly conserved Leu44, Leu60, Leu70, Phe80, Phe83 and Leu139 as shown by Figure 26.

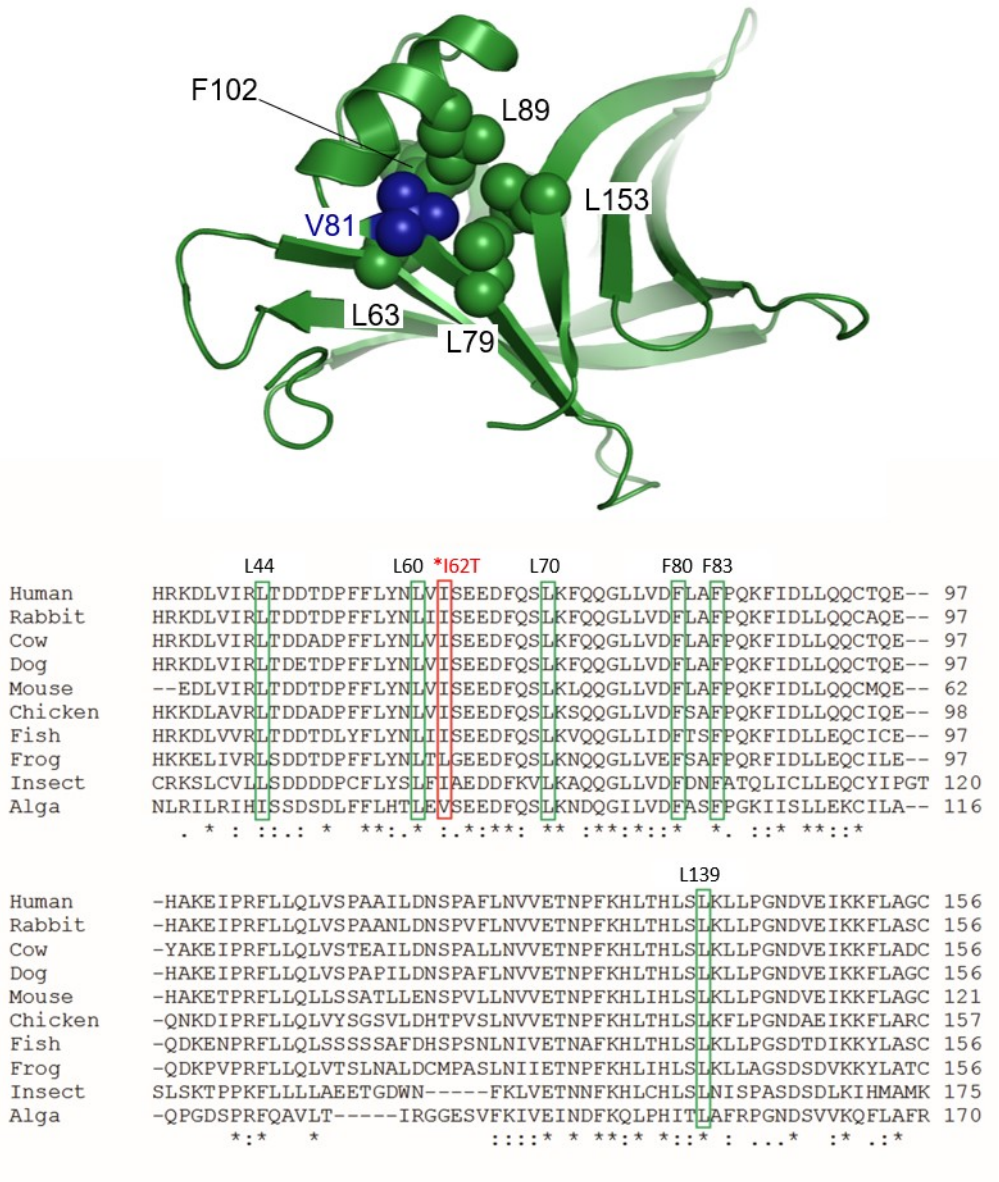

Figure 26: Crystal structure of the head domain of danio rerio (Dr) SAS-6 and conserved residues interacting with it. The I62 residue (indicated in blue spheres) lies within the hydrophobic core in close proximity to highly conserved hydrophobic amino acid residues (marked as green spheres). HsL44=DrL63, HsL60=DrL79, HsI62=DrV81, HsL70=DrL89, HsF83=DrF103, HsL139=DrL153. The picture was prepared using PyMOL (The PyMOL Molecular Graphics System, Version 1.5.0.5 Schrödinger,LLC). Alignment of full-length SAS-6 sequences of various species via ClustalW (http://www.genome.jp/tools-bin/clustalw) proves strict conservation of residues packed against Ile62. *= strong conservation of only one amino acid; :=conservation of a strong amino acid group (methionine, isoleucine, leucine and phenylalanine); .=conservation of weaker groups. The crystal structure was provided by Michel Steinmetz (figure and text reproduced from (Khan, Rupp et al. 2014) with permission of Human Molecular Genetics).

These data suggested an impaired or weakened folding of the N-terminal head domain due to the exchange of the hydrophobic isoleucine with the hydrophilic threonine. A model of the affected domain in the *clamydomonas reinhardtii* homolog crSAS-6, were the corresponding residue crVal81 is highlighted in yellow, shows that this core is in direct proximity to the head-head interaction site between two homodimers (Figure 27).

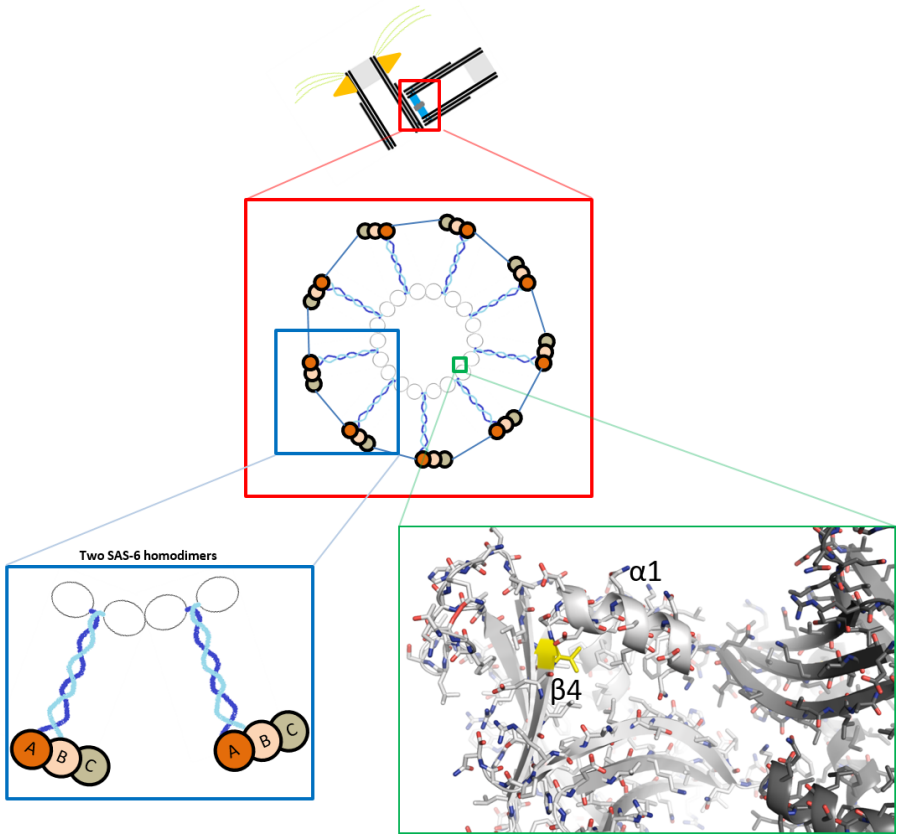

Figure 27: SAS-6 location in procentriole and composition. Nine homodimers form a ring-like structure via N-terminal head domain interactions. On their tail they are associated through A, B and C-tubulin. A model of the head domain of the *chlamydomonas reinhardtii* homolog crSAS-6 depicts the location of the mutated residue (in this case crSAS-6 V81) at the end of the β4 sheet directly before the α1 helix. Two interacting crSAS-6 head domains are presented- a lighter shaded domain on the left and the darker colored domain on the right (green box).

To therefore study the potential effect of the *HsSASS-6* mutation on localization, we transfected U2OS cells with either doxycycline-inducible wildtype or c.185T>C mutant constructs fused to EGFP. This was performed at the EPFl in Lausanne in

the laboratory of Pierre Gönczy by Meritxell Orpinell Mercadé. After 48 hours of induction, cells were analyzed for subcellular SAS-6 localization. To enhance the achieved GFP signal, the cells were fixed and stained with anit-GFP and anti-centrin2 (centriole marker) antibodies. This initial experiment highlighted that the localization to the centriole (marked by centrin2) was not impaired (Figure 28a) and that the protein was correctly folded.

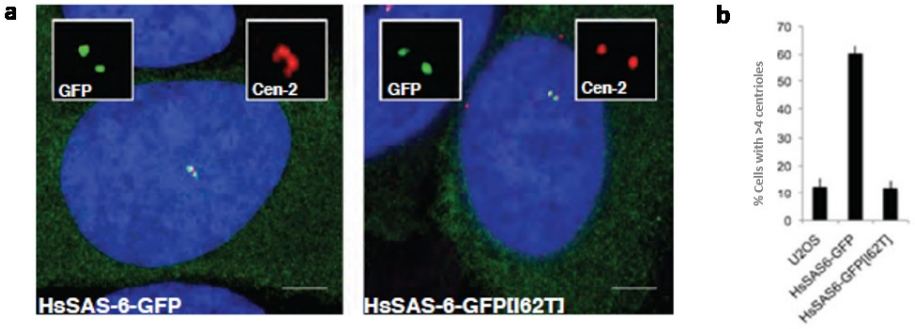

Figure 28: Subcellular localization of HsSAS-6 wildype and mutant. a. No significant differences in localization can be recognized upon induced overexpression of HsSAS-6-GFP [Ile62] (picture on the right) and HsSAS-6-GFP (picture on the left) (centrin=red, GFP=green). **b**. Percentage of cells harboring more than four centrioles after 48 hours of doxycyclin induction. The number is significantly higher in mitotic cells expressing the wildtype construct compared with HsSAS-6-GFP [I62T] expressing cells. Levels in cells transfected with the mutated construct are comparable to untransfected U2OS cells (data from ≥3 experiments and ≥ 50 cells scored) (figures and text reproduced from (Khan, Rupp et al. 2014) with permission of Human Molecular Genetics).

Subsequently, we investigated whether the mutated hsSAS-6 had an influence on centriole formation. Overexpression of wildype *hsSASS-6* normally increases the number of centrioles in a cell (Strnad, Leidel et al. 2007). This was, however, not the case for cells expressing the I62T mutant construct (Figure 28b). Moreover, while only about 1% of wildtype *HsSASS-6* expressing cells were observed to have less than 3 centrioles, expression of the mutant construct increased this to 7% of observed cells (Figure 29b). This suggested that the mutation indeed had an effect on centriole formation. We therefore subsequently knocked down the endogenous *HsSASS-6* using siRNA's directed against the 3'UTR region to ensure that we were not targeting our constructs. The knockdown efficiency was confirmed by Western

Blot analysis of the iU2OS protein extracts (Figure 29a). hsSAS-6 levels were increased upon doxycycline induction while endogenous hsSAS-6 expression was concomitantly inhibited upon siRNA knock-down (see Figure 29a, e & f).

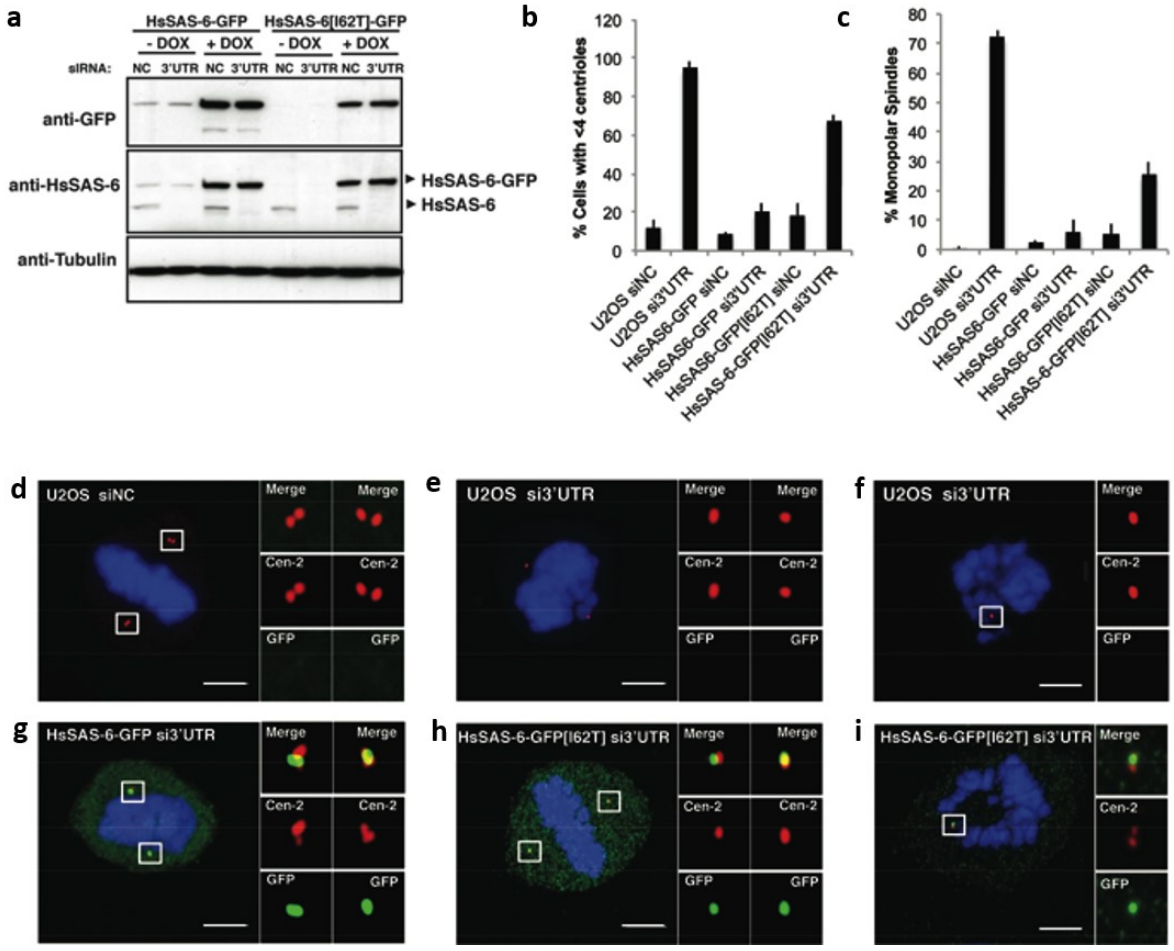

Figure 29: siRNA knock down of endogenously expressed *HsSASS-6.* **a**. Western Blot showing the expression of HsSAS-6 WT and mutant constructs upon doxycycline induction, which highlights the knockdown efficiency of the siRNA compared to negative control siRNA (NC). **b & c**. Frequency of cells with less than four centrioles and monopolar spindles in untransfected control U2OS, HsSAS-6-GFP or HsSAS6-GFP[I62T] cells, transfected with either negative control siRNA (siNC) or siRNa knocking-down endogenous HsSAS-6 (3'UTR) (data from ≥3 experiments and ≥ 50 cells scored). **d-i**. U2OS **(d-f)**, iU2OS HsSAS-6-GFP **(g)** or iU2OS HsSAS-6-GFP[I62T] **(h & i)** cells in mitosis, stained for GFP (green), Centrin-2 (red) and DNA (blue). In **(g-i)**, doxycycline induction for 48h was concomitant with siHsSAS-6 3'UTR (3'UTR) treatment. Monopolar spindles were found in **f** and **i**. Scale bars represent 5µm. (Figures and text reproduced from (Khan, Rupp et al. 2014) with permission of Human Molecular Genetics).

As we wanted to see if the number of centrioles changed upon endogenous *HsSASS-6* knockdown we only concentrated on mitotic cells. Knockdown in U2OS cells was extremely efficient (Figure 29e) with up to 95% of cells having less than four centrin foci whereas the number of foci for cells transfected with negative control siRNA was equal to untreated cells (see Figure 28 versus Figure 29b). We also noted a large increase in monopolar cells in these control cells upon HsSAS-6 depletion (Figure 29f). By trying to rescue this phenotype through overexpression of either HsSAS-6-GFP or HsSAS-6-GFP[I62T] we found significant differences. While we successfully rescued the amount of monopolar spindles (less than 10%) and increased the number of cells having four foci (~80%) by expressing the wildtype construct the results for the construct containing the p.Ile62Thr mutation were less promising. In terms of centriole numbers, the mutant construct was only able to reduce the number of cells having less than four foci in 27% of cells. Moreover, monopolar spindle formation was still observed in nearly 30% of transfected cells.
These experiments clearly provide evidence that the mutation has an impact on cell division and especially centriole formation, though it must be noted that HsSAS-6 function is not completely impaired. As altered cell division is a major cause of autosomal recessive primary microcephaly, we conclude that the c.185T>C transition in *HsSASS-6* is most likely pathogenic and causes the development of MCPH14.

4. Discussion

In this thesis, we report the discovery of two genes, *Kif1bβ* and *hsSASS-6*, associated with an autosomal recessive inherited brain disorder. Moreover, we describe for the first time a yet unreported syndromal intellectual disability with agenesis of the corpus callosum, which we found appears to be linked with a mutation in *Kif1bβ.* While *Kif1bβ* has already been identified as a causative gene for CMT2A (Zhao, Takita et al. 2001) and has furthermore been associated with the development of multiple sclerosis (Aulchenko, Hoppenbrouwers et al. 2008), *hsSASS-6* has previously not been established as causative gene for any known syndromes or diseases. Interestingly, both genes identified in our experiments have different functions: while the plays a major role in cell division (*hsSASS-6*), the other (*Kif1bβ*) codes for a transport molecule in neurons (Zhao, Takita et al. 2001, Leidel, Delattre et al. 2005).

In chapter 3.1 we discussed the discovery of a single base pair exchange in the donor splice site of the second to last exon of *Kif1bβ*. As a result, this exon is skipped, causing a frameshift in the remaining C-terminal sequence. Accordingly, more than a third of the Pleckstrin homology region and the entire remaining tail domain are replaced by the novel frame generated by the single base pair exchange, which subsequently encodes a different amino acid sequence and thus for a completely different tail.

Kinesins are motor proteins that transport different cargos through the cell. Their movement along microtubules is driven by ATP binding to the motor. Forty-two genes coding for kinesins are known and all are assigned to one of 14 different superfamilies (Wang, Cao et al. 2015). Together with *Kif1A*, *Kif1C*, *Kif13A*, *Kif13B*, *KIF14* and *Kif16B*, *Kif1B* is member of the kinesin-3 family (Hirokawa, Noda 2008, Siddiqui, Straube 2017). In the unbound state, kinesin-3 motors reside as monomers within the cells, but dimerize upon cargo binding to guarantee vesicle transport in neurons (Hammond, Cai et al. 2009, Soppina, Norris et al. 2014). *Kif1b* gives rise to two major isoforms, namely *KIF1bβ* and *KIF1bα*. As depicted in Figure 7, we found that Sanger Sequencing confirmed the c.5270+2T>G transition in *Kif1bβ.* The longer β isoform is the main isoform expressed in the brain (see Figure 10b), encoding a kinesin interacting with synaptic vesicle membranes containing

synaptotagmin, SV2 and synaptophysin (Zhao, Takita et al. 2001), whereas the shorter α isoform has a mitochondrial binding site not present in the β variant (Conforti, Dell'Agnello et al. 2003). Despite the general assumption that Kif1bβ is implemented solely in anterograde vesicle transport in axons, Niovi Santama's research group has observed mRNA (Arc and CaM) transporting Kif1Bβ molecules within dendrites moving in both directions, antero- and retrogradely (Charalambous, Pasciuto et al. 2013). In general, kinesin-3 members share an amino terminal motor and a FHA domain (fork head associated domain), which allows kinesins to interact with phosphorylated proteins or peptides and interacts with another Kinesin-3 domain (CC2) to control intramolecular autoinhibition (J. R. Lee, Shin et al. 2004, Westerholm-Parvinen, Vernos et al. 2000)). However, only KIF1A, KIF1bβ and KIF16B possess a C-terminal PH domain (Hirokawa, Noda 2008). As mentioned in chapter 3.1, this region is responsible for the interaction with phosphatidylinositol 4,5-bisphosphate in vesicle membranes in order to transport its cargos (Klopfenstein, Tomishige et al. 2002, Klopfenstein, Vale 2004). It has been shown, that kinesin-3 motors remain in an autoinhibited state until they bind to a vesicle. Only upon binding are they able to localize to microtubules and membranes (Niwa, Lipton et al. 2016, Hammond, Cai et al. 2009) which could explain the more cytosolic distribution we observed in cells overexpressing the defective PH domain molecule when compared with wildtype pcDNA3.1-KIF1bβ-GFP transfected cells. As neither movements of GFP expressing *KIF1bβ* mutant molecules nor a co-localization of the mutated isoform with $p75^{NTR}$ containing vesicles could be seen in cells, we conclude that the mutated kinesin remains inactivated as monomers in the cell and even in the presence of its cargo is not able to dimerize, bind to and move along microtubules (Soppina, Norris et al. 2014) (Figure 30).

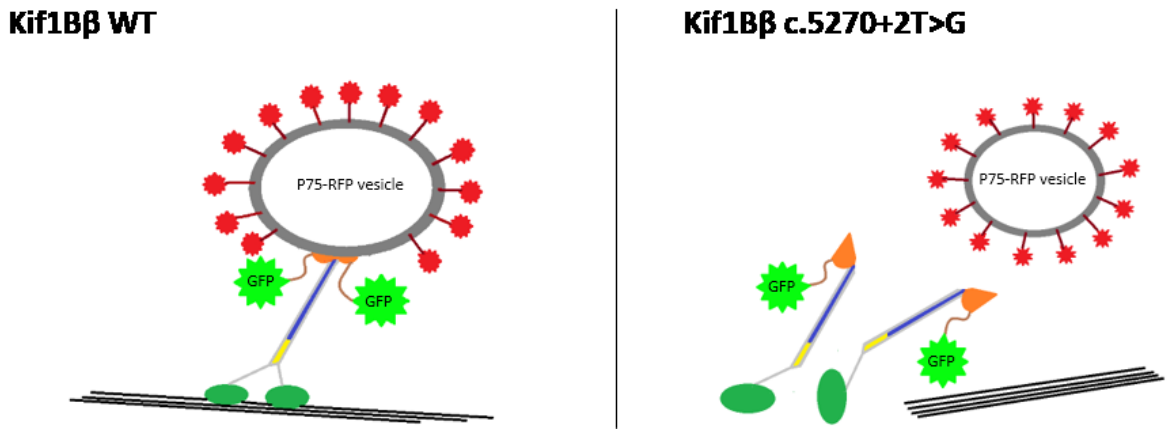

Figure 30: Hypothetic model of Kif1Bβ loss-of-function due to altered tail domain. Orange part of dimeric kinesin indicates tails with PH domains interacting with $p75^{NTR}$ transporting vesicle membrane. In the mutated molecule it is altered. Thus vesicle-kinesin binding, subsequent kinesin activation, dimerization and its recruitment to microtubules is inhibited. The suggested pathomechanism according to the kinesin-3 activity model was first proposed by Soppina et al. (Soppina, Norris et al. 2014). The GFP molecule is connected to kinesin via the brown linker. RFP-expressing $p75^{NTR}$ is anchored in vesicle membrane. Blue = stalk domain; yellow = FHA domain; green= motor domain. Black lines depict microtubules.

Looking at the phenotype, neurological diseases are frequently related to mutations in kinesins or genes interacting with them (Hirokawa, Niwa et al. 2010). For example, mutations in *Kif1a,* which is highly homologous to *KIF1bβ*, have been linked to three neurological diseases, including autosomal dominant mental retardation syndrome 9 (OMIM 614255), autosomal recessive hereditary sensory neuropathy type 2C (OMIM 614213) and autosomal recessive spastic paraplegia 30 (OMIM 610357) (Erlich, Edvardson et al. 2011, Hamdan, Gauthier et al. 2011, Riviere, Ramalingam et al. 2011). Interestingly, in addition to other neurological abnormalities brain MRIs of patients with mutations in *Kif1c*, *Kif2a, Kif5c, Kif7* or *Kif14* revealed total loss or thinning of the corpus callosum (Moawia, Shaheen et al. 2017, Dor, Cinnamon et al. 2014, Michels, Foss et al. 2017, Putoux, Thomas et al. 2011). This highlights that some kinesins are indeed essential for neuronal and corpus callosum development. The importance of *Kif1bβ* during neuronal development may already be suggested by its Pax6 dependent activation (Xie, Yang et al. 2013). *Pax6* is one of the first genes to be specifically expressed in stem cells upon differentiation into the neuronal lineage in humans (X. Zhang, Huang et al.

2010) and is essential for proper brain development (Xie, Yang et al. 2013, Glaser, Jepeal et al. 1994, X. Zhang, Huang et al. 2010, Mo, Zecevic 2008). Just like *Kif1b* knock-out mice, homozygous *Pax6* mutant mice die shortly after birth due to neurological defects (Favor, Bradley et al. 2009, Estivill-Torrus, Vitalis et al. 2001). There has been one report on a compound heterozygous mutation in *Pax6*, which was associated with facial dysmorphisms, no development of the eyes, an absent corpus callosum, hypotonia, missing optic nerves and chiasm as well as severe CNS defects. The patient died within eight days after birth (Glaser, Jepeal et al. 1994). Additional evidence for the importance of *Kif1bβ* in neuronal development comes from detailed studies in zebrafish where *Kif1bβ*, but not *Kif1bα,* was identified as essential for axonal outgrowth (Lyons, Naylor et al. 2009). Compared with wildtype animals, long axons in Kif1b transgenic fish with a mutation in the motor domain were shortened by 50-70% (Drerup, Lusk et al. 2016). In addition to defective axonal outgrowth, Lyons et al (Lyons, Naylor et al. 2009) also noted a 30% reduction in the total number of neurons in *Kif1b* mutant fish. These data correlate with studies conducted in $p75^{NTR}$ knockdown neurons. Marco Canossa's group provided evidence that neuronal polarization is dependent on $p75^{NTR}$ since depletion of $p75^{NTR}$ prevents axongenesis (Zuccaro, Bergami et al. 2014). As $p75^{NTR}$ transport is not solely dependent on Kif1Bβ but also on Kif1A (X. Xue, Jaulin et al. 2010), axonal outgrowth is perhaps not completely impaired in all cells. The loss of anterograde commissural fibers in Kif1Bβ knock out mice (Zhao, Takita et al. 2001), however, lets us assume that Kif1Bβ plays an important role in axonal development of long projection fibers. As the longest commissural fibers in the brain are found in the corpus callosum (Paul, Brown et al. 2007), we therefore suggest a high correlation between the C-terminal loss-of-function mutation in our patients with reduced $p75^{NTR}$ vesicle transport and the absence of this fiber tract.

Zebrafish models of Kif1B also exhibited myelination defects due to abberant myelin binding protein (mbp) transport (Lyons, Naylor et al. 2009). The *Kif1b* variant rs10492972 was formerly linked to a higher susceptibility for the demyelinating disease multiple sclerosis (MS) (Aulchenko, Hoppenbrouwers et al. 2008). However, Sombekke et al. later rebutted this claim (Sombekke, Jafari et al. 2011). As myelination was normal in our patients and no cases of MS have been reported in the healthy family members, we assume that mutations in human *Kif1bβ* are unlikely related to myelination defects.

It is to note that the Kif1B binding protein, KBP, has been reported to be causative for brain developmental disorders associated with intellectual disability, microcephaly, polymicrogyria, dilated ventricles and hypoplastic corpus callosum development (Valence, Poirier et al. 2013, Brooks, Bertoli-Avella et al. 2005), and that similar brain abnormalities that were seen in the MRIs of our IDACC patients. Furthermore, depletion of KBP in zebrafish revealed reduced outgrowth of long axons, axonal degeneration but also disorganization of the axonal cytoskeleton (Lyons, Naylor et al. 2008). These effects of KBP depletion were suggested to result in impaired SCG10 transport to extending axonal growth cones, as it is required to stabilize microtubules (Drerup, Lusk et al. 2016).

Additionally, we have shown that the interaction between calmodulin and Kif1Bβ is disrupted in lymphoblastoid cells of our patients (Figure 17). This interaction has been suggested to support Ca^{2+}-dependent recruitment of Kif1Bβ to synapses upon depolarization, triggering synaptic vesicle transport when needed (Charalambous, Pasciuto et al. 2013). In addition to the fact that vesicle binding seems to be prevented by the altered tail of Kif1Bβ, the impaired interaction between CaM and Kif1Bβ may also have a negative impact on the translocation to the growing axons. The most interesting aspect, however, is that electrophysiological studies in our patients were normal, not matching those with other reported CMT2A patients. The severity of the mutation in our homozygous mouse models seems to be in line with results seen in the *Kif1b* knock-out mice from Zhao (Zhao, Takita et al. 2001). Also, as our mutation was shown to cause a loss of function according to our cellular co-expression studies, it is therefore surprising that a heterozygous mutation in the ATP binding site of the motor domain can cause a phenotype but that neither our homo- nor heterozygous affected individuals show signs of peripheral neuropathies. Of course, depending on the location of each mutation, phenotypic development can vary (for example mutations in *Kif1A* account for three different phenotypes). The mutation in the CMT2A family published by Zhao et al (Zhao, Takita et al. 2001) is located in the ATP binding site of the motor domain shared by both isoforms. Zhao et al suggested that the neurological phenotypes are caused by the impairment of the β isoform, as rescue experiments in Kif1B-depleted neurons succeeded only upon overexpression of *Kif1bβ* but not *α*. This is interesting as our mutation specifically impairs the longer β isoform resulting in a totally different phenotype. A study published in Neurology by Carvill et al also raised the question if CMT2A is

truly associated with Kif1B. Here, during the course of whole exome sequencing in patients with Dravet syndrome, a disease characterized by infantile epileptic seizures combined with progressive intellectual disability, the groups of Ingrid Scheffer and Heather Mefford found a compound heterozygous mutation (p.T606I and p.R942C) in Kif1B (Carvill, Weckhuysen et al. 2014). The researchers did not report any CMT-related phenotypical abnormalities. While the T606 residue is shared by both Kif1B isoforms, the latter R942 amino acid is specific for the α isoform, located in its putative mitochondria binding site (Conforti, Dell'Agnello et al. 2003). Therefore, only the shorter alpha isoform is affected by both mutations. Some studies have linked Dravet syndrome to mitochondrial dysfunction and abnormalities (reviewed in (Castro-Gago, Perez-Gay et al. 2011)). Although not discussed in their paper, the Carvill mutations could perhaps be linked to defective Kif1Bα-dependent mitochondria transport. As mentioned in the results section of this thesis, CMT2A is frequently associated with abnormal mitochondria and defective transport along peripheral nerves. Taking into account that *Kif1bα* has a slightly higher abundance in muscle than *Kif1bβ* and that no signs of peripheral neuropathies were observed in our patients, one could therefore suggest that the CMT phenotype is more likely caused by mutations in the alpha but not the beta isoform of Kif1B. Since the mutation in the report of Zhao et al (Zhao, Takita et al. 2001) was heterozygous, the brain was perhaps not affected. This, however, would be contrary to the Dravet paper (Carvill, Weckhuysen et al. 2014) where no peripheral neuropathies were detected either.

Considering these data and the fact that our healthy mutation carriers showed no symptoms, this raised the question about the causality of the heterozygous p.Q98T in the CMT2A family of Zhao et al (Zhao, Takita et al. 2001). According to entries published on the 'Neuromuscular Disease Center' website (http://neuromuscular.wustl.edu/time/hmsn.html#2a1) patients reported for CMT2A1 by Zhao et al in 2001 also carry a mutation in the CMT2A gene *mitofusin2*, *MFN2*, situated just a few genes further downstream of *Kif1b*. *MFN2* as another causative CMT2A gene was published three years after the Zhao paper by the groups of Schröder and Vance (Zuchner, Mersiyanova et al. 2004). According to the human genome mutation database HGMD (Stenson, Mort et al. 2017, Stenson, Ball et al. 2003), since then more than 220 mutations in *MFN2* have been reported compared to three additional but questionable mutations in *Kif1B*. While one of the

2 mutations (p.V1358A) published by Drew et al (Drew, Zhu et al. 2015) was also found in an unaffected parent, and secondly, not predicted to be pathogenic by Polyphen2 analysis, the amino acid conservation on the site of the other mutation (p.E758D) was low. Moreover, the phenotype of the patient with the p.E758D mutation was not a classical CMT neuropathy but rather a hereditary motor neuropathy with pyramidal signs. A third mutation in *Kif1b* was found in the course of a larger NGS study in Norwegian CMT families (Hoyer, Braathen et al. 2014). In this study, only one affected family member was tested but none of the unaffected individuals of the family. Therefore, the pathogenic effect of these three mutations has to be considered as uncertain.

Recently we have tried to generate induced pluripotent stem cells (iPSC) from our lymphoblastoid cell lines using the coMIP method (Diecke, Lu et al. 2015) to investigate the neuronal differentiation capability and axon elongation in heterozygous and homozygous c.5270 +2T>G *Kif1bβ* stem cells, but we were not successful in establishing iPSC clones from these cells. Instead, we are currently trying to integrate the splice site mutation into the genome of commercially purchased iPSCs via CrispR-Cas9 to get a better understanding of the impact of this mutation on neuronal development using a human cell model. In addition to testing the neurogenic potential of these mutated stem cells, this model will allow us to investigate the influence of our mutation on various other tissue types. Especially renal cells would be of interest as in addition to the neurological phenotype, kidney abnormalities were noted in one patient and one terminated fetus. If Kif1Bβ indeed has an impact on kidney development, this would indicate that Kif1Bβ, like Kif3A, is also involved in ciliogenesis (F. Lin, Hiesberger et al. 2003). This hypothesis is supported by reports on Kif7 mutations. Kif7 is a kinesin-4 member, which is esential for primary cilia function causing acrocallosal syndrome upon loss of function (Edwards, Sherr et al. 2014, Tunovic, Baranano et al. 2015, Ibisler, Hehr et al. 2015, Karaer, Yuksel et al. 2015, Barakeh, Faqeih et al. 2015, Walsh, Shalev et al. 2013, Putoux, Thomas et al. 2011, Putoux, Nampoothiri et al. 2012). Cilia are important throughout the body and are divided into motile and non-motile (primary) cilia (Baker, Beales 2009). In the brain, the motile cilium is found on ependymal cells aligning the lateral ventricles where they beat in waves to control the flow of the cerebrospinal fluid to support the nutrient supply for neurons (Korzh 2018). Ventricles in the brain are connected via channels and cilia defects have been linked

to abnormal accumulation of the cerebral fluid within the ventricles causing a massive enlargement and eventually leading to the development of a hydrocephalus (Korzh 2018, Al Omran, Saternos et al. 2015). In line with the findings of dilated ventricles in Kif7 patients (Putoux, Thomas et al. 2011), the enlarged ventricles in our patients could further support the theory of a potential ciliopathy in our patients.

In our second family we identified the *spindle assembly homolog 6* gene (*HsSASS-6* or *SASS6*), as the causative gene for MCPH14. Like the majority of all other known primary microcephaly genes to date (see Table 1), its protein product HsSAS-6 is required for cell division by ensuring centrosome duplication (Leidel, Delattre et al. 2005, Strnad, Leidel et al. 2007). In order to establish the daughter centriole, two HsSAS-6 monomers initially dimerize to homodimers via the coiled-coil domain and these subsequently oligomerize to a symmetric 9-fold cartwheel structure by interacting with each other via their head domains (see Figure 27) (van Breugel, Hirono et al. 2011, Nakazawa, Hiraki et al. 2007, Kitagawa, Vakonakis et al. 2011). For a long time, a scaffold model has been proposed, which suggests that the HsSAS-6 cartwheel is initially built orthogonally attached to its mother centriole before the microtubules are stepwise assembled to its C-terminal domain (Hirono 2014, Hilbert, Noga et al. 2016). However, a more recent interdependence model suggests that the HsSAS-6 and microtubule scaffold are generated in parallel but separately and assemble to create a stable pro-centriole (Hilbert, Noga et al. 2016). HsSAS-6 is not permanently expressed. It can only be detected between S-phase and mitosis, before it is degraded via ubiquitination during the final phase of cell division. Thus HsSAS-6 cannot be found in mature centrioles. This tight regulation of molecule levels ensures the generation of only one new centriole (procentriole or daughter centriole) per cell cycle (Strnad, Leidel et al. 2007). Some of the already identified microcephaly proteins closely interact with HsSAS-6 helping to establish the procentriole. Before procentriole formation takes place, CEP125 and CEP63 form a ring-like structure surrounding the mother centriole (Tang 2013). This enables the recruitment of PLK4, which closely interacts with CEP192 and CEP152 (Sonnen, Gabryjonczyk et al. 2013). PLK4, in turn, recruits and phosphorylates STIL at its STAN domain thus enabling the interaction of STIL with the C-terminal domain of HsSAS-6 triggering the cartwheel formation (Moyer, Clutario et al. 2015). At its C-terminal coiled-coil domain HsSAS-6 harbors a binding site for CEP135. This

protein facilitates the attachment of the cartwheel scaffold to the A-tubule and links it indirectly via CPAP (protein product of the *CENPJ* gene) to the B and C tubules (Hatzopoulos, Erat et al. 2013). In addition to CEP192, all of the above mentioned proteins have been reported to be involved in the pathogenesis of microcephaly (Martin, Ahmad et al. 2014, Bond, Roberts et al. 2005, Kumar, Girimaji et al. 2009, Hussain, Baig et al. 2012, Guernsey, Jiang et al. 2010, Sir, Barr et al. 2011). In our MCPH patients we have identified a missense mutation in *HsSASS-6* located within the highly conserved PISA domain of the gene (Leidel, Delattre et al. 2005). This domain spans the region between the β3 sheet and the α2 helix in the head. Being part of the hydrophobic core of the V-terminal domain of HsSAS-6, we expected the mutation located at the end of β4 and shortly before α1 to destabilize the folding of the globular head domain, thus impairing homodimer aggregation. As published by Kitagawa et al (Kitagawa, Vakonakis et al. 2011) oligomerization is mediated by phenylalanine at position 131 reaching into the hydrophobic cavity between α1 and α3. Targeted mutagenesis of this residue abrogated the head-head interactions between the homodimers as well as bipolar spindle formation in *Caenorhabditis elegans*, indicating a complete loss-of-function of HsSAS-6. The p.Ile62Thr found in our patient exchanges a hydrophobic with a hydrophilic residue. As this area is part of the hydrophobic core where the F131 inserts and acts according to the lock-and-key principle, we wanted to see if this mutation had the same impact on centriole formation as has been shown for the mutated F131. Although overexpression of the mutated construct in cells did not reveal obvious changes in localization, we saw that compared with wild type HsSAS-6 overexpressing cells the number of cells containing more than four centrioles was significantly reduced, while the number of cell with less than three centrioles slightly increased. Assuming this to represent a dominant-negative effect, we knocked down the endogenous HsSAS-6. As expected, this resulted in an impaired procentriole formation, thereby increasing the number of cells with monopolar spindles and the percentage of cells with less than three centrioles. Trying to rescue this phenotype by overexpressing the p.Ile62Thr *HsSASS-6* construct succeeded only partially compared with an almost complete rescue upon WT HsSAS-6 overexpression. Impairing the N-N interaction by mutating F131 has been shown to completely prevent mitosis (Kitagawa, Vakonakis et al. 2011). However, since our phenotype was rescued to some extent we propose that the remaining activity of the mutated HsSAS-6 is sufficient for human

development, but still has an impact on neurogenesis as centrosome duplication is severely affected and the number of cells undergoing mitotic cleavage is reduced.
As we suggested that the folding of the head domain was perhaps loosened or the interaction between the nine homodimers was weakened, we also set out to produce a recombinant p.Ile62Thr HsSAS-6 protein to determine the impact of the mutation on the cartwheel structure as well as on the protein folding of the head domain (data not included in this thesis). Unfortunately, the recombinant HsSAS-6 protein was not soluble, keeping us from performing electrospray experiments.
Still, we were able to ivestigated the effect of the mutated HsSAS-6 on a non-neurological osteosarcoma cell line. To unravel the real pathomechanism affecting brain development, it would be interesting to create a homozygous c.185T>C *SASS-6* mouse. As already mentioned, brain developmental processes are tightly regulated. Slight tilts in the mitotic spindle during symmetric cell divisions of neuroepithelial stem cells severely affect the establishment of a large enough stem cell progenitor pool since divisions become asymmetric too early and thus neurogenic (Homem, Repic et al. 2015, Lizarraga, Margossian et al. 2010). This, for instance, is the case for NEs in *MCPH1* or *CENPJ* knockout mice (Gruber, Zhou et al. 2011, Garcez, Diaz-Alonso et al. 2015). As cell culture experiments revealed an increase in monopolar spindles, it is to be assumed that the mutation indeed has an impact on spindle formation. Additionally, the impaired centriole formation resulting from the knock-down of CPAP in U2OS cells can just partially be rescued by overexpression of CPAP p.Glu1235Val (*CENPJ* c.3704A>T) (Kitagawa, Kohlmaier et al. 2011, Bond, Roberts et al. 2005), which is in line with our rescue experiments for HsSAS-6. The close interaction of HsSAS-6 with CPAP would suggest a similar impairment in *HsSASS-6* mutated neuronal stem cell progenitors, as seen in CPAP mouse models, but this does not necessarily have to be the case. As an example, a total knockout of ASPM in mice drastically influences the orientation of the cleavage planes in NEs (Fish, Kosodo et al. 2006), in contrast to disease causing mutations in ASPM that did not show such effects (Pulvers, Bryk et al. 2010). Another pathomechanism was demonstrated by the overexpression of PLK4, the STIL-recruiting protein. Too high levels of PLK4 produced a surplus of centrosomes, resulting in aneuploid cells. These, in turn, were eliminated by p53, reducing the total number of cells and eventually triggering the development of a microcephalic

brain (Marthiens, Rujano et al. 2013). A similar phenotype has also been proposed for some STIL mutations (Arquint, Nigg 2014).

Interestingly, compared to humans affected, MCPH gene knock-out mice often develop different phenotypes (McIntyre, Lakshminarasimhan Chavali et al. 2012, Pulvers, Bryk et al. 2010, Trimborn, Ghani et al. 2010, Liang, Gao et al. 2010). As the architecture of the subventricular zones in mice and humans is not the same (only humans have an oSVZ and an inner fiber layer, splitting the inner and outer SVZ), altered phenotypical development has been linked to this morphological difference (Lancaster, Renner et al. 2013, Shitamukai, Konno et al. 2011). To study such alterations in a more authentic disease model, Jürgen Knoblich's group developed the generation of brain organoids, elegantly reflecting human cortical development and cerebral layer organization. By using a compound heterozygous *CDK5RAP2* human iPSC line, they successfully mimicked microcephalic brain development in a spinner culture flask. The resulting patient-derived organoids were not only smaller in size, they also contained significantly smaller neuroepithelial tissues reflecting premature neurogenesis. The researchers confirmed this by analyzing the spindle orientation of radial glial cells, proving tilted orientations (Lancaster, Renner et al. 2013). Since their publication in 2013, the method has been improved and several other neurological diseases have been modeled depicting it as a powerful tool to investigate neurogenesis and brain developmental disorders (reviewed in (C. T. Lee, Bendriem et al. 2017)). Producing such an organoid from iPSCs containing the *HsSASS-6* c.185T>C mutation would help to unravel the pathomechanism in humans and definitely confirm the disease-causing nature of our mutation.

To conclude, we are the first to report the herein described mutations in two genes associated with developmental neurological disorders, which both play different roles during brain development. By performing a variety of experiments we were able to prove that the impaired function (HsSAS-6) or loss-of-function (Kif1Bβ) caused by these mutations, which are both located in highly conserved and/or functionally important regions of the encoding proteins, appeared to cause the disease. Mouse models for Kif1Bβ supporting our theory are on the way to show the phenotypical consequences of the herein described mutation in a model organism.

Although our experiments provide evidence of the pathogenic effect of the *hsSASS-6* mutation identified in our patients, an animal or stem cell model would substantiate our theory.

Eventually, the molecular findings shed light on the actual role of the detected genes in the physiological and developmental context, revealing both as fundamental for brain development in the embryo. The identification of *hsSASS-6* in association with MCPH substantially increases the complexity of the genetic heterogeneity of MCPH. In terms of autosomal recessive primary microcephaly, most genes encode for proteins required for centriole formation and cell division. By identifying hsSAS-6, another centrosomal protein has thereby be linked to brain development.

Although these findings do unfortunately not provide any instant treatment options for the patients, knowing the familial mutation allows genetic testing and genetic counselling of relatives upon family planning. Additionally, including both genes in prenatal diagnostic NGS panels for mental disabilities or microcephaly will further facilitate the detection of disease causing mutations during prenatal testing, thereby allowing parents to make an early decision on the further course of their pregnancy. However, current advances in the field of genome editing provide hope for the future and suggest that embryonic gene editing might one day be used to increase the chances of normal embryonic development. First attempts to correct mutated genes in human embryos using CrispR-Cas9 have already been published (Ma, Marti-Gutierrez et al. 2017). Nevertheless, before this comes to the clinic, many obstacles such as low editing efficiency and off-target effects, must be overcome.

5. Bibliography

ABDEL-HAMID, M.S., ISMAIL, M.F., DARWISH, H.A., EFFAT, L.K., ZAKI, M.S. and ABDEL-SALAM, G.M., 2016. Molecular and phenotypic spectrum of ASPM-related primary microcephaly: Identification of eight novel mutations. *American journal of medical genetics.Part A,* **170**(8), pp. 2133-2140.

ABECASIS, G.R., CHERNY, S.S., COOKSON, W.O. and CARDON, L.R., 2002. Merlin--rapid analysis of dense genetic maps using sparse gene flow trees. *Nature genetics,* **30**(1), pp. 97-101.

ACHIRON, R. and ACHIRON, A., 2001. Development of the human fetal corpus callosum: a high-resolution, cross-sectional sonographic study. *Ultrasound in obstetrics & gynecology : the official journal of the International Society of Ultrasound in Obstetrics and Gynecology,* **18**(4), pp. 343-347.

AGHA, N., 2016. Kinship in rural Pakistan: Consanguineous marriages and their implications for women. *Women's Studies International Forum,* **54**, pp. 1-10.

AL OMRAN, A.J., SATERNOS, H.C., LIU, T., NAULI, S.M. and ABOUALAIWI, W.A., 2015. Live Imaging of the Ependymal Cilia in the Lateral Ventricles of the Mouse Brain. *Journal of visualized experiments : JoVE,* **(100):e52853. doi**(100), pp. e52853.

ALAKBARZADE, V., HAMEED, A., QUEK, D.Q., CHIOZA, B.A., BAPLE, E.L., CAZENAVE-GASSIOT, A., NGUYEN, L.N., WENK, M.R., AHMAD, A.Q., SREEKANTAN-NAIR, A., WEEDON, M.N., RICH, P., PATTON, M.A., WARNER, T.T., SILVER, D.L. and CROSBY, A.H., 2015. A partially inactivating mutation in the sodium-dependent lysophosphatidylcholine transporter MFSD2A causes a non-lethal microcephaly syndrome. *Nature genetics,* **47**(7), pp. 814-817.

AL-HASHIM, A.H., BLASER, S., RAYBAUD, C. and MACGREGOR, D., 2016. Corpus callosum abnormalities: neuroradiological and clinical correlations. *Developmental medicine and child neurology,* **58**(5), pp. 475-484.

ALKURAYA, F.S., 2010. Homozygosity mapping: one more tool in the clinical geneticist's toolbox. *Genetics in medicine : official journal of the American College of Medical Genetics,* **12**(4), pp. 236-239.

AL-QAHTANI, A.A., NAZIR, N., AL-ANAZI, M.R., RUBINO, S. and AL-AHDAL, M.N., 2016. Zika virus: a new pandemic threat. *Journal of infection in developing countries,* **10**(3), pp. 201-207.

ANDRADE-MORAES, C.H., OLIVEIRA-PINTO, A.V., CASTRO-FONSECA, E., DA SILVA, C.G., GUIMARAES, D.M., SZCZUPAK, D., PARENTE-BRUNO, D.R., CARVALHO, L.R., POLICHISO, L., GOMES, B.V., OLIVEIRA, L.M., RODRIGUEZ, R.D., LEITE, R.E., FERRETTI-REBUSTINI, R.E., JACOB-FILHO, W., PASQUALUCCI, C.A., GRINBERG, L.T. and LENT, R., 2013. Cell number changes in Alzheimer's disease relate to dementia, not to plaques and tangles. *Brain : a journal of neurology,* **136**(Pt 12), pp. 3738-3752.

ARQUINT, C. and NIGG, E.A., 2014. STIL microcephaly mutations interfere with APC/C-mediated degradation and cause centriole amplification. *Current biology : CB,* **24**(4), pp. 351-360.

AULCHENKO, Y.S., HOPPENBROUWERS, I.A., RAMAGOPALAN, S.V., BROER, L., JAFARI, N., HILLERT, J., LINK, J., LUNDSTROM, W., GREINER, E., DESSA SADOVNICK, A., GOOSSENS, D., VAN BROECKHOVEN, C., DEL-FAVERO, J., EBERS, G.C., OOSTRA, B.A., VAN DUIJN, C.M. and HINTZEN, R.Q., 2008. Genetic variation in the KIF1B locus influences susceptibility to multiple sclerosis. *Nature genetics,* **40**(12), pp. 1402-1403.

AWAD, S., AL-DOSARI, M.S., AL-YACOUB, N., COLAK, D., SALIH, M.A., ALKURAYA, F.S. and POIZAT, C., 2013. Mutation in PHC1 implicates chromatin remodeling in primary microcephaly pathogenesis. *Human molecular genetics,* **22**(11), pp. 2200-2213.

BACH, M., GRIGAT, S., PAWLIK, B., FORK, C., UTERMOHLEN, O., PAL, S., BANCZYK, D., LAZAR, A., SCHOMIG, E. and GRUNDEMANN, D., 2007. Fast set-up of doxycycline-inducible protein expression in human cell lines with a single plasmid based on Epstein-Barr virus replication and the simple tetracycline repressor. *The FEBS journal,* **274**(3), pp. 783-790.

BAKER, K. and BEALES, P.L., 2009. Making sense of cilia in disease: the human ciliopathies. *American journal of medical genetics.Part C, Seminars in medical genetics,* **151C**(4), pp. 281-295.

BARAKEH, D., FAQEIH, E., ANAZI, S., S AL-DOSARI, M., SOFTAH, A., ALBADR, F., HASSAN, H., ALAZAMI, A.M. and ALKURAYA, F.S., 2015. The many faces of KIF7. *Human genome variation,* **2**, pp. 15006.

BARBELANNE, M. and TSANG, W.Y., 2014. Molecular and cellular basis of autosomal recessive primary microcephaly. *BioMed research international,* **2014**, pp. 547986.

BARRERA, J.A., KAO, L.R., HAMMER, R.E., SEEMANN, J., FUCHS, J.L. and MEGRAW, T.L., 2010. CDK5RAP2 regulates centriole engagement and cohesion in mice. *Developmental cell,* **18**(6), pp. 913-926.

BASIT, S., AL-HARBI, K.M., ALHIJJI, S.A., ALBALAWI, A.M., ALHARBY, E., ELDARDEAR, A. and SAMMAN, M.I., 2016. CIT, a gene involved in neurogenic cytokinesis, is mutated in human primary microcephaly. *Human genetics,* **135**(10), pp. 1199-1207.

BAYLY, P.V., TABER, L.A. and KROENKE, C.D., 2014. Mechanical forces in cerebral cortical folding: a review of measurements and models. *Journal of the mechanical behavior of biomedical materials,* **29**, pp. 568-581.

BILGUVAR, K., OZTURK, A.K., LOUVI, A., KWAN, K.Y., CHOI, M., TATLI, B., YALNIZOGLU, D., TUYSUZ, B., CAGLAYAN, A.O., GOKBEN, S., KAYMAKCALAN, H., BARAK, T., BAKIRCIOGLU, M., YASUNO, K., HO, W., SANDERS, S., ZHU, Y., YILMAZ, S., DINCER, A., JOHNSON, M.H., BRONEN, R.A., KOCER, N., PER, H., MANE, S., PAMIR, M.N., YALCINKAYA, C., KUMANDAS, S., TOPCU, M., OZMEN, M., SESTAN, N., LIFTON, R.P., STATE, M.W. and GUNEL, M., 2010. Whole-exome sequencing identifies recessive WDR62 mutations in severe brain malformations. *Nature,* **467**(7312), pp. 207-210.

BISCHOF, H., REHBERG, M., STRYECK, S., ARTINGER, K., EROGLU, E., WALDECK-WEIERMAIR, M., GOTTSCHALK, B., ROST, R., DEAK, A.T., NIEDRIST, T., VUJIC, N., LINDERMUTH, H., PRASSL, R., PELZMANN, B., GROSCHNER, K., KRATKY, D., ELLER, K., ROSENKRANZ, A.R., MADL, T., PLESNILA, N., GRAIER, W.F. and MALLI, R., 2017. Novel genetically encoded fluorescent probes enable real-time detection of potassium in vitro and in vivo. *Nature communications,* **8**(1), pp. 1422-017-01615-z.

BITTLES, A.H. and BLACK, M.L., 2015-last update, Global Patterns & Tables of Consanguinity. Available: http://consang.net [11/02, 2017].

BITTLES, A., 2001. Consanguinity and its relevance to clinical genetics. *Clinical genetics,* **60**(2), pp. 89-98.

BLOOM, J.S. and HYND, G.W., 2005. The role of the corpus callosum in interhemispheric transfer of information: excitation or inhibition? *Neuropsychology review,* **15**(2), pp. 59-71.

BOMBELLI, F., STOJKOVIC, T., DUBOURG, O., ECHANIZ-LAGUNA, A., TARDIEU, S., LARCHER, K., AMATI-BONNEAU, P., LATOUR, P., VIGNAL, O., CAZENEUVE, C., BRICE, A. and LEGUERN, E., 2014. Charcot-Marie-Tooth disease type 2A: from typical to rare phenotypic and genotypic features. *JAMA neurology,* **71**(8), pp. 1036-1042.

BOND, J., ROBERTS, E., MOCHIDA, G.H., HAMPSHIRE, D.J., SCOTT, S., ASKHAM, J.M., SPRINGELL, K., MAHADEVAN, M., CROW, Y.J., MARKHAM, A.F., WALSH, C.A. and WOODS, C.G., 2002. ASPM is a major determinant of cerebral cortical size. *Nature genetics,* **32**(2), pp. 316-320.

BOND, J., ROBERTS, E., SPRINGELL, K., LIZARRAGA, S.B., SCOTT, S., HIGGINS, J., HAMPSHIRE, D.J., MORRISON, E.E., LEAL, G.F., SILVA, E.O., COSTA, S.M., BARALLE, D., RAPONI, M., KARBANI, G., RASHID, Y., JAFRI, H., BENNETT, C., CORRY, P., WALSH, C.A. and WOODS, C.G., 2005. A centrosomal mechanism involving CDK5RAP2 and CENPJ controls brain size. *Nature genetics,* **37**(4), pp. 353-355.

BORRELL, V. and CALEGARI, F., 2014. Mechanisms of brain evolution: regulation of neural progenitor cell diversity and cell cycle length. *Neuroscience research,* **86**, pp. 14-24.

BROOKS, A.S., BERTOLI-AVELLA, A.M., BURZYNSKI, G.M., BREEDVELD, G.J., OSINGA, J., BOVEN, L.G., HURST, J.A., MANCINI, G.M., LEQUIN, M.H., DE COO, R.F., MATERA, I., DE GRAAFF, E., MEIJERS, C., WILLEMS, P.J., TIBBOEL, D., OOSTRA, B.A. and HOFSTRA, R.M., 2005. Homozygous nonsense mutations in KIAA1279 are associated with malformations of the central and enteric nervous systems. *American Journal of Human Genetics,* **77**(1), pp. 120-126.

BUDDAY, S., STEINMANN, P. and KUHL, E., 2015. Physical biology of human brain development. *Frontiers in cellular neuroscience,* **9**, pp. 257.

CALDAS, G.V. and DELUCA, J.G., 2014. KNL1: bringing order to the kinetochore. *Chromosoma,* **123**(3), pp. 169-181.

CARVILL, G.L., WECKHUYSEN, S., MCMAHON, J.M., HARTMANN, C., MOLLER, R.S., HJALGRIM, H., COOK, J., GERAGHTY, E., O'ROAK, B.J., PETROU, S., CLARKE, A., GILL, D., SADLEIR, L.G., MUHLE, H., VON SPICZAK, S., NIKANOROVA, M., HODGSON, B.L., GAZINA, E.V., SULS, A., SHENDURE, J., DIBBENS, L.M., DE JONGHE, P., HELBIG, I., BERKOVIC, S.F., SCHEFFER, I.E. and MEFFORD, H.C., 2014. GABRA1 and STXBP1: novel genetic causes of Dravet syndrome. *Neurology,* **82**(14), pp. 1245-1253.

CASTRO-GAGO, M., PEREZ-GAY, L. and EIRIS-PUNAL, J., 2011. Dravet syndrome and mitochondrial dysfunction. *Journal of child neurology,* **26**(10), pp. 1331-1332.

CHARALAMBOUS, D.C., PASCIUTO, E., MERCALDO, V., PILO BOYL, P., MUNCK, S., BAGNI, C. and SANTAMA, N., 2013. KIF1Bbeta transports dendritically localized mRNPs in neurons and is recruited to synapses in an activity-dependent manner. *Cellular and molecular life sciences : CMLS,* **70**(2), pp. 335-356.

CHEN, H. and CHAN, D.C., 2006. Critical dependence of neurons on mitochondrial dynamics. *Current opinion in cell biology,* **18**(4), pp. 453-459.

CLARKE, L.E. and BARRES, B.A., 2013. Emerging roles of astrocytes in neural circuit development. *Nature reviews.Neuroscience,* **14**(5), pp. 311-321.

CONFORTI, L., DELL'AGNELLO, C., CALVARESI, N., TORTAROLO, M., GIORGINI, A., COLEMAN, M.P. and BENDOTTI, C., 2003. Kif1Bbeta isoform is enriched in motor neurons but does not change in a mouse model of amyotrophic lateral sclerosis. *Journal of neuroscience research,* **71**(5), pp. 732-739.

DARVISH, H., ESMAEELI-NIEH, S., MONAJEMI, G.B., MOHSENI, M., GHASEMI-FIROUZABADI, S., ABEDINI, S.S., BAHMAN, I., JAMALI, P., AZIMI, S., MOJAHEDI, F., DEHGHAN, A., SHAFEGHATI, Y., JANKHAH, A., FALAH, M., SOLTANI BANAVANDI, M.J., GHANI-KAKHI, M., GARSHASBI, M., RAKHSHANI, F., NAGHAVI, A., TZSCHACH, A., NEITZEL, H., ROPERS, H.H., KUSS, A.W., BEHJATI, F., KAHRIZI, K. and NAJMABADI, H., 2010. A clinical and molecular genetic study of 112 Iranian families with primary microcephaly. *Journal of medical genetics,* **47**(12), pp. 823-828.

DEHAY, C. and KENNEDY, H., 2007. Cell-cycle control and cortical development. *Nature reviews.Neuroscience,* **8**(6), pp. 438-450.

DIECKE, S., LU, J., LEE, J., TERMGLINCHAN, V., KOOREMAN, N.G., BURRIDGE, P.W., EBERT, A.D., CHURKO, J.M., SHARMA, A., KAY, M.A. and WU, J.C., 2015. Novel codon-optimized mini-intronic plasmid for efficient, inexpensive, and xeno-free induction of pluripotency. *Scientific reports,* **5**, pp. 8081.

DOBYNS, W.B., 1996. Absence makes the search grow longer. *American Journal of Human Genetics,* **58**(1), pp. 7-16.

DOR, T., CINNAMON, Y., RAYMOND, L., SHAAG, A., BOUSLAM, N., BOUHOUCHE, A., GAUSSEN, M., MEYER, V., DURR, A., BRICE, A., BENOMAR, A., STEVANIN, G., SCHUELKE, M. and EDVARDSON, S., 2014. KIF1C mutations in two families with hereditary spastic paraparesis and cerebellar dysfunction. *Journal of medical genetics,* **51**(2), pp. 137-142.

DRERUP, C.M., LUSK, S. and NECHIPORUK, A., 2016. Kif1B Interacts with KBP to Promote Axon Elongation by Localizing a Microtubule Regulator to Growth Cones. *The Journal of neuroscience : the official journal of the Society for Neuroscience,* **36**(26), pp. 7014-7026.

DREW, A.P., ZHU, D., KIDAMBI, A., LY, C., TEY, S., BREWER, M.H., AHMAD-ANNUAR, A., NICHOLSON, G.A. and KENNERSON, M.L., 2015. Improved inherited peripheral neuropathy genetic diagnosis by whole-exome sequencing. *Molecular genetics & genomic medicine,* **3**(2), pp. 143-154.

DWYER, N.D., CHEN, B., CHOU, S.J., HIPPENMEYER, S., NGUYEN, L. and GHASHGHAEI, H.T., 2016. Neural Stem Cells to Cerebral Cortex: Emerging Mechanisms Regulating Progenitor Behavior and Productivity. *The Journal of neuroscience : the official journal of the Society for Neuroscience,* **36**(45), pp. 11394-11401.

EDWARDS, T.J., SHERR, E.H., BARKOVICH, A.J. and RICHARDS, L.J., 2014. Clinical, genetic and imaging findings identify new causes for corpus callosum development syndromes. *Brain : a journal of neurology,* **137**(Pt 6), pp. 1579-1613.

ERLICH, Y., EDVARDSON, S., HODGES, E., ZENVIRT, S., THEKKAT, P., SHAAG, A., DOR, T., HANNON, G.J. and ELPELEG, O., 2011. Exome sequencing and disease-network analysis of a single family implicate a mutation in KIF1A in hereditary spastic paraparesis. *Genome research,* **21**(5), pp. 658-664.

ESCUDERO, C.A., LAZO, O.M., GALLEGUILLOS, C., PARRAGUEZ, J.I., LOPEZ-VERRILLI, M.A., CABEZA, C., LEON, L., SAEED, U., RETAMAL, C., GONZALEZ, A., MARZOLO, M.P., CARTER, B.D., COURT, F.A. and BRONFMAN, F.C., 2014. The p75 neurotrophin receptor evades the endolysosomal route in neuronal cells, favouring multivesicular bodies specialised for exosomal release. *Journal of cell science,* **127**(Pt 9), pp. 1966-1979.

ESTIVILL-TORRUS, G., VITALIS, T., FERNANDEZ-LLEBREZ, P. and PRICE, D.J., 2001. The transcription factor Pax6 is required for development of the diencephalic dorsal midline secretory radial glia that form the subcommissural organ. *Mechanisms of development,* **109**(2), pp. 215-224.

FAVOR, J., BRADLEY, A., CONTE, N., JANIK, D., PRETSCH, W., REITMEIR, P., ROSEMANN, M., SCHMAHL, W., WIENBERG, J. and ZAUS, I., 2009. Analysis of Pax6 contiguous gene deletions in the mouse, Mus musculus, identifies regions distinct from Pax6 responsible for extreme small-eye and belly-spotting phenotypes. *Genetics,* **182**(4), pp. 1077-1088.

FILIPPI, C.G. and CAULEY, K.A., 2014. Lesions of the corpus callosum and other commissural fibers: diffusion tensor studies. *Seminars in ultrasound, CT, and MR,* **35**(5), pp. 445-458.

FIRAT-KARALAR, E.N., RAUNIYAR, N., YATES, J.R.,3rd and STEARNS, T., 2014. Proximity interactions among centrosome components identify regulators of centriole duplication. *Current biology : CB,* **24**(6), pp. 664-670.

FISH, J.L., KOSODO, Y., ENARD, W., PAABO, S. and HUTTNER, W.B., 2006. Aspm specifically maintains symmetric proliferative divisions of neuroepithelial cells. *Proceedings of the National Academy of Sciences of the United States of America,* **103**(27), pp. 10438-10443.

FITSIORI, A., NGUYEN, D., KARENTZOS, A., DELAVELLE, J. and VARGAS, M.I., 2011. The corpus callosum: white matter or terra incognita. *The British journal of radiology,* **84**(997), pp. 5-18.

FLORIO, M. and HUTTNER, W.B., 2014. Neural progenitors, neurogenesis and the evolution of the neocortex. *Development (Cambridge, England),* **141**(11), pp. 2182-2194.

FRATELLI, N., PAPAGEORGHIOU, A.T., PREFUMO, F., BAKALIS, S., HOMFRAY, T. and THILAGANATHAN, B., 2007. Outcome of prenatally diagnosed agenesis of the corpus callosum. *Prenatal diagnosis,* **27**(6), pp. 512-517.

FUJITA, P.A., RHEAD, B., ZWEIG, A.S., HINRICHS, A.S., KAROLCHIK, D., CLINE, M.S., GOLDMAN, M., BARBER, G.P., CLAWSON, H., COELHO, A., DIEKHANS, M., DRESZER, T.R., GIARDINE, B.M., HARTE, R.A., HILLMAN-JACKSON, J., HSU, F., KIRKUP, V., KUHN, R.M., LEARNED, K., LI, C.H., MEYER, L.R., POHL, A., RANEY, B.J., ROSENBLOOM, K.R., SMITH, K.E., HAUSSLER, D. and KENT, W.J., 2011. The UCSC Genome Browser database: update 2011. *Nucleic acids research,* **39**(Database issue), pp. D876-82.

GABRIEL, E., RAMANI, A., KAROW, U., GOTTARDO, M., NATARAJAN, K., GOOI, L.M., GORANCI-BUZHALA, G., KRUT, O., PETERS, F., NIKOLIC, M., KUIVANEN, S., KORHONEN, E., SMURA, T., VAPALAHTI, O., PAPANTONIS, A., SCHMIDT-CHANASIT, J., RIPARBELLI, M., CALLAINI, G., KRONKE, M., UTERMOHLEN, O. and GOPALAKRISHNAN, J., 2017. Recent Zika Virus Isolates Induce Premature Differentiation of Neural Progenitors in Human Brain Organoids. *Cell stem cell,* **20**(3), pp. 397-406.e5.

GAL, J.S., MOROZOV, Y.M., AYOUB, A.E., CHATTERJEE, M., RAKIC, P. and HAYDAR, T.F., 2006. Molecular and morphological heterogeneity of neural precursors in the mouse neocortical proliferative zones. *The Journal of neuroscience : the official journal of the Society for Neuroscience,* **26**(3), pp. 1045-1056.

GAO, P., POSTIGLIONE, M.P., KRIEGER, T.G., HERNANDEZ, L., WANG, C., HAN, Z., STREICHER, C., PAPUSHEVA, E., INSOLERA, R., CHUGH, K., KODISH, O., HUANG, K., SIMONS, B.D., LUO, L., HIPPENMEYER, S. and SHI, S.H., 2014. Deterministic progenitor behavior and unitary production of neurons in the neocortex. *Cell,* **159**(4), pp. 775-788.

GARCEZ, P.P., DIAZ-ALONSO, J., CRESPO-ENRIQUEZ, I., CASTRO, D., BELL, D. and GUILLEMOT, F., 2015. Cenpj/CPAP regulates progenitor divisions and neuronal migration in the cerebral cortex downstream of Ascl1. *Nature communications,* **6**, pp. 6474.

GARZORZ, N., 2009. *Neuroanatomie.* 1 edn. München: Urban & Fischer.

GASTEIGER, E., GATTIKER, A., HOOGLAND, C., IVANYI, I., APPEL, R.D. and BAIROCH, A., 2003. ExPASy: The proteomics server for in-depth protein knowledge and analysis. *Nucleic acids research,* **31**(13), pp. 3784-3788.

GENIN, A., DESIR, J., LAMBERT, N., BIERVLIET, M., VAN DER AA, N., PIERQUIN, G., KILLIAN, A., TOSI, M., URBINA, M., LEFORT, A., LIBERT, F., PIRSON, I. and ABRAMOWICZ, M., 2012. Kinetochore KMN network gene CASC5 mutated in primary microcephaly. *Human molecular genetics,* **21**(24), pp. 5306-5317.

GERFEN, C.R., ECONOMO, M.N. and CHANDRASHEKAR, J., 2016. Long distance projections of cortical pyramidal neurons. *Journal of neuroscience research*.

GLASER, T., JEPEAL, L., EDWARDS, J.G., YOUNG, S.R., FAVOR, J. and MAAS, R.L., 1994. PAX6 gene dosage effect in a family with congenital cataracts, aniridia, anophthalmia and central nervous system defects. *Nature genetics,* **7**(4), pp. 463-471.

GONCZY, P., 2012. Towards a molecular architecture of centriole assembly. *Nature reviews.Molecular cell biology,* **13**(7), pp. 425-435.

GOPALAKRISHNAN, J., GUICHARD, P., SMITH, A.H., SCHWARZ, H., AGARD, D.A., MARCO, S. and AVIDOR-REISS, T., 2010. Self-assembling SAS-6 Multimer Is a Core Centriole Building Block*. *The Journal of Biological Chemistry,* **285**(12), pp. 8759-8770.

GOTZ, M. and HUTTNER, W.B., 2005. The cell biology of neurogenesis. *Nature reviews.Molecular cell biology,* **6**(10), pp. 777-788.

GRUBER, R., ZHOU, Z., SUKCHEV, M., JOERSS, T., FRAPPART, P.O. and WANG, Z.Q., 2011. MCPH1 regulates the neuroprogenitor division mode by coupling the centrosomal cycle with mitotic entry through the Chk1-Cdc25 pathway. *Nature cell biology,* **13**(11), pp. 1325-1334.

GRUNEBERG, U., NEEF, R., LI, X., CHAN, E.H., CHALAMALASETTY, R.B., NIGG, E.A. and BARR, F.A., 2006. KIF14 and citron kinase act together to promote efficient cytokinesis. *The Journal of cell biology,* **172**(3), pp. 363-372.

GUDBJARTSSON, D.F., JONASSON, K., FRIGGE, M.L. and KONG, A., 2000. Allegro, a new computer program for multipoint linkage analysis. *Nature genetics,* **25**(1), pp. 12-13.

GUEMEZ-GAMBOA, A., NGUYEN, L.N., YANG, H., ZAKI, M.S., KARA, M., BEN-OMRAN, T., AKIZU, N., ROSTI, R.O., ROSTI, B., SCOTT, E., SCHROTH, J., COPELAND, B., VAUX, K.K., CAZENAVE-GASSIOT, A., QUEK, D.Q., WONG, B.H., TAN, B.C., WENK, M.R., GUNEL, M., GABRIEL, S., CHI, N.C., SILVER, D.L. and GLEESON, J.G., 2015. Inactivating mutations in MFSD2A, required for omega-3 fatty acid transport in brain, cause a lethal microcephaly syndrome. *Nature genetics,* **47**(7), pp. 809-813.

GUERNSEY, D.L., JIANG, H., HUSSIN, J., ARNOLD, M., BOUYAKDAN, K., PERRY, S., BABINEAU-STURK, T., BEIS, J., DUMAS, N., EVANS, S.C., FERGUSON, M., MATSUOKA, M., MACGILLIVRAY, C., NIGHTINGALE, M., PATRY, L., RIDEOUT, A.L., THOMAS, A., ORR, A., HOFFMANN, I., MICHAUD, J.L., AWADALLA, P., MEEK, D.C., LUDMAN, M. and SAMUELS, M.E., 2010. Mutations in centrosomal protein CEP152 in primary microcephaly families linked to MCPH4. *American Journal of Human Genetics,* **87**(1), pp. 40-51.

HAMDAN, F.F., GAUTHIER, J., ARAKI, Y., LIN, D.T., YOSHIZAWA, Y., HIGASHI, K., PARK, A.R., SPIEGELMAN, D., DOBRZENIECKA, S., PITON, A., TOMITORI, H., DAOUD, H., MASSICOTTE, C., HENRION, E., DIALLO, O., S2D GROUP, SHEKARABI, M., MARINEAU, C., SHEVELL, M., MARANDA, B., MITCHELL, G., NADEAU, A., D'ANJOU, G., VANASSE, M., SROUR, M., LAFRENIERE, R.G., DRAPEAU, P., LACAILLE, J.C., KIM, E., LEE, J.R., IGARASHI, K., HUGANIR, R.L., ROULEAU, G.A. and MICHAUD, J.L., 2011. Excess of de novo deleterious mutations in genes associated with glutamatergic systems in nonsyndromic intellectual disability. *American Journal of Human Genetics,* **88**(3), pp. 306-316.

HAMMOND, J.W., CAI, D., BLASIUS, T.L., LI, Z., JIANG, Y., JIH, G.T., MEYHOFER, E. and VERHEY, K.J., 2009. Mammalian Kinesin-3 motors are dimeric in vivo and move by processive motility upon release of autoinhibition. *PLoS biology,* **7**(3), pp. e72.

HANNA, R.M., MARSH, S.E., SWISTUN, D., AL-GAZALI, L., ZAKI, M.S., ABDEL-SALAM, G.M., AL-TAWARI, A., BASTAKI, L., KAYSERILI, H., RAJAB, A., BOGLARKA, B., DIETRICH, R.B., DOBYNS, W.B., TRUWIT, C.L., SATTAR, S., CHUANG, N.A., SHERR, E.H. and GLEESON, J.G., 2011. Distinguishing 3 classes of corpus callosal abnormalities in consanguineous families. *Neurology,* **76**(4), pp. 373-382.

HANSEN, D.V., LUI, J.H., PARKER, P.R. and KRIEGSTEIN, A.R., 2010. Neurogenic radial glia in the outer subventricular zone of human neocortex. *Nature,* **464**(7288), pp. 554-561.

HATZOPOULOS, G.N., ERAT, M.C., CUTTS, E., ROGALA, K.B., SLATER, L.M., STANSFELD, P.J. and VAKONAKIS, I., 2013. Structural analysis of the G-box domain of the microcephaly protein CPAP suggests a role in centriole architecture. *Structure (London, England : 1993),* **21**(11), pp. 2069-2077.

HEVNER, R.F., DAZA, R.A., RUBENSTEIN, J.L., STUNNENBERG, H., OLAVARRIA, J.F. and ENGLUND, C., 2003. Beyond laminar fate: toward a molecular classification of cortical projection/pyramidal neurons. *Developmental neuroscience,* **25**(2-4), pp. 139-151.

HILBERT, M., ERAT, M.C., HACHET, V., GUICHARD, P., BLANK, I.D., FLUCKIGER, I., SLATER, L., LOWE, E.D., HATZOPOULOS, G.N., STEINMETZ, M.O., GONCZY, P. and VAKONAKIS, I., 2013. Caenorhabditis elegans centriolar protein SAS-6 forms a spiral that is consistent with imparting a ninefold symmetry. *Proceedings of the National Academy of Sciences of the United States of America,* **110**(28), pp. 11373-11378.

HILBERT, M., NOGA, A., FREY, D., HAMEL, V., GUICHARD, P., KRAATZ, S.H., PFREUNDSCHUH, M., HOSNER, S., FLUCKIGER, I., JAUSSI, R., WIESER, M.M., THIELTGES, K.M., DEUPI, X., MULLER, D.J., KAMMERER, R.A., GONCZY, P., HIRONO, M. and STEINMETZ, M.O., 2016. SAS-6 engineering reveals interdependence between cartwheel and microtubules in determining centriole architecture. *Nature cell biology,* **18**(4), pp. 393-403.

HILDEBRANDT, F., HEERINGA, S.F., RUSCHENDORF, F., ATTANASIO, M., NURNBERG, G., BECKER, C., SEELOW, D., HUEBNER, N., CHERNIN, G., VLANGOS, C.N., ZHOU, W., O'TOOLE, J.F., HOSKINS, B.E., WOLF, M.T., HINKES, B.G., CHAIB, H., ASHRAF, S., SCHOEB, D.S., OVUNC, B., ALLEN, S.J., VEGA-WARNER, V., WISE, E., HARVILLE, H.M., LYONS, R.H., WASHBURN, J., MACDONALD, J., NURNBERG, P. and OTTO, E.A., 2009. A systematic approach to mapping recessive disease genes in individuals from outbred populations. *PLoS genetics,* **5**(1), pp. e1000353.

HIROKAWA, N., NIWA, S. and TANAKA, Y., 2010. Molecular motors in neurons: transport mechanisms and roles in brain function, development, and disease. *Neuron,* **68**(4), pp. 610-638.

HIROKAWA, N. and NODA, Y., 2008. Intracellular transport and kinesin superfamily proteins, KIFs: structure, function, and dynamics. *Physiological Reviews,* **88**(3), pp. 1089-1118.

HIRONO, M., 2014. Cartwheel assembly. *Philosophical transactions of the Royal Society of London.Series B, Biological sciences,* **369**(1650), pp. 10.1098/rstb.2013.0458.

HOERDER-SUABEDISSEN, A. and MOLNAR, Z., 2015. Development, evolution and pathology of neocortical subplate neurons. *Nature reviews.Neuroscience,* **16**(3), pp. 133-146.

HOLLAND, M.A., MILLER, K.E. and KUHL, E., 2015. Emerging Brain Morphologies from Axonal Elongation. *Annals of Biomedical Engineering,* **43**(7), pp. 1640-1653.

HOMEM, C.C., REPIC, M. and KNOBLICH, J.A., 2015. Proliferation control in neural stem and progenitor cells. *Nature reviews.Neuroscience,* **16**(11), pp. 647-659.

HOYER, H., BRAATHEN, G.J., BUSK, O.L., HOLLA, O.L., SVENDSEN, M., HILMARSEN, H.T., STRAND, L., SKJELBRED, C.F. and RUSSELL, M.B., 2014. Genetic diagnosis of Charcot-Marie-Tooth disease in a population by next-generation sequencing. *BioMed research international,* **2014**, pp. 210401.

HUANG, E.J. and REICHARDT, L.F., 2001. Neurotrophins: roles in neuronal development and function. *Annual Review of Neuroscience,* **24**, pp. 677-736.

HUANG, H., XUE, R., ZHANG, J., REN, T., RICHARDS, L.J., YAROWSKY, P., MILLER, M.I. and MORI, S., 2009. Anatomical characterization of human fetal brain development with diffusion tensor magnetic resonance imaging. *The Journal of neuroscience : the official journal of the Society for Neuroscience,* **29**(13), pp. 4263-4273.

HUSSAIN, M.S., BAIG, S.M., NEUMANN, S., NURNBERG, G., FAROOQ, M., AHMAD, I., ALEF, T., HENNIES, H.C., TECHNAU, M., ALTMULLER, J., FROMMOLT, P., THIELE, H., NOEGEL, A.A. and NURNBERG, P., 2012. A Truncating Mutation of CEP135 Causes Primary Microcephaly and Disturbed Centrosomal Function. *American Journal of Human Genetics,* **90**(5), pp. 871-878.

HUSSAIN, M.S., BAIG, S.M., NEUMANN, S., PECHE, V.S., SZCZEPANSKI, S., NURNBERG, G., TARIQ, M., JAMEEL, M., KHAN, T.N., FATIMA, A., MALIK, N.A., AHMAD, I., ALTMULLER, J., FROMMOLT, P., THIELE, H., HOHNE, W., YIGIT, G., WOLLNIK, B., NEUBAUER, B.A., NURNBERG, P. and NOEGEL, A.A., 2013. CDK6 associates with the centrosome during mitosis and is mutated in a large Pakistani family with primary microcephaly. *Human molecular genetics,* .

IBISLER, A., HEHR, U., BARTH, A., KOCH, M., EPPLEN, J.T. and HOFFJAN, S., 2015. Novel KIF7 Mutation in a Tunisian Boy with Acrocallosal Syndrome: Case Report and Review of the Literature. *Molecular syndromology,* **6**(4), pp. 173-180.

INSTITUTE OF MEDICINE (US) COMMITTEE ON ACCELERATING RARE DISEASES RESEARCH AND ORPHAN PRODUCT DEVELOPMENT, 2010.

JABAUDON, D., 2017. Fate and freedom in developing neocortical circuits. *Nature communications,* **8**, pp. 16042.

JACKSON, A.P., EASTWOOD, H., BELL, S.M., ADU, J., TOOMES, C., CARR, I.M., ROBERTS, E., HAMPSHIRE, D.J., CROW, Y.J., MIGHELL, A.J., KARBANI, G., JAFRI, H., RASHID, Y., MUELLER, R.F., MARKHAM, A.F. and WOODS, C.G., 2002. Identification of microcephalin, a protein implicated in determining the size of the human brain. *American Journal of Human Genetics,* **71**(1), pp. 136-142.

JAVED, F., MANZOOR, K.N., ALI, M., HAQ, I.U., KHAN, A.A., ZAIB, A. and MANZOOR, S., 2018. Zika virus: what we need to know? *Journal of Basic Microbiology,* **58**(1), pp. 3-16.

JERET, J.S., SERUR, D., WISNIEWSKI, K. and FISCH, C., 1985. Frequency of agenesis of the corpus callosum in the developmentally disabled population as determined by computerized tomography. *Pediatric neuroscience,* **12**(2), pp. 101-103.

JO, H.M., CHO, H.K., JANG, S.H., YEO, S.S., LEE, E., KIM, H.S. and SON, S.M., 2012. A comparison of microstructural maturational changes of the corpus callosum in preterm and full-term children: a diffusion tensor imaging study. *Neuroradiology,* **54**(9), pp. 997-1005.

KADIR, R., HAREL, T., MARKUS, B., PEREZ, Y., BAKHRAT, A., COHEN, I., VOLODARSKY, M., FEINTSEIN-LINIAL, M., CHERVINSKI, E., ZLOTOGORA, J., SIVAN, S., BIRNBAUM, R.Y., ABDU, U., SHALEV, S. and BIRK, O.S., 2016. ALFY-Controlled DVL3 Autophagy Regulates Wnt Signaling, Determining Human Brain Size. *PLoS genetics,* **12**(3), pp. e1005919.

KARAER, K., YUKSEL, Z., ICHKOU, A., CALISIR, C. and ATTIE-BITACH, T., 2015. A novel KIF7 mutation in two affected siblings with acrocallosal syndrome. *Clinical dysmorphology,* **24**(2), pp. 61-64.

KATOH, K., KUMA, K., TOH, H. and MIYATA, T., 2005. MAFFT version 5: improvement in accuracy of multiple sequence alignment. *Nucleic acids research,* **33**(2), pp. 511-518.

KAUFMANN, T., KUKOLJ, E., BRACHNER, A., BELTZUNG, E., BRUNO, M., KOSTRHON, S., OPRAVIL, S., HUDECZ, O., MECHTLER, K., WARREN, G. and SLADE, D., 2016. SIRT2 regulates nuclear envelope reassembly through ANKLE2 deacetylation. *Journal of cell science,* **129**(24), pp. 4607-4621.

KENT, W.J., SUGNET, C.W., FUREY, T.S., ROSKIN, K.M., PRINGLE, T.H., ZAHLER, A.M. and HAUSSLER, D., 2002. The human genome browser at UCSC. *Genome research,* **12**(6), pp. 996-1006.

KHAN, M.A., RUPP, V.M., ORPINELL, M., HUSSAIN, M.S., ALTMULLER, J., STEINMETZ, M.O., ENZINGER, C., THIELE, H., HOHNE, W., NURNBERG, G., BAIG, S.M., ANSAR, M., NURNBERG, P., VINCENT, J.B., SPEICHER, M.R., GONCZY, P. and WINDPASSINGER, C., 2014. A missense mutation in the PISA domain of HsSAS-6 causes autosomal recessive primary microcephaly in a large consanguineous Pakistani family. *Human molecular genetics,* **23**(22). pp. 5940-5949.

KIM, Y.S., FURMAN, S., SINK, H. and VANBERKUM, M.F., 2001. Calmodulin and profilin coregulate axon outgrowth in Drosophila. *Journal of neurobiology,* **47**(1), pp. 26-38.

KITAGAWA, D., KOHLMAIER, G., KELLER, D., STRNAD, P., BALESTRA, F.R., FLUCKIGER, I. and GONCZY, P., 2011. Spindle positioning in human cells relies on proper centriole formation and on the microcephaly proteins CPAP and STIL. *Journal of cell science,* **124**(Pt 22), pp. 3884-3893.

KITAGAWA, D., VAKONAKIS, I., OLIERIC, N., HILBERT, M., KELLER, D., OLIERIC, V., BORTFELD, M., ERAT, M.C., FLUCKIGER, I., GONCZY, P. and STEINMETZ, M.O., 2011. Structural basis of the 9-fold symmetry of centrioles. *Cell,* **144**(3), pp. 364-375.

KLOPFENSTEIN, D.R., TOMISHIGE, M., STUURMAN, N. and VALE, R.D., 2002. Role of phosphatidylinositol(4,5)bisphosphate organization in membrane transport by the Unc104 kinesin motor. *Cell,* **109**(3), pp. 347-358.

KLOPFENSTEIN, D.R. and VALE, R.D., 2004. The lipid binding pleckstrin homology domain in UNC-104 kinesin is necessary for synaptic vesicle transport in Caenorhabditis elegans. *Molecular biology of the cell,* **15**(8), pp. 3729-3739.

KLOSE, M. and BENTLEY, D., 1989. Transient pioneer neurons are essential for formation of an embryonic peripheral nerve. *Science (New York, N.Y.),* **245**(4921), pp. 982-984.

KOHLMAIER, G., LONCAREK, J., MENG, X., MCEWEN, B.F., MOGENSEN, M.M., SPEKTOR, A., DYNLACHT, B.D., KHODJAKOV, A. and GONCZY, P., 2009. Overly long centrioles and defective cell division upon excess of the SAS-4-related protein CPAP. *Current biology : CB,* **19**(12), pp. 1012-1018.

KORZH, V., 2018. Development of brain ventricular system. *Cellular and molecular life sciences : CMLS,* **75**(3), pp. 375-383.

KOWALCZYK, T., PONTIOUS, A., ENGLUND, C., DAZA, R.A., BEDOGNI, F., HODGE, R., ATTARDO, A., BELL, C., HUTTNER, W.B. and HEVNER, R.F., 2009. Intermediate neuronal progenitors (basal progenitors) produce pyramidal-projection neurons for all layers of cerebral cortex. *Cerebral cortex (New York, N.Y.: 1991),* **19**(10), pp. 2439-2450.

KUMAR, A., GIRIMAJI, S.C., DUVVARI, M.R. and BLANTON, S.H., 2009. Mutations in STIL, encoding a pericentriolar and centrosomal protein, cause primary microcephaly. *American Journal of Human Genetics,* **84**(2), pp. 286-290.

KUWADA, J.Y., 1986. Cell recognition by neuronal growth cones in a simple vertebrate embryo. *Science (New York, N.Y.),* **233**(4765), pp. 740-746.

KWAN, K.Y., SESTAN, N. and ANTON, E.S., 2012. Transcriptional co-regulation of neuronal migration and laminar identity in the neocortex. *Development (Cambridge, England),* **139**(9), pp. 1535-1546.

LAGUESSE, S., PEYRE, E. and NGUYEN, L., 2015. Progenitor genealogy in the developing cerebral cortex. *Cell and tissue research,* **359**(1), pp. 17-32.

LAMONICA, B.E., LUI, J.H., HANSEN, D.V. and KRIEGSTEIN, A.R., 2013. Mitotic spindle orientation predicts outer radial glial cell generation in human neocortex. *Nature communications,* **4**, pp. 1665.

LANCASTER, M.A., RENNER, M., MARTIN, C.A., WENZEL, D., BICKNELL, L.S., HURLES, M.E., HOMFRAY, T., PENNINGER, J.M., JACKSON, A.P. and KNOBLICH, J.A., 2013. Cerebral organoids model human brain development and microcephaly. *Nature,* **501**(7467), pp. 373-379.

LAVADO, A., WARE, M., PARE, J. and CAO, X., 2014. The tumor suppressor Nf2 regulates corpus callosum development by inhibiting the transcriptional coactivator Yap. *Development (Cambridge, England),* **141**(21), pp. 4182-4193.

LEE, C.T., BENDRIEM, R.M., WU, W.W. and SHEN, R.F., 2017. 3D brain Organoids derived from pluripotent stem cells: promising experimental models for brain development and neurodegenerative disorders. *Journal of Biomedical Science,* **24**(1), pp. 59-017-0362-8.

LEE, J.R., SHIN, H., CHOI, J., KO, J., KIM, S., LEE, H.W., KIM, K., RHO, S.H., LEE, J.H., SONG, H.E., EOM, S.H. and KIM, E., 2004. An intramolecular interaction between the FHA domain and a coiled coil negatively regulates the kinesin motor KIF1A. *The EMBO journal,* **23**(7), pp. 1506-1515.

LEIDEL, S., DELATTRE, M., CERUTTI, L., BAUMER, K. and GONCZY, P., 2005. SAS-6 defines a protein family required for centrosome duplication in C. elegans and in human cells. *Nature cell biology,* **7**(2), pp. 115-125.

LI, C., XU, D., YE, Q., HONG, S., JIANG, Y., LIU, X., ZHANG, N., SHI, L., QIN, C.F. and XU, Z., 2016. Zika Virus Disrupts Neural Progenitor Development and Leads to Microcephaly in Mice. *Cell stem cell,* **19**(1), pp. 120-126.

LI, H. and DURBIN, R., 2009. Fast and accurate short read alignment with Burrows-Wheeler transform. *Bioinformatics (Oxford, England),* **25**(14), pp. 1754-1760.

LIANG, Y., GAO, H., LIN, S.Y., PENG, G., HUANG, X., ZHANG, P., GOSS, J.A., BRUNICARDI, F.C., MULTANI, A.S., CHANG, S. and LI, K., 2010. BRIT1/MCPH1 is essential for mitotic and meiotic recombination DNA repair and maintaining genomic stability in mice. *PLoS genetics,* **6**(1), pp. e1000826.

LIN, F., HIESBERGER, T., CORDES, K., SINCLAIR, A.M., GOLDSTEIN, L.S., SOMLO, S. and IGARASHI, P., 2003. Kidney-specific inactivation of the KIF3A subunit of kinesin-II inhibits renal ciliogenesis and produces polycystic kidney disease. *Proceedings of the National Academy of Sciences of the United States of America,* **100**(9), pp. 5286-5291.

LIN, M., WEI, L.J., SELLERS, W.R., LIEBERFARB, M., WONG, W.H. and LI, C., 2004. dChipSNP: significance curve and clustering of SNP-array-based loss-of-heterozygosity data. *Bioinformatics (Oxford, England),* **20**(8), pp. 1233-1240.

LIN, Y.C., CHANG, C.W., HSU, W.B., TANG, C.J., LIN, Y.N., CHOU, E.J., WU, C.T. and TANG, T.K., 2013. Human microcephaly protein CEP135 binds to hSAS-6 and CPAP, and is required for centriole assembly. *The EMBO journal,* **32**(8), pp. 1141-1154.

LIZARRAGA, S.B., MARGOSSIAN, S.P., HARRIS, M.H., CAMPAGNA, D.R., HAN, A.P., BLEVINS, S., MUDBHARY, R., BARKER, J.E., WALSH, C.A. and FLEMING, M.D., 2010. Cdk5rap2 regulates centrosome function and chromosome segregation in neuronal progenitors. *Development (Cambridge, England),* **137**(11), pp. 1907-1917.

LUDERS, E., STEINMETZ, H. and JANCKE, L., 2002. Brain size and grey matter volume in the healthy human brain. *Neuroreport,* **13**(17), pp. 2371-2374.

LUDERS, E., THOMPSON, P.M. and TOGA, A.W., 2010. The development of the corpus callosum in the healthy human brain. *The Journal of neuroscience : the official journal of the Society for Neuroscience,* **30**(33), pp. 10985-10990.

LUI, J.H., HANSEN, D.V. and KRIEGSTEIN, A.R., 2011. Development and evolution of the human neocortex. *Cell,* **146**(1), pp. 18-36.

LYONS, D.A., NAYLOR, S.G., MERCURIO, S., DOMINGUEZ, C. and TALBOT, W.S., 2008. KBP is essential for axonal structure, outgrowth and maintenance in zebrafish, providing insight into the cellular basis of Goldberg-Shprintzen syndrome. *Development (Cambridge, England),* **135**(3), pp. 599-608.

LYONS, D.A., NAYLOR, S.G., SCHOLZE, A. and TALBOT, W.S., 2009. Kif1b is essential for mRNA localization in oligodendrocytes and development of myelinated axons. *Nature genetics,* **41**(7), pp. 854-858.

MA, H., MARTI-GUTIERREZ, N., PARK, S.W., WU, J., LEE, Y., SUZUKI, K., KOSKI, A., JI, D., HAYAMA, T., AHMED, R., DARBY, H., VAN DYKEN, C., LI, Y., KANG, E., PARK, A.R., KIM, D., KIM, S.T., GONG, J., GU, Y., XU, X., BATTAGLIA, D., KRIEG, S.A., LEE, D.M., WU, D.H., WOLF, D.P., HEITNER, S.B., BELMONTE, J.C.I., AMATO, P., KIM, J.S., KAUL, S. and MITALIPOV, S., 2017. Correction of a pathogenic gene mutation in human embryos. *Nature,* **548**(7668), pp. 413-419.

MALATESTA, P., HARTFUSS, E. and GOTZ, M., 2000. Isolation of radial glial cells by fluorescent-activated cell sorting reveals a neuronal lineage. *Development (Cambridge, England),* **127**(24), pp. 5253-5263.

MARKRAM, H., TOLEDO-RODRIGUEZ, M., WANG, Y., GUPTA, A., SILBERBERG, G. and WU, C., 2004. Interneurons of the neocortical inhibitory system. *Nature reviews.Neuroscience,* **5**(10), pp. 793-807.

MARTHIENS, V., RUJANO, M.A., PENNETIER, C., TESSIER, S., PAUL-GILLOTEAUX, P. and BASTO, R., 2013. Centrosome amplification causes microcephaly. *Nature cell biology,* **15**(7), pp. 731-740.

MARTIN, C.A., AHMAD, I., KLINGSEISEN, A., HUSSAIN, M.S., BICKNELL, L.S., LEITCH, A., NURNBERG, G., TOLIAT, M.R., MURRAY, J.E., HUNT, D., KHAN, F., ALI, Z., TINSCHERT, S., DING, J., KEITH, C., HARLEY, M.E., HEYN, P., MULLER, R., HOFFMANN, I., CORMIER-DAIRE, V., DOLLFUS, H., DUPUIS, L., BASHAMBOO, A., MCELREAVEY, K., KARIMINEJAD, A., MENDOZA-LONDONO, R., MOORE, A.T., SAGGAR, A., SCHLECHTER, C., WELEBER, R., THIELE, H., ALTMULLER, J., HOHNE, W., HURLES, M.E., NOEGEL, A.A., BAIG, S.M., NURNBERG, P. and JACKSON, A.P., 2014. Mutations in PLK4, encoding a master regulator of centriole biogenesis, cause microcephaly, growth failure and retinopathy. *Nature genetics,* **46**(12), pp. 1283-1292.

MATISE, T.C., CHEN, F., CHEN, W., DE LA VEGA, F.M., HANSEN, M., HE, C., HYLAND, F.C., KENNEDY, G.C., KONG, X., MURRAY, S.S., ZIEGLE, J.S., STEWART, W.C. and BUYSKE, S., 2007. A second-generation combined linkage physical map of the human genome. *Genome research,* **17**(12), pp. 1783-1786.

MAUN, N.A., SPEICHER, D.W., DINUBILE, M.J. and SOUTHWICK, F.S., 1996. Purification and properties of a Ca(2+)-independent barbed-end actin filament capping protein, CapZ, from human polymorphonuclear leukocytes. *Biochemistry,* **35**(11), pp. 3518-3524.

MCINTYRE, R.E., LAKSHMINARASIMHAN CHAVALI, P., ISMAIL, O., CARRAGHER, D.M., SANCHEZ-ANDRADE, G., FORMENT, J.V., FU, B., DEL CASTILLO VELASCO-HERRERA, M., EDWARDS, A., VAN DER WEYDEN, L., YANG, F., SANGER MOUSE GENETICS PROJECT, RAMIREZ-SOLIS, R., ESTABEL, J., GALLAGHER, F.A., LOGAN, D.W., ARENDS, M.J., TSANG, S.H., MAHAJAN, V.B., SCUDAMORE, C.L., WHITE, J.K., JACKSON, S.P., GERGELY, F. and ADAMS, D.J., 2012. Disruption of mouse Cenpj, a regulator of centriole biogenesis, phenocopies Seckel syndrome. *PLoS genetics,* **8**(11), pp. e1003022.

MCKENNA, A., HANNA, M., BANKS, E., SIVACHENKO, A., CIBULSKIS, K., KERNYTSKY, A., GARIMELLA, K., ALTSHULER, D., GABRIEL, S., DALY, M. and DEPRISTO, M.A., 2010. The Genome Analysis Toolkit: a MapReduce framework for analyzing next-generation DNA sequencing data. *Genome research,* **20**(9), pp. 1297-1303.

MCKUSICK-NATHANS INSTITUTE OF GENETIC MEDICINE, JOHNS HOPKINS UNIVERSITY (BALTIMORE, MD), 2012-last update, Online Mendelian Inheritance in Man, OMIM®. Available: http://omim.org/ [05/14, 2012].

MICHELS, S., FOSS, K., PARK, K., GOLDEN-GRANT, K., SANETO, R., LOPEZ, J. and MIRZAA, G.M., 2017. Mutations of KIF5C cause a neurodevelopmental disorder of infantile-onset epilepsy, absent language, and distinctive malformations of cortical development. *American journal of medical genetics.Part A,* **173**(12), pp. 3127-3131.

MIHALAS, A.B., ELSEN, G.E., BEDOGNI, F., DAZA, R.A.M., RAMOS-LAGUNA, K.A., ARNOLD, S.J. and HEVNER, R.F., 2016. Intermediate Progenitor Cohorts Differentially Generate Cortical Layers and Require Tbr2 for Timely Acquisition of Neuronal Subtype Identity. *Cell reports,* **16**(1), pp. 92-105.

MIRZAA, G.M., VITRE, B., CARPENTER, G., ABRAMOWICZ, I., GLEESON, J.G., PACIORKOWSKI, A.R., CLEVELAND, D.W., DOBYNS, W.B. and O'DRISCOLL, M., 2014. Mutations in CENPE define a novel kinetochore-centromeric mechanism for microcephalic primordial dwarfism. *Human genetics,* **133**(8), pp. 1023-1039.

MIYAMOTO, T., AKUTSU, S.N., FUKUMITSU, A., MORINO, H., MASATSUNA, Y., HOSOBA, K., KAWAKAMI, H., YAMAMOTO, T., SHIMIZU, K., OHASHI, H. and MATSUURA, S., 2017. PLK1-mediated phosphorylation of WDR62/MCPH2 ensures proper mitotic spindle orientation. *Human molecular genetics,* **26**(22), pp. 4429-4440.

MO, Z. and ZECEVIC, N., 2008. Is Pax6 critical for neurogenesis in the human fetal brain? *Cerebral cortex (New York, N.Y.: 1991),* **18**(6), pp. 1455-1465.

MOAWIA, A., SHAHEEN, R., RASOOL, S., WASEEM, S.S., EWIDA, N., BUDDE, B., KAWALIA, A., MOTAMENY, S., KHAN, K., FATIMA, A., JAMEEL, M., ULLAH, F., AKRAM, T., ALI, Z., ABDULLAH, U., IRSHAD, S., HOHNE, W., NOEGEL, A.A., AL-OWAIN, M., HORTNAGEL, K., STOBE, P., BAIG, S.M., NURNBERG, P., ALKURAYA, F.S., HAHN, A. and HUSSAIN, M.S., 2017. Mutations of KIF14 cause primary microcephaly by impairing cytokinesis. *Annals of Neurology,* **82**(4), pp. 562-577.

MOLYNEAUX, B.J., ARLOTTA, P., MENEZES, J.R. and MACKLIS, J.D., 2007. Neuronal subtype specification in the cerebral cortex. *Nature reviews.Neuroscience,* **8**(6), pp. 427-437.

MOTA, B. and HERCULANO-HOUZEL, S., 2015. BRAIN STRUCTURE. Cortical folding scales universally with surface area and thickness, not number of neurons. *Science (New York, N.Y.),* **349**(6243), pp. 74-77.

MOUNTCASTLE, V.B., 1997. The columnar organization of the neocortex. *Brain : a journal of neurology,* **120 (Pt 4)**(Pt 4), pp. 701-722.

MOYER, T.C., CLUTARIO, K.M., LAMBRUS, B.G., DAGGUBATI, V. and HOLLAND, A.J., 2015. Binding of STIL to Plk4 activates kinase activity to promote centriole assembly. *The Journal of cell biology,* **209**(6), pp. 863-878.

NAKAZAWA, Y., HIRAKI, M., KAMIYA, R. and HIRONO, M., 2007. SAS-6 is a cartwheel protein that establishes the 9-fold symmetry of the centriole. *Current biology : CB,* **17**(24), pp. 2169-2174.

NATIONAL INSTITUTE OF NEUROLOGICAL DISORDERS AND STROKE, 2017-last update, All Disorders. Available: https://www.ninds.nih.gov/Disorders/All-Disorders [07/16, 2017].

NEUMANN, B., WALTER, T., HERICHE, J.K., BULKESCHER, J., ERFLE, H., CONRAD, C., ROGERS, P., POSER, I., HELD, M., LIEBEL, U., CETIN, C., SIECKMANN, F., PAU, G., KABBE, R., WUNSCHE, A., SATAGOPAM, V., SCHMITZ, M.H., CHAPUIS, C., GERLICH, D.W., SCHNEIDER, R., EILS, R., HUBER, W., PETERS, J.M., HYMAN, A.A., DURBIN, R., PEPPERKOK, R. and ELLENBERG, J., 2010. Phenotypic profiling of the human genome by time-lapse microscopy reveals cell division genes. *Nature,* **464**(7289), pp. 721-727.

NIWA, S., LIPTON, D.M., MORIKAWA, M., ZHAO, C., HIROKAWA, N., LU, H. and SHEN, K., 2016. Autoinhibition of a Neuronal Kinesin UNC-104/KIF1A Regulates the Size and Density of Synapses. *Cell reports,* **16**(8), pp. 2129-2141.

NOCTOR, S.C., FLINT, A.C., WEISSMAN, T.A., DAMMERMAN, R.S. and KRIEGSTEIN, A.R., 2001. Neurons derived from radial glial cells establish radial units in neocortex. *Nature,* **409**(6821), pp. 714-720.

NOCTOR, S.C., MARTINEZ-CERDENO, V., IVIC, L. and KRIEGSTEIN, A.R., 2004. Cortical neurons arise in symmetric and asymmetric division zones and migrate through specific phases. *Nature neuroscience,* **7**(2), pp. 136-144.

O'DELL, R.S., CAMERON, D.A., ZIPFEL, W.R. and OLSON, E.C., 2015. Reelin Prevents Apical Neurite Retraction during Terminal Translocation and Dendrite Initiation. *The Journal of neuroscience : the official journal of the Society for Neuroscience,* **35**(30), pp. 10659-10674.

O'LEARY, D.D. and KOESTER, S.E., 1993. Development of projection neuron types, axon pathways, and patterned connections of the mammalian cortex. *Neuron,* **10**(6), pp. 991-1006.

OLSON, E.C., 2014. Analysis of preplate splitting and early cortical development illuminates the biology of neurological disease. *Frontiers in pediatrics,* **2**, pp. 121.

OMIM Clinical Synopsis Search - corpus callosum agenesis. Available: https://www.omim.org/search/?index=entry&search=corpus+callosum+agenesis&filter=cs_exists:true&sort=score+desc&start=1&limit=10&retrieve=clinicalSynopsis [11/22/2017, 2017].

OSTREM, B.E., LUI, J.H., GERTZ, C.C. and KRIEGSTEIN, A.R., 2014. Control of outer radial glial stem cell mitosis in the human brain. *Cell reports,* **8**(3), pp. 656-664.

PAGNAMENTA, A.T., MURRAY, J.E., YOON, G., SADIGHI AKHA, E., HARRISON, V., BICKNELL, L.S., AJILOGBA, K., STEWART, H., KINI, U., TAYLOR, J.C., KEAYS, D.A., JACKSON, A.P. and KNIGHT, S.J., 2012. A novel nonsense CDK5RAP2 mutation in a Somali child with primary microcephaly and sensorineural hearing loss. *American journal of medical genetics.Part A,* **158A**(10), pp. 2577-2582.

PALMER, E.E. and MOWAT, D., 2014. Agenesis of the corpus callosum: a clinical approach to diagnosis. *American journal of medical genetics.Part C, Seminars in medical genetics,* **166C**(2), pp. 184-197.

PAUL, L.K., 2011. Developmental malformation of the corpus callosum: a review of typical callosal development and examples of developmental disorders with callosal involvement. *Journal of neurodevelopmental disorders,* **3**(1), pp. 3-27.

PAUL, L.K., BROWN, W.S., ADOLPHS, R., TYSZKA, J.M., RICHARDS, L.J., MUKHERJEE, P. and SHERR, E.H., 2007. Agenesis of the corpus callosum: genetic, developmental and functional aspects of connectivity. *Nature reviews.Neuroscience,* **8**(4), pp. 287-299.

PEFEROEN, L., KIPP, M., VAN DER VALK, P., VAN NOORT, J.M. and AMOR, S., 2014. Oligodendrocyte-microglia cross-talk in the central nervous system. *Immunology,* **141**(3), pp. 302-313.

PERKINS, L., HUGHES, E., SRINIVASAN, L., ALLSOP, J., GLOVER, A., KUMAR, S., FISK, N. and RUTHERFORD, M., 2008. Exploring cortical subplate evolution using magnetic resonance imaging of the fetal brain. *Developmental neuroscience,* **30**(1-3), pp. 211-220.

POLLEN, A.A., NOWAKOWSKI, T.J., CHEN, J., RETALLACK, H., SANDOVAL-ESPINOSA, C., NICHOLAS, C.R., SHUGA, J., LIU, S.J., OLDHAM, M.C., DIAZ, A., LIM, D.A., LEYRAT, A.A., WEST, J.A. and KRIEGSTEIN, A.R., 2015. Molecular identity of human outer radial glia during cortical development. *Cell,* **163**(1), pp. 55-67.

PONTIOUS, A., KOWALCZYK, T., ENGLUND, C. and HEVNER, R.F., 2008. Role of intermediate progenitor cells in cerebral cortex development. *Developmental neuroscience,* **30**(1-3), pp. 24-32.

PULVERS, J.N., BRYK, J., FISH, J.L., WILSCH-BRAUNINGER, M., ARAI, Y., SCHREIER, D., NAUMANN, R., HELPPI, J., HABERMANN, B., VOGT, J., NITSCH, R., TOTH, A., ENARD, W., PAABO, S. and HUTTNER, W.B., 2010. Mutations in mouse Aspm (abnormal spindle-like microcephaly associated) cause not only microcephaly but also major defects in the germline. *Proceedings of the National Academy of Sciences of the United States of America,* **107**(38), pp. 16595-16600.

PUTOUX, A., NAMPOOTHIRI, S., LAURENT, N., CORMIER-DAIRE, V., BEALES, P.L., SCHINZEL, A., BARTHOLDI, D., ALBY, C., THOMAS, S., ELKHARTOUFI, N., ICHKOU, A., LITZLER, J., MUNNICH, A., ENCHA-RAZAVI, F., KANNAN, R., FAIVRE, L., BODDAERT, N., RAUCH, A., VEKEMANS, M. and ATTIE-BITACH, T., 2012. Novel KIF7 mutations extend the phenotypic spectrum of acrocallosal syndrome. *Journal of medical genetics,* **49**(11), pp. 713-720.

PUTOUX, A., THOMAS, S., COENE, K.L., DAVIS, E.E., ALANAY, Y., OGUR, G., UZ, E., BUZAS, D., GOMES, C., PATRIER, S., BENNETT, C.L., ELKHARTOUFI, N., FRISON, M.H., RIGONNOT, L., JOYE, N., PRUVOST, S., UTINE, G.E., BODUROGLU, K., NITSCHKE, P., FERTITTA, L., THAUVIN-ROBINET, C., MUNNICH, A., CORMIER-DAIRE, V., HENNEKAM, R., COLIN, E., AKARSU, N.A., BOLE-FEYSOT, C., CAGNARD, N., SCHMITT, A., GOUDIN, N., LYONNET, S., ENCHA-RAZAVI, F., SIFFROI, J.P., WINEY, M., KATSANIS, N., GONZALES, M., VEKEMANS, M., BEALES, P.L. and ATTIE-BITACH, T., 2011. KIF7 mutations cause fetal hydrolethalus and acrocallosal syndromes. *Nature genetics,* **43**(6), pp. 601-606.

RAYBAUD, C., AHMAD, T., RASTEGAR, N., SHROFF, M. and AL NASSAR, M., 2013. The premature brain: developmental and lesional anatomy. *Neuroradiology,* **55 Suppl 2**, pp. 23-40.

REESE, M.G., EECKMAN, F.H., KULP, D. and HAUSSLER, D., 1997. Improved splice site detection in Genie. *Journal of computational biology : a journal of computational molecular cell biology,* **4**(3), pp. 311-323.

REN, T., ANDERSON, A., SHEN, W.B., HUANG, H., PLACHEZ, C., ZHANG, J., MORI, S., KINSMAN, S.L. and RICHARDS, L.J., 2006. Imaging, anatomical, and

molecular analysis of callosal formation in the developing human fetal brain. *The anatomical record.Part A, Discoveries in molecular, cellular, and evolutionary biology,* **288**(2), pp. 191-204.

RILEY, E.P., MATTSON, S.N., SOWELL, E.R., JERNIGAN, T.L., SOBEL, D.F. and JONES, K.L., 1995. Abnormalities of the corpus callosum in children prenatally exposed to alcohol. *Alcoholism, Clinical and Experimental Research,* **19**(5), pp. 1198-1202.

RIVIERE, J.B., RAMALINGAM, S., LAVASTRE, V., SHEKARABI, M., HOLBERT, S., LAFONTAINE, J., SROUR, M., MERNER, N., ROCHEFORT, D., HINCE, P., GAUDET, R., MES-MASSON, A.M., BAETS, J., HOULDEN, H., BRAIS, B., NICHOLSON, G.A., VAN ESCH, H., NAFISSI, S., DE JONGHE, P., REILLY, M.M., TIMMERMAN, V., DION, P.A. and ROULEAU, G.A., 2011. KIF1A, an axonal transporter of synaptic vesicles, is mutated in hereditary sensory and autonomic neuropathy type 2. *American Journal of Human Genetics,* **89**(2), pp. 219-230.

ROBERTS, E., HAMPSHIRE, D.J., PATTISON, L., SPRINGELL, K., JAFRI, H., CORRY, P., MANNON, J., RASHID, Y., CROW, Y., BOND, J. and WOODS, C.G., 2002. Autosomal recessive primary microcephaly: an analysis of locus heterogeneity and phenotypic variation. *Journal of medical genetics,* **39**(10), pp. 718-721.

RODRIGUES-MARTINS, A., BETTENCOURT-DIAS, M., RIPARBELLI, M., FERREIRA, C., FERREIRA, I., CALLAINI, G. and GLOVER, D.M., 2007. DSAS-6 organizes a tube-like centriole precursor, and its absence suggests modularity in centriole assembly. *Current biology : CB,* **17**(17), pp. 1465-1472.

RONAN, L. and FLETCHER, P.C., 2015. From genes to folds: a review of cortical gyrification theory. *Brain structure & function,* **220**(5), pp. 2475-2483.

ROZEN, S. and SKALETSKY, H., 2000. Primer3 on the WWW for general users and for biologist programmers. *Methods in molecular biology (Clifton, N.J.),* **132**, pp. 365-386.

SCHELL-APACIK, C.C., WAGNER, K., BIHLER, M., ERTL-WAGNER, B., HEINRICH, U., KLOPOCKI, E., KALSCHEUER, V.M., MUENKE, M. and VON VOSS, H., 2008. Agenesis and dysgenesis of the corpus callosum: clinical, genetic and neuroimaging findings in a series of 41 patients. *American journal of medical genetics.Part A,* **146A**(19), pp. 2501-2511.

SCHINDELIN, J., ARGANDA-CARRERAS, I., FRISE, E., KAYNIG, V., LONGAIR, M., PIETZSCH, T., PREIBISCH, S., RUEDEN, C., SAALFELD, S., SCHMID, B., TINEVEZ, J.Y., WHITE, D.J., HARTENSTEIN, V., ELICEIRI, K., TOMANCAK, P. and CARDONA, A., 2012. Fiji: an open-source platform for biological-image analysis. *Nature methods,* **9**(7), pp. 676-682.

SCHNEIDER, C.A., RASBAND, W.S. and ELICEIRI, K.W., 2012. NIH Image to ImageJ: 25 years of image analysis. *Nature methods,* **9**(7), pp. 671-675.

SEMLITSCH, M., SHACKELFORD, R.E., ZIRKL, S., SATTLER, W. and MALLE, E., 2011. ATM protects against oxidative stress induced by oxidized low-density lipoprotein. *DNA repair,* **10**(8), pp. 848-860.

SHITAMUKAI, A., KONNO, D. and MATSUZAKI, F., 2011. Oblique radial glial divisions in the developing mouse neocortex induce self-renewing progenitors outside the germinal zone that resemble primate outer subventricular zone progenitors. *The Journal of neuroscience : the official journal of the Society for Neuroscience,* **31**(10), pp. 3683-3695.

SHITAMUKAI, A. and MATSUZAKI, F., 2012. Control of asymmetric cell division of mammalian neural progenitors. *Development, growth & differentiation,* **54**(3), pp. 277-286.

SIDDIQUI, N. and STRAUBE, A., 2017. Intracellular Cargo Transport by Kinesin-3 Motors. *Biochemistry.Biokhimiia,* **82**(7), pp. 803-815.

SILBEREIS, J.C., POCHAREDDY, S., ZHU, Y., LI, M. and SESTAN, N., 2016. The Cellular and Molecular Landscapes of the Developing Human Central Nervous System. *Neuron,* **89**(2), pp. 248-268.

SIR, J.H., BARR, A.R., NICHOLAS, A.K., CARVALHO, O.P., KHURSHID, M., SOSSICK, A., REICHELT, S., D'SANTOS, C., WOODS, C.G. and GERGELY, F., 2011. A primary microcephaly protein complex forms a ring around parental centrioles. *Nature genetics,* **43**(11), pp. 1147-1153.

SOLE, G., FERRER, X., VITAL, C., MARTIN-NEGRIER, M.L., VITAL, A. and LATOUR, P., 2009. Ultrastructural mitochondrial modifications characteristic of mitofusin 2 mutations (CMT2A). *Journal of the peripheral nervous system : JPNS,* **14**(3), pp. 206-207.

SOMBEKKE, M.H., JAFARI, N., BENDFELDT, K., MUELLER-LENKE, N., RADUE, E.W., NAEGELIN, Y., KAPPOS, L., MATTHEWS, P.M., POLMAN, C.H., BARKHOF, F., HINTZEN, R. and GEURTS, J.J., 2011. No influence of KIF1B on neurodegenerative markers in multiple sclerosis. *Neurology,* **76**(21), pp. 1843-1845.

SONNEN, K.F., GABRYJONCZYK, A.M., ANSELM, E., STIERHOF, Y.D. and NIGG, E.A., 2013. Human Cep192 and Cep152 cooperate in Plk4 recruitment and centriole duplication. *Journal of cell science,* **126**(Pt 14), pp. 3223-3233.

SOPPINA, V., NORRIS, S.R., DIZAJI, A.S., KORTUS, M., VEATCH, S., PECKHAM, M. and VERHEY, K.J., 2014. Dimerization of mammalian kinesin-3 motors results in superprocessive motion. *Proceedings of the National Academy of Sciences of the United States of America,* **111**(15), pp. 5562-5567.

SOTIRIADIS, A. and MAKRYDIMAS, G., 2012. Neurodevelopment after prenatal diagnosis of isolated agenesis of the corpus callosum: an integrative review. *American Journal of Obstetrics and Gynecology,* **206**(4), pp. 337.e1-337.e5.

STANCIK, E.K., NAVARRO-QUIROGA, I., SELLKE, R. and HAYDAR, T.F., 2010. Heterogeneity in ventricular zone neural precursors contributes to neuronal fate diversity in the postnatal neocortex. *The Journal of neuroscience : the official journal of the Society for Neuroscience,* **30**(20), pp. 7028-7036.

STENSON, P.D., BALL, E.V., MORT, M., PHILLIPS, A.D., SHIEL, J.A., THOMAS, N.S., ABEYSINGHE, S., KRAWCZAK, M. and COOPER, D.N., 2003. Human Gene Mutation Database (HGMD): 2003 update. *Human mutation,* **21**(6), pp. 577-581.

STENSON, P.D., MORT, M., BALL, E.V., EVANS, K., HAYDEN, M., HEYWOOD, S., HUSSAIN, M., PHILLIPS, A.D. and COOPER, D.N., 2017. The Human Gene Mutation Database: towards a comprehensive repository of inherited mutation data for medical research, genetic diagnosis and next-generation sequencing studies. *Human genetics,* **136**(6), pp. 665-677.

STILES, J. and JERNIGAN, T.L., 2010. The basics of brain development. *Neuropsychology review,* **20**(4), pp. 327-348.

STRNAD, P., LEIDEL, S., VINOGRADOVA, T., EUTENEUER, U., KHODJAKOV, A. and GONCZY, P., 2007. Regulated HsSAS-6 levels ensure formation of a single procentriole per centriole during the centrosome duplication cycle. *Developmental cell,* **13**(2), pp. 203-213.

SUN, T. and HEVNER, R.F., 2014. Growth and folding of the mammalian cerebral cortex: from molecules to malformations. *Nature reviews.Neuroscience,* **15**(4), pp. 217-232.

TAKAHASHI, T., NOWAKOWSKI, R.S. and CAVINESS, V.S.,Jr, 1993. Cell cycle parameters and patterns of nuclear movement in the neocortical proliferative zone of the fetal mouse. *The Journal of neuroscience : the official journal of the Society for Neuroscience,* **13**(2), pp. 820-833.

TALLINEN, T., CHUNG, J.Y., BIGGINS, J.S. and MAHADEVAN, L., 2014. Gyrification from constrained cortical expansion. *Proceedings of the National Academy of Sciences of the United States of America,* **111**(35), pp. 12667-12672.

TAN, X. and SHI, S.H., 2013. Neocortical neurogenesis and neuronal migration. *Wiley interdisciplinary reviews.Developmental biology,* **2**(4), pp. 443-459.

TANG, T.K., 2013. Centriole biogenesis in multiciliated cells. *Nature cell biology,* **15**(12), pp. 1400-1402.

TEEUW, M.E., LOUKILI, G., BARTELS, E.A., TEN KATE, L.P., CORNEL, M.C. and HENNEMAN, L., 2014. Consanguineous marriage and reproductive risk: attitudes and understanding of ethnic groups practising consanguinity in Western society. *European journal of human genetics : EJHG,* **22**(4), pp. 452-457.

TOMA, K. and HANASHIMA, C., 2015. Switching modes in corticogenesis: mechanisms of neuronal subtype transitions and integration in the cerebral cortex. *Frontiers in neuroscience,* **9**, pp. 274.

TOVAR-MOLL, F., MOLL, J., DE OLIVEIRA-SOUZA, R., BRAMATI, I., ANDREIUOLO, P.A. and LENT, R., 2007. Neuroplasticity in human callosal dysgenesis: a diffusion tensor imaging study. *Cerebral cortex (New York, N.Y.: 1991),* **17**(3), pp. 531-541.

TRIMBORN, M., GHANI, M., WALTHER, D.J., DOPATKA, M., DUTRANNOY, V., BUSCHE, A., MEYER, F., NOWAK, S., NOWAK, J., ZABEL, C., KLOSE, J., ESQUITINO, V., GARSHASBI, M., KUSS, A.W., ROPERS, H.H., MUELLER, S., POEHLMANN, C., GAVVOVIDIS, I., SCHINDLER, D., SPERLING, K. and NEITZEL, H., 2010. Establishment of a mouse model with misregulated chromosome condensation due to defective Mcph1 function. *PloS one,* **5**(2), pp. e9242.

TUNOVIC, S., BARANANO, K.W., BARKOVICH, J.A., STROBER, J.B., JAMAL, L. and SLAVOTINEK, A.M., 2015. Novel KIF7 missense substitutions in two patients presenting with multiple malformations and features of acrocallosal syndrome. *American journal of medical genetics.Part A,* **167A**(11), pp. 2767-2776.

TYLER, W.A. and HAYDAR, T.F., 2013. Multiplex genetic fate mapping reveals a novel route of neocortical neurogenesis, which is altered in the Ts65Dn mouse model of Down syndrome. *The Journal of neuroscience : the official journal of the Society for Neuroscience,* **33**(12), pp. 5106-5119.

UNNI, D.K., PIPER, M., MOLDRICH, R.X., GOBIUS, I., LIU, S., FOTHERGILL, T., DONAHOO, A.L., BAISDEN, J.M., COOPER, H.M. and RICHARDS, L.J., 2012. Multiple Slits regulate the development of midline glial populations and the corpus callosum. *Developmental biology,* **365**(1), pp. 36-49.

VALENCE, S., POIRIER, K., LEBRUN, N., SAILLOUR, Y., SONIGO, P., BESSIERES, B., ATTIE-BITACH, T., BENACHI, A., MASSON, C., ENCHA-RAZAVI, F., CHELLY, J. and BAHI-BUISSON, N., 2013. Homozygous truncating mutation of the KBP gene, encoding a KIF1B-binding protein, in a familial case of fetal polymicrogyria. *Neurogenetics,* **14**(3-4), pp. 215-224.

VAN BREUGEL, M., HIRONO, M., ANDREEVA, A., YANAGISAWA, H.A., YAMAGUCHI, S., NAKAZAWA, Y., MORGNER, N., PETROVICH, M., EBONG, I.O., ROBINSON, C.V., JOHNSON, C.M., VEPRINTSEV, D. and ZUBER, B., 2011. Structures of SAS-6 suggest its organization in centrioles. *Science (New York, N.Y.),* **331**(6021), pp. 1196-1199.

VAN DER KNAAP, L.J. and VAN DER HAM, I.J., 2011. How does the corpus callosum mediate interhemispheric transfer? A review. *Behavioural brain research,* **223**(1), pp. 211-221.

VASISTHA, N.A., GARCIA-MORENO, F., ARORA, S., CHEUNG, A.F., ARNOLD, S.J., ROBERTSON, E.J. and MOLNAR, Z., 2015. Cortical and Clonal Contribution of Tbr2 Expressing Progenitors in the Developing Mouse Brain. *Cerebral cortex (New York, N.Y.: 1991),* **25**(10), pp. 3290-3302.

VERLOES, A., DRUNAT, S., GRESSENS, P. and PASSEMARD, S., 1993. Primary Autosomal Recessive Microcephalies and Seckel Syndrome Spectrum Disorders. In: R.A. PAGON, M.P. ADAM, H.H. ARDINGER, T.D. BIRD, C.R. DOLAN, C.T. FONG, R.J.H. SMITH and K. STEPHENS, eds, *GeneReviews(R).* Seattle (WA): University of Washington, Seattle, .

VOLPE, J.J., 2000. Overview: normal and abnormal human brain development. *Mental retardation and developmental disabilities research reviews,* **6**(1), pp. 1-5.

VULPRECHT, J., DAVID, A., TIBELIUS, A., CASTIEL, A., KONOTOP, G., LIU, F., BESTVATER, F., RAAB, M.S., ZENTGRAF, H., IZRAELI, S. and KRAMER, A., 2012. STIL is required for centriole duplication in human cells. *Journal of cell science,* **125**(Pt 5), pp. 1353-1362.

WAISMAN, A., GINHOUX, F., GRETER, M. and BRUTTGER, J., 2015. Homeostasis of Microglia in the Adult Brain: Review of Novel Microglia Depletion Systems. *Trends in immunology,* **36**(10), pp. 625-636.

WALDECK-WEIERMAIR, M., BISCHOF, H., BLASS, S., DEAK, A.T., KLEC, C., GRAIER, T., ROLLER, C., ROST, R., EROGLU, E., GOTTSCHALK, B., HOFMANN, N.A., GRAIER, W.F. and MALLI, R., 2015. Generation of Red-Shifted Cameleons for Imaging Ca(2)(+) Dynamics of the Endoplasmic Reticulum. *Sensors (Basel, Switzerland),* **15**(6), pp. 13052-13068.

WALSH, D.M., SHALEV, S.A., SIMPSON, M.A., MORGAN, N.V., GELMAN-KOHAN, Z., CHEMKE, J., TREMBATH, R.C. and MAHER, E.R., 2013. Acrocallosal syndrome: identification of a novel KIF7 mutation and evidence for oligogenic inheritance. *European journal of medical genetics,* **56**(1), pp. 39-42.

WANG, W., CAO, L., WANG, C., GIGANT, B. and KNOSSOW, M., 2015. Kinesin, 30 years later: Recent insights from structural studies. *Protein science : a publication of the Protein Society,* **24**(7), pp. 1047-1056.

WATERHOUSE, A.M., PROCTER, J.B., MARTIN, D.M., CLAMP, M. and BARTON, G.J., 2009. Jalview Version 2--a multiple sequence alignment editor and analysis workbench. *Bioinformatics (Oxford, England),* **25**(9), pp. 1189-1191.

WESTERHOLM-PARVINEN, A., VERNOS, I. and SERRANO, L., 2000. Kinesin subfamily UNC104 contains a FHA domain: boundaries and physicochemical characterization. *FEBS letters,* **486**(3), pp. 285-290.

WOLMAN, D., 2012. The split brain: a tale of two halves. *Nature,* **483**(7389), pp. 260-263.

WOODS, C.G., BOND, J. and ENARD, W., 2005. Autosomal recessive primary microcephaly (MCPH): a review of clinical, molecular, and evolutionary findings. *American Journal of Human Genetics,* **76**(5), pp. 717-728.

XIE, Q., YANG, Y., HUANG, J., NINKOVIC, J., WALCHER, T., WOLF, L., VITENZON, A., ZHENG, D., GOTZ, M., BEEBE, D.C., ZAVADIL, J. and CVEKL, A., 2013. Pax6 interactions with chromatin and identification of its novel direct target genes in lens and forebrain. *PloS one,* **8**(1), pp. e54507.

XUE, X., JAULIN, F., ESPENEL, C. and KREITZER, G., 2010. PH-domain-dependent selective transport of p75 by kinesin-3 family motors in non-polarized MDCK cells. *Journal of cell science,* **123**(Pt 10), pp. 1732-1741.

XUE, Y., SCHOSER, B., RAO, A.R., QUADRELLI, R., VAGLIO, A., RUPP, V., BEICHLER, C., NELSON, S.F., SCHAPACHER-TILP, G., WINDPASSINGER, C. and WILCOX, W.R., 2016. Exome Sequencing Identified a Splice Site Mutation in FHL1 that Causes Uruguay Syndrome, an X-Linked Disorder With Skeletal Muscle Hypertrophy and Premature Cardiac Death. *Circulation.Cardiovascular genetics,* **9**(2), pp. 130-135.

YAMAMOTO, S., JAISWAL, M., CHARNG, W.L., GAMBIN, T., KARACA, E., MIRZAA, G., WISZNIEWSKI, W., SANDOVAL, H., HAELTERMAN, N.A., XIONG, B., ZHANG, K., BAYAT, V., DAVID, G., LI, T., CHEN, K., GALA, U., HAREL, T., PEHLIVAN, D., PENNEY, S., VISSERS, L.E.L.M., DE LIGT, J., JHANGIANI, S.N., XIE, Y., TSANG, S.H., PARMAN, Y., SIVACI, M., BATTALOGLU, E., MUZNY, D., WAN, Y.W., LIU, Z., LIN-MOORE, A.T., CLARK, R.D., CURRY, C.J., LINK, N., SCHULZE, K.L., BOERWINKLE, E., DOBYNS, W.B., ALLIKMETS, R., GIBBS, R.A., CHEN, R., LUPSKI, J.R., WANGLER, M.F. and BELLEN, H.J., 2014. A drosophila genetic resource of mutants to study mechanisms underlying human genetic diseases. *Cell,* **159**(1), pp. 200-214.

YANG, Y.J., BALTUS, A.E., MATHEW, R.S., MURPHY, E.A., EVRONY, G.D., GONZALEZ, D.M., WANG, E.P., MARSHALL-WALKER, C.A., BARRY, B.J., MURN, J., TATARAKIS, A., MAHAJAN, M.A., SAMUELS, H.H., SHI, Y., GOLDEN, J.A., MAHAJNAH, M., SHENHAV, R. and WALSH, C.A., 2012. Microcephaly gene links trithorax and REST/NRSF to control neural stem cell proliferation and differentiation. *Cell,* **151**(5), pp. 1097-1112.

YEO, G. and BURGE, C.B., 2004. Maximum entropy modeling of short sequence motifs with applications to RNA splicing signals. *Journal of computational biology : a journal of computational molecular cell biology,* **11**(2-3), pp. 377-394.

YEUNG, M.S., ZDUNEK, S., BERGMANN, O., BERNARD, S., SALEHPOUR, M., ALKASS, K., PERL, S., TISDALE, J., POSSNERT, G., BRUNDIN, L., DRUID, H. and FRISEN, J., 2014. Dynamics of oligodendrocyte generation and myelination in the human brain. *Cell,* **159**(4), pp. 766-774.

YOSHIDA, R., ISHIZU, K., YAMADA, S., UWABE, C., OKADA, T., TOGASHI, K. and TAKAKUWA, T., 2017. Dynamics of gyrification in the human cerebral cortex during development. *Congenital anomalies,* **57**(1), pp. 8-14.

YU, T.W., MOCHIDA, G.H., TISCHFIELD, D.J., SGAIER, S.K., FLORES-SARNAT, L., SERGI, C.M., TOPCU, M., MCDONALD, M.T., BARRY, B.J., FELIE, J.M., SUNU, C., DOBYNS, W.B., FOLKERTH, R.D., BARKOVICH, A.J. and WALSH, C.A., 2010. Mutations in WDR62, encoding a centrosome-associated protein, cause microcephaly with simplified gyri and abnormal cortical architecture. *Nature genetics,* **42**(11), pp. 1015-1020.

YUAN, L., HUANG, X.Y., LIU, Z.Y., ZHANG, F., ZHU, X.L., YU, J.Y., JI, X., XU, Y.P., LI, G., LI, C., WANG, H.J., DENG, Y.Q., WU, M., CHENG, M.L., YE, Q., XIE, D.Y., LI, X.F., WANG, X., SHI, W., HU, B., SHI, P.Y., XU, Z. and QIN, C.F., 2017. A single mutation in the prM protein of Zika virus contributes to fetal microcephaly. *Science (New York, N.Y.),* **358**(6365), pp. 933-936.

ZECEVIC, N., CHEN, Y. and FILIPOVIC, R., 2005. Contributions of cortical subventricular zone to the development of the human cerebral cortex. *The Journal of comparative neurology,* **491**(2), pp. 109-122.

ZECEVIC, N., HU, F. and JAKOVCEVSKI, I., 2011. Interneurons in the developing human neocortex. *Developmental neurobiology,* **71**(1), pp. 18-33.

ZECHEL, S., NAKAGAWA, Y. and IBANEZ, C.F., 2016. Thalamo-cortical axons regulate the radial dispersion of neocortical GABAergic interneurons. *eLife,* **5**, pp. 10.7554/eLife.20770.

ZHANG, F., WANG, H.J., WANG, Q., LIU, Z.Y., YUAN, L., HUANG, X.Y., LI, G., YE, Q., YANG, H., SHI, L., DENG, Y.Q., QIN, C.F. and XU, Z., 2017. American Strain of Zika Virus Causes More Severe Microcephaly Than an Old Asian Strain in Neonatal Mice. *EBioMedicine,* **25**, pp. 95-105.

ZHANG, X., HUANG, C.T., CHEN, J., PANKRATZ, M.T., XI, J., LI, J., YANG, Y., LAVAUTE, T.M., LI, X.J., AYALA, M., BONDARENKO, G.I., DU, Z.W., JIN, Y., GOLOS, T.G. and ZHANG, S.C., 2010. Pax6 is a human neuroectoderm cell fate determinant. *Cell stem cell,* **7**(1), pp. 90-100.

ZHAO, C., TAKITA, J., TANAKA, Y., SETOU, M., NAKAGAWA, T., TAKEDA, S., YANG, H.W., TERADA, S., NAKATA, T., TAKEI, Y., SAITO, M., TSUJI, S., HAYASHI, Y. and HIROKAWA, N., 2001. Charcot-Marie-Tooth disease type 2A caused by mutation in a microtubule motor KIF1Bbeta. *Cell,* **105**(5), pp. 587-597.

ZLOTOGORA, J., 1997. Genetic disorders among Palestinian Arabs: 1. Effects of consanguinity. *American Journal of Medical Genetics,* **68**(4), pp. 472-475.

ZUCCARO, E., BERGAMI, M., VIGNOLI, B., BONY, G., PIERCHALA, B.A., SANTI, S., CANCEDDA, L. and CANOSSA, M., 2014. Polarized expression of p75(NTR) specifies axons during development and adult neurogenesis. *Cell reports,* **7**(1), pp. 138-152.

ZUCHNER, S., MERSIYANOVA, I.V., MUGLIA, M., BISSAR-TADMOURI, N., ROCHELLE, J., DADALI, E.L., ZAPPIA, M., NELIS, E., PATITUCCI, A., SENDEREK, J., PARMAN, Y., EVGRAFOV, O., JONGHE, P.D., TAKAHASHI, Y., TSUJI, S., PERICAK-VANCE, M.A., QUATTRONE, A., BATTALOGLU, E., POLYAKOV, A.V., TIMMERMAN, V., SCHRODER, J.M. and VANCE, J.M., 2004. Mutations in the mitochondrial GTPase mitofusin 2 cause Charcot-Marie-Tooth neuropathy type 2A. *Nature genetics,* **36**(5), pp. 449-451.